



ADVANCED MASTERS IN STRUCTURAL ANALYSIS
OF MONUMENTS AND HISTORICAL CONSTRUCTIONS



Master's Thesis

Marian Fresneda Cardani

**Fatigue assessment of
riveted connections in old
metallic bridges.**

This Masters Course has been funded with support from the European Commission. This publication reflects the views only of the author, and the Commission cannot be held responsible for any use which may be made of the information contained therein.

DECLARATION

Name: Marian Fresneda Cardani

Email: marian.cardani@gmail.com

Title of the
Msc Dissertation: Fatigue assessment of riveted connections in old metallic bridges

Supervisor(s): Isabel Valente

Co-supervisor: José António Fonseca de Oliveira Correia

Year: 2017

I hereby declare that all information in this document has been obtained and presented in accordance with academic rules and ethical conduct. I also declare that, as required by these rules and conduct, I have fully cited and referenced all material and results that are not original to this work.

I hereby declare that the MSc Consortium responsible for the Advanced Masters in Structural Analysis of Monuments and Historical Constructions is allowed to store and make available electronically the present MSc Dissertation.

University: Universidade do Minho

Date: 17/07/2017

Signature: _____

ACKNOWLEDGEMENTS

Firstly, I would like to thank my supervisor Isabel B. Valente and co-supervisor José A. F. O. Correia for their guidance, patience and sharing of knowledge throughout this process.

I also like to thank all SAHC professors for their teaching and assistance. Also, my SAHC friends for this fulfilling experience.

My especial and deep gratitude to my parents, for always supporting and encouraging me. For providing me with opportunities that I know many people will never experience in their lives.

This page was intentionally left blank.

ABSTRACT

This thesis aim to extend the interpretation of data collected from experimental tests developed to analyze the fatigue phenomena on the material and on riveted connections obtained from old Portuguese metallic bridges. The analysis of the results is made following a conventional point of view (i.e. by considering the statistical models proposed in actual codes) and by following probabilistic fatigue models (i.e. modern interpretational proposals, such as Tara and Grainer model, and Castillo and Fernández-Canteli model).

The metallic bridges addressed in the analysis were built in the late nineteenth and early twentieth centuries and have now become important historical heritage. The main materials used at that time were steel and puddle iron.

There is an increasing interest of governmental agencies for their conservation and maintenance, not only for their historical value, but also for being structures that are still in use. These bridges were designed for a very different scenario of cars and trains flow than the one that is being used nowadays. Due to this situation, the materials and connections that exist in these bridges may be prone to suffer failure.

An important phenomenon, not always well known by engineering designers, is fatigue. Such phenomenon was only studied in the twentieth century. The fatigue failure is a problem in steel bridges, due to the likelihood of the steel to deteriorate under variable stresses. Fatigue is recognised as the major cause of failure in metallic bridges.

In due time, the technical community became aware of the phenomena and studies were developed so that it is now possible to find a treatment of fatigue life of structural details in the European, British and North American standards, such as, Eurocode 3, BS 5400 and AASHTO LRFD Bridge Design Specifications. The approaches proposed by these codes are based in the S-N curves and related to the total number of cycles to failure and the applied stress range. However, the fatigue resistance of riveted shear connections is not directly mentioned in the referred codes.

In the present work, a statistical analysis based on experimental data collected in fatigue tests previously performed by others authors, is developed. The main objective is to obtain characteristic S-N curves for riveted joints as well as design fatigue curves for several fatigue damage parameters for materials, calibrated for old Portuguese metallic bridges.

The statistical analysis will be achieved with the used of ASTM E 739–91 American Standard and probabilistic fatigue model proposed by Castillo and Fernández-Canteli. The experimental results are compared to the characteristic S-N curves obtained by applying a statistical analysis.

This page was intentionally left blank.

RESUMO

A tese visa a interpretação de testes obtidos através de dados experimentais do fenômeno da fadiga em rebites em antigas pontes metálicas portuguesas. A análise dos resultados foi realizada através de modelos convencionais (como os propostos por códigos e normas) e com modelos probabilísticos voltados à fadiga (como propostas modernas de interpretação, o modelo de Tara e Grainer, e o modelo de Castillo e Fernández-Canteli).

As pontes metálicas construídas no final do século XIX e início do século XX tornaram-se patrimônio histórico importante. Assim, despertando o interesse das agências governamentais para sua conservação e manutenção. Não somente pelo valor histórico que estas representam, mas também por serem pontes que ainda em uso. No entanto, estas pontes foram projetadas para situações muito diferente para as quais são usadas no presente. O fluxo de carros e comboios são diferentes para o qual as pontes foram originalmente projetadas. Devido a esta situação, os materiais e conexões presentes nestas apresentam ruptura. A fadiga é fenômeno importante, porém desconhecido pelos engenheiros projetistas da época. O fenômeno só foi ser estudado no século XX.

O principal material usado naquela época era ferro e aço. As rupturas causadas pela fadiga são preocupantes em pontes feitas de aço, já que quando submetidas a tensões variáveis há probabilidade de deterioração tanto do material como das conexões. Assim, o fenômeno da fadiga é apontado como uma das principais causas de falhas e rupturas em pontes metálicas.

Por tanto, foram desenvolvidos métodos para avaliação e tratamento da vida à fadiga em estruturas e conexões metálicas foram normalizadas em códigos europeus, britânico e norte americano, como o Euro código 3, BS 5400 e as especificações de projeto de pontes AASHTO. As abordagens são baseadas nas curvas S-N e relacionada ao número total de ciclos para a ruptura na faixa de tensões estudada. Mas a resistência à fadiga ao cisalhamento de rebites não é mencionada nos códigos mencionados.

Nesta tese, será apresentada uma análise estatística dos dados experimentais obtidos em testes experimentais de fadiga previamente realizados por outros autores. O objetivo principal é obter curvas S-N características para conexões rebitadas e para os materiais presentes nas antigas pontes metálicas portuguesa aqui em estudo.

A análise estatística será realizada com o auxílio do código norte americano ASTM E 739-91 e modelo de fadiga probabilístico proposto por Castillo e Fernández-Cantelo. Os resultados experimentais utilizados neste estudo serão comparados com as curvas S-N características obtidas pela aplicação das análises estatísticas consideradas.

This page was intentionally left blank.

Table of Contents

1	Introduction	1
1.1	Objectives	2
1.2	Thesis organization.....	2
2	STATE-OF-ART	5
2.1	Historical Point of View	5
2.2	The Rivet	6
2.3	The Fatigue Phenomenon	9
2.4	Methods that consider the Fatigue Life	11
2.4.1	Stress-Life Method or S-N Curve	11
2.4.2	Nominal Stress Method	12
2.5	Codes related to Fatigue Calculation	12
2.5.1	Eurocode 3	12
2.5.2	ASTM E 793 -91	18
2.5.3	British Code - BS 5400.....	19
2.5.4	Taras and Greiner approach	20
3	Fatigue on connecting elements.....	27
3.1	The Portuguese bridges in study.....	27
3.2	Probabilistic models directed to fatigue	30
3.2.1	Global interpretation of probabilistic models	31
3.2.2	Probabilistic fatigue damage	31
3.2.3	Castillo and Fernández-Canteli probabilistic model	32
3.3	Study of the riveted connections	33
3.3.1	Probabilistic study of riveted connection	35
3.4	Results of the connections elements.....	46
3.4.1	Proposed S-N curves for double shear and single shear riveted connections	46
3.4.2	Statistical analysis based on comparison between ASTM E 739-91 and Castillo and Fernández-Canteli model.....	48

3.4.3	Statistical Analysis based on Castillo and Fernández-Canteli model	49
4	Fatigue characterization of the material	51
4.1	Stress-life test	52
4.1.1	Stress test on Viana bridge material - Strain ratio equal 0	53
4.1.2	Stress test on Fão bridge material.....	54
4.1.3	Analysis on the material behavior of Trezói bridge through stress test - strain ratio equal -1	58
4.1.4	Analysis on the material behavior of Luiz I bridge through stress test - strain ratio equal -1	59
4.2	Strain-life test	61
4.2.1	Material behavior Viana bridge through strain test - Study carried out with strain ratio equal -1	61
4.2.2	Analysis on the material behavior of Fão bridge through strain test	62
4.2.3	Analysis on the material behavior of Trezói bridge through strain test - strain ratio equal -1	66
4.2.4	Analysis on the material behavior Luiz I bridge through strain test - strain ratio equal -1	68
4.3	Smith – Watson – Topper - life test (SWT)	69
4.3.1	Analysis on the material behavior Viana bridge through SWT test - strain ratio equal -1	69
4.3.2	Analysis on the material behavior Viana bridge through SWT test	70
4.3.3	Analysis on the material behavior of Trezói bridge through SWT test - strain ratio equal -1	74
4.3.4	Analysis on the material behavior of Luiz I bridge through SWT test - strain ratio equal -1	76
4.4	Comparison of the experimental data	77
4.4.1	Statistical analysis based on ASTM E739-91 standard.....	77
4.5	Results from the fatigue damage parameters.....	79
5	Final remarks.....	81
5.1	Future developments	82

References.....	83
Appendix A: Tables of the data of the riveted connection	87
1 RESULTS OBTAINED FOR THE MATERIALS SUBMITTED TO STRESS	87
2 RESULTS OBTAINED FOR THE MATERIALS SUBMITTED TO STRAIN	92
3 RESULTS OBTAINED FOR THE MATERIALS SUBMITTED TO SMITH-WATSON-TOPPER (SWT)	96

This page was intentionally left blank.

List of Figures

Figure 1 - Representation of a rivet (Collette Q. , 2014)	7
Figure 2 - Common processes adopted in the production of rivets (Lindenberg, 2016).....	7
Figure 3 - Elevation and plan views of a riveted specimen (Collette, Sire, & Wouters, 2014).....	8
Figure 4 - Representation of the tools used to the positioning and installation of the rivets (Collette Q. , 2014)	9
Figure 5 - Group of men responsible for the hot-riveting installation (Collette Q. , 2014).....	9
Figure 6 - Three period of the fatigue life (Correia, 2014).....	10
Figure 7 - Representation of the sliding movement of the slip plans (ASM, 2008).....	11
Figure 8 - Example of plain members and mechanically fastened joints (EUROPEAN STANDARD, 2005)	13
Figure 9 – Example of attachments and stiffeners (EUROPEAN STANDARD, 2005)	14
Figure 10 - Example of load carrying joints (EUROPEAN STANDARD, 2005)	15
Figure 11 – Fatigue strength curves for normal stress ranges (EUROPEAN STANDARD, 2005).....	17
Figure 12 - Fatigue strength curve for shear stress ranges (EUROPEAN STANDARD, 2005)	17
Figure 13 – Example of Fatigue Life N (Y) vs. Plastic Strain Amplitude $\Delta\epsilon/2$ (X) (ASTM E739-91, 2004)	19
Figure 14 – Classification of non-welding components used in the calculation of fatigue life	20
Figure 15 – S-N curve result from Taras and Greiner research (Taras & Greiner, 2009)	21
Figure 16 - Increase or reduction of fatigue strength, as function of the stress ratio (Taras & Greiner, 2009)	22
Figure 17 – Most important categories for the statistical evaluation (Taras & Greiner, 2009).....	22
Figure 18 - Classification of construction details (Taras & Greiner, 2009).....	24
Figure 19 - Minimum values (Taras & Greiner, 2009).....	25
Figure 20 - Location of the bridges in study (onestopmap, 2017).....	27
Figure 21 – Luiz I bridge (author, 2017)	28
Figure 22 - Fão road bridge (Jesus, Silva, & Correia, 2014)	28
Figure 23 - Pinhão bridge (Correia, 2014)	29
Figure 24 - Viana bridge (Correia, 2014)	30

Figure 25 - Trezói railway bridge (Correia, 2014).....	30
Figure 26 – Distribution band in a S-N curve (Correia, 2014)	31
Figure 27 – Representation of the probabilistic curves (Correia, 2014).....	32
Figure 28 – Probabilistic representation of $\epsilon\sigma$ -N field (Correia, 2014).....	33
Figure 29 - example of round specimens put in to submitted to monotonic tensile test (Correia, 2014)	33
Figure 30 - Photos of the specimens with double shear riveted connections, cut from Viana bridge (Correia, 2014)	35
Figure 31 - (a) S-N Curve of Viana bridge riveted connections obtained with ProFatigue® software; .	37
Figure 32 – Illustration of the Luiz I bridge connection, before testing (Correia, 2014)	38
Figure 33 – (a) S-N Curve of Fão bridge riveted connections obtained with the ProFatigue® software ; (b) - Probabilistic paper of Fão bridge riveted connections; Weibull distribution on Fão bridge riveted connections	39
Figure 34 - Photo of the specimens from Trezói bridge (Correia, 2014).....	40
Figure 35 – (a) S-N Curve of Trezói bridge riveted connections obtained with the ProFatigue® software, (b) Probabilistic paper of Trezói bridge of the riveted connections, (c) Weibull distribution Trezói bridge of the riveted connections	41
Figure 36 - Representation of the Luiz I bridge connection.....	42
Figure 37 – (a) S-N Curve of Luiz I bridge riveted connections obtained with the ProFatigue® software, (b) Probabilistic paper of Luiz I bridge of the riveted connections, (c) Weibull distribution Luiz I bridge of the riveted connections	43
Figure 38 - Illustration of the specimens from Pinhão bridge	44
Figure 39 – (a) S-N Curve of Pinhão bridge riveted connections obtained with the ProFatigue® software, (b) Probabilistic paper of Pinhão bridge of the riveted connections, (c) Weibull distribution Pinhão bridge of the riveted connections	45
Figure 40 - Curves for double shear riveted connections.....	47
Figure 41 - Curves for single shear riveted connections	47
Figure 42 – Statistical analysis on the results obtained with double shear specimens.....	48
Figure 43 – Statistical analysis on the results obtained with single shear specimens	49
Figure 44 - Statistical Analysis based on the Castillo & Fernández-Canteli model, applied to double shear.....	50

Figure 45 - Statistical Analysis based on the Castillo & Fernández-Canteli model, applied to single shear	50
Figure 46 – Geometry of the specimen used in the fatigue tests (Correia, 2014)	52
Figure 47 – Example of specimens of material extracted from Fão bridge used (Correia, 2014)	52
Figure 48 - Example of specimens of material extracted from the Viana bridge (Correia, 2014)	52
Figure 49 – (a) S-N Curve of Viana bridge material stress test ($R_{\varepsilon}=-1$), (b) Probabilistic paper of the material behavior of Viana bridge; stress test ($R_{\varepsilon}=-1$), (c) Weibull distribution Viana bridge material; stress test ($R_{\varepsilon}=-1$)	53
Figure 50 – (a) S-N Curve of Fão bridge material stress test ($R_{\varepsilon}= 0$), (b) - Probabilistic paper of the material behavior of Fão bridge; stress test ($R_{\varepsilon}= 0$), (c) Weibull material distribution on Fão bridge; stress test ($R_{\varepsilon}= 0$)	55
Figure 51 – (a) S-N Curve of Fão bridge material stress test ($R_{\varepsilon}=-1$), (b) Probabilistic paper of the material behavior of Fão bridge; stress test ($R_{\varepsilon}=-1$), (c) Weibull material distribution on Fão bridge; stress test ($R_{\varepsilon}=-1$)	56
Figure 52 – (a) S-N Curve of Fão bridge material stress test ($R_{\varepsilon}=0$ and $R_{\varepsilon}=-1$), (b) Probabilistic paper of the material behavior of Fão bridge; stress test ($R_{\varepsilon}=0$ and $R_{\varepsilon}=-1$), (c) Weibull material distribution on Fão bridge; stress test ($R_{\varepsilon}=0$ and $R_{\varepsilon}=-1$)	57
Figure 53 – (a) S-N Curve of Trezói bridge material stress test ($R_{\varepsilon}=-1$), (b) Probabilistic paper of the material behavior of Trezói bridge; stress test ($R_{\varepsilon}=-1$), (c) Weibull material distribution on Trezói bridge; stress test ($R_{\varepsilon}=-1$)	59
Figure 54 – (a) S-N Curve of Luiz I bridge material stress test ($R_{\varepsilon}=-1$), (b) Probabilistic paper of the material behavior of Luiz I bridge; stress test ($R_{\varepsilon}=-1$), (c) Weibull material distribution of Luiz I bridge, stress test ($R_{\varepsilon}=-1$)	60
Figure 55 – (a) S-N Curve of Viana bridge material strain test ($R_{\varepsilon}=-1$), (b) Probabilistic paper of the material behavior of Viana bridge; strain test ($R_{\varepsilon}=-1$), (c) Weibull material distribution of Viana bridge, strain test ($R_{\varepsilon}=-1$)	62
Figure 56 – (a) S-N Curve of Fão bridge material strain test ($R_{\varepsilon}=0$), (b) Probabilistic paper of the material behavior of Fão bridge; strain test ($R_{\varepsilon}=0$), (c) Weibull material distribution of Fão bridge, strain test ($R_{\varepsilon}=0$)	63
Figure 57 – (a) Curve of Fão bridge material strain test ($R_{\varepsilon}=-1$), (b) Probabilistic paper of the material behavior of Fão bridge; strain test ($R_{\varepsilon}=-1$), (c) Weibull material distribution of Fão bridge, strain test ($R_{\varepsilon}=-1$)	64

Figure 58 – (a) S-N Curve of Fão bridge material strain test ($R_{\epsilon}=0$ and $R_{\epsilon}=-1$), (b) Probabilistic paper of the material behavior of Fão bridge; strain test ($R_{\epsilon}=0$ and $R_{\epsilon}=-1$), (c) Weibull material distribution of Fão bridge, strain test ($R_{\epsilon}=0$ and $R_{\epsilon}=-1$) 66

Figure 59 – (a) S-N Curve of Trezói bridge material strain test ($R_{\epsilon}=-1$), (b) Probabilistic paper of the material behavior of Trezói bridge; strain test ($R_{\epsilon}=-1$), (c) Weibull material distribution of Trezói bridge, strain test ($R_{\epsilon}=-1$) 67

Figure 60 – (a) S-N Curve of Luiz I bridge material strain test ($R_{\epsilon}=-1$), (b) Probabilistic paper of the material behavior of Luiz I bridge; strain test ($R_{\epsilon}=-1$), (c) Weibull material distribution of Luiz I bridge, strain test ($R_{\epsilon}=-1$) 68

Figure 61 – (a) S-N Curve of Viana bridge material SWT test ($R_{\epsilon}=-1$), (b) Probabilistic paper of the material behavior of Viana bridge; SWT test ($R_{\epsilon}=-1$), (c) Weibull material distribution of Viana bridge, SWT test ($R_{\epsilon}=-1$) 70

Figure 62 – (a) S-N Curve of Fão bridge material SWT test ($R_{\epsilon}=0$), (b) - Probabilistic paper of the material behavior of Fão bridge; SWT test ($R_{\epsilon}=0$), (c) Weibull material distribution of Fão bridge, SWT test ($R_{\epsilon}=0$) 71

Figure 63 – (a) S-N Curve of Fão bridge, based on material SWT test ($R_{\epsilon}=-1$), (b) Probabilistic paper of the material behavior of Fão bridge; SWT test ($R_{\epsilon}=-1$), (c) Weibull material distribution on Fão bridge1, SWT test ($R_{\epsilon}=-1$) 72

Figure 64 – (a) S-N Curve of Fão bridge, based on material SWT test ($R_{\epsilon}=0$ and $R_{\epsilon}=-1$), (b) Probabilistic paper of the material behavior of Fão bridge; SWT test ($R_{\epsilon}=0$ and $R_{\epsilon}=-1$), Weibull material distribution on Fão bridge, SWT test ($R_{\epsilon}=0$ and $R_{\epsilon}=-1$) 74

Figure 65 – (a) S-N Curve of Trezói’s bridge, based on material SWT test ($R_{\epsilon}=-1$), (b) Probabilistic paper of the material behavior of Trezói bridge; SWT test ($R_{\epsilon}=-1$), (c) Weibull material distribution Trezói bridge, SWT test ($R_{\epsilon}=-1$) 75

Figure 66 – (a) S-N Curve of Luiz I bridge, based on material SWT test ($R_{\epsilon}=-1$), (b) Probabilistic paper of the material behavior of Luiz I bridge; SWT test ($R_{\epsilon}=-1$), (c) Weibull material distribution on Luiz I bridge, SWT test ($R_{\epsilon}=-1$) 76

Figure 67 – Statistical analysis on the stress-life of all bridge materials 77

Figure 68 - Statistical analysis on the strain-life of all bridge materials..... 78

Figure 69 - Statistical analysis on the SWT-life of all bridge materials 78

Figure 70 – Stress-life fatigue damage of all bridge materials 79

Figure 71 - Strain-life fatigue damage of all bridge materials 80

Figure 72 - SWT-life fatigue damage of all bridge materials 80

This page was intentionally left blank.

List of Tables

Table 1 - The dimension of the round specimens submitted to monotonic tensile test (Correia, 2014)	34
Table 2 - Results from Viana bridge stress test on connections (Correia, 2014)	36
Table 3 - Estimated parameters on the connections of Viana bridge	37
Table 4 – Results from Fão bridge stress test on connections (Correia, An Integral Probabilistic Approach for Fatigue Lifetime Prediction of Mechanical and Structural Components, 2014)	38
Table 5 - Estimated parameters on the connections of Fão bridge	39
Table 6 – Results from Trezói bridge stress test connections (Correia, An Integral Probabilistic Approach for Fatigue Lifetime Prediction of Mechanical and Structural Components, 2014)	40
Table 7 - Estimated parameters on the connections of Trezói bridge	42
Table 8 - Results from Luiz I bridge stress test connections (Correia, 2014)	42
Table 9 - Estimated parameters on the connections of Luiz I bridge	44
Table 10 – Results from Pinhão bridge stress test connections (Correia, 2014)	44
Table 11 - Estimated parameters on the connections of Pinhão bridge	46
Table 12 – Nominal dimensions of specimens used in fatigue test (Correia, 2014)	51
Table 13 - Material parameters estimated from the stress test results of Viana bridge	54
Table 14 - Material parameters estimated from the stress test results of Fão bridge ($R_{\varepsilon}= 0$)	55
Table 15 - Material parameters estimated from the stress test results of Fão bridge ($R_{\varepsilon}= -1$)	57
Table 16 - Material parameters estimated from the stress test results of Fão bridge ($R_{\varepsilon}=0$ and $R_{\varepsilon}=-1$)	58
Table 17 - Material parameters estimated from the stress test results of Trezói bridge ($R_{\varepsilon}= -1$)	59
Table 18 - Material parameters estimated from the stress test results of Luiz I bridge ($R_{\varepsilon}= -1$)	61
Table 19 - Estimated material parameters to stain test for Viana’s bridge ($R_{\varepsilon}= -1$)	62
Table 20 - Material parameters estimated from the stress test results of Fão bridge ($R_{\varepsilon}= 0$)	64
Table 21 - Material parameters estimated from the stress test results of Fão bridge ($R_{\varepsilon}= -1$)	65
Table 22 - Material parameters estimated from the stress test results of Fão bridge ($R_{\varepsilon}=0$ and $R_{\varepsilon}=-1$)	66
Table 23 - Material parameters estimated from the stress test results of Trezói bridge ($R_{\varepsilon}=-1$)	68

Table 24 - Material parameters estimated from the stress test results of Luiz I bridge ($R_{\varepsilon}=-1$).....	69
Table 25 - Material parameters estimated from the SWT test of Viana bridge ($R_{\varepsilon}=-1$)	70
Table 26 - Material parameters estimated from the SWT test of Fão bridge ($R_{\varepsilon}=0$).....	72
Table 27 - Material parameters estimated from the SWT test of Fão bridge ($R_{\varepsilon}=-1$)	73
Table 28 - Material parameters estimated from the SWT test of Fão bridge ($R_{\varepsilon}=0$ and $R_{\varepsilon}=-1$)	74
Table 29 - Material parameters estimated from the SWT test of Trezói bridge ($R_{\varepsilon}=-1$)	75
Table 30 - Material parameters estimated from the SWT test of Trezói bridge ($R_{\varepsilon}=-1$)	77
Table 31 – Results obtained from Correia’s research; Viana bridge stress test ($R_{\varepsilon}=-1$); (Correia, 2014)	87
Table 32 - Results obtained from Correia’s research; Fão bridge stress test ($R_{\varepsilon}=0$); (Correia, 2014) ..	88
Table 33 – Results obtained from Correia’s research; Fão bridge stress test ($R_{\varepsilon}=-1$); (Correia, 2014)	89
Table 34 – Results obtained from Correia’s research; Fão bridge stress test ($R_{\varepsilon}=0$ and $R_{\varepsilon}=-1$); (Correia, 2014)	90
Table 35 - Results obtained from Correia’s research; Trezói bridge stress test ($R_{\varepsilon}=-1$); (Correia, 2014)	91
Table 36 - Results obtained from Correia’s research; Luiz I bridge stress test ($R_{\varepsilon}=-1$); (Correia, 2014)	91
Table 37 - Results obtained from Correia’s research; Viana bridge strain test ($R_{\varepsilon}=-1$); (Correia, 2014)	92
Table 38 - Results obtained from Correia’s research; Fão bridge strain test ($R_{\varepsilon}=0$); (Correia, 2014) ..	93
Table 39 - Results obtained from Correia’s research; Fão bridge strain test ($R_{\varepsilon}=-1$); (Correia, 2014) ..	93
Table 40 - Results obtained from Correia’s research; Fão bridge strain test ($R_{\varepsilon}=0$ and $R_{\varepsilon}=-1$); (Correia, 2014)	94
Table 41 - Results obtained from Correia’s research; Trezói bridge strain test ($R_{\varepsilon}=-1$); (Correia, 2014)	95
Table 42 - Results obtained from Correia’s research; Luiz I bridge strain test ($R_{\varepsilon}=-1$); (Correia, 2014)	95
Table 43 - Results obtained from Correia’s research; Viana bridge SWT test ($R_{\varepsilon}=-1$); (Correia, 2014)	96
Table 44 - Results obtained from Correia’s research; Fão bridge SWT test ($R_{\varepsilon}=0$); (Correia, 2014) ...	97

Table 45 - Results obtained from Correia's research; Fão bridge SWT test ($R_{\varepsilon}=-1$); (Correia, 2014) .	97
Table 46 - Results obtained from Correia's research; Fão bridge SWT test ($R_{\varepsilon}=0$ and $R_{\varepsilon}=-1$); (Correia, 2014)	98
Table 47 - Results obtained from Correia's research; Trezói bridge SWT test ($R_{\varepsilon}=-1$); (Correia, 2014)	99
Table 48 - Results obtained from Correia's research; Luiz I bridge SWT test ($R_{\varepsilon}=-1$); (Correia, 2014)	99

This page was intentionally left blank.

1 INTRODUCTION

Nowadays, governmental agencies put considerable concern and effort in is the maintenance and safety of historical bridges. Railway and roadway metallic riveted bridges that were put in to service in the last half of the 19th century and beginning of the 20th century are included in this group. These bridges were designed for different traffic conditions than the ones they face today. The type of vehicles (trains, trams, cars, buses, etc), the population and the needs for transportation varied greatly both in mass and in vehicle flow, in a short period in history. Therefore, the loadings on these bridges have changed significantly. Considering this, it is likely that the calculations made at the time of their construction are now obsolete.

At that time, the design engineers did not consider the fatigue phenomenon in structures or more specifically in riveted connections, because the fatigue phenomena were only later studied in the 20th century.

In bridges made of metallic materials, i.e. steel or puddled iron, the fatigue failures relies on the likelihood of deterioration on the metallic material under variable loads. The fatigue phenomenon is the most recognised cause of failure in metallic bridges. Maintenance and retrofitting has to be done periodically in order to avoid the failure of such structures.

Therefore, the residual life calculation of existing bridges in operation should take into account fatigue as a progressive damaging mechanism. A consistent residual life prediction should be based on actual fatigue data from bridge members being assessed.

The verification of the remaining fatigue life of old steel bridges structural relies on details related to the riveted material and the connections. These details have to be identified and categorized. The methods used to analyse the fatigue lifetime in metal structures are described in European, North American and British codes, such as the Eurocode 3, ASTM 739 and BS 5400. The general approach is based on the construction of the S-N curves, where the total number of cycles up to failure is related to the applied stress range. In the existing codes, previously mentioned, there is no method specifically dedicated to the evaluation of riveted connections. Thus, many authors recommend the use of category 71 curve presented in Eurocode 3 for the evaluation of riveted connections. Since the riveted connections may use single shear riveted joints or double shear riveted joints, some authors propose specific S-N curves, based on previously obtained experimental data. The data depends on many factors, such as the properties of the original material and its connections or details to the old bridge under analysis. Therefore, the obtained curves are not always similar to each other.

This thesis develops a statistical approach on the experimental results obtained in fatigue tests previously performed by other authors, in order to obtain characteristic S-N curves for riveted joints from old Portuguese metallic bridges. The results obtained are compared with other models, such as the

ones proposed by Taras and Greiner (Taras & Greiner, 2009) and by Castillo and Fernández- Canteli (Castillo, et al., 2005).

1.1 Objectives

The work performed for this thesis aims to fulfil the following general objectives:

- Review about fatigue phenomena, fatigue design codes (e.g. EC3, AASHTO, and BS5400) and fatigue class catalogue for riveted components proposed by Taras and Greiner.
- Fatigue statistical analysis for structural details and materials using ASTM 739 standard and the probabilistic S-N model proposed by Castillo and Fernández-Canteli;
- Full range fatigue curves assessment for structural details and materials from old metallic bridges and current steels;
- Development of probabilistic fully range fatigue fields using several fatigue damage parameters;

1.2 Thesis organization

This thesis is organized in 5 chapters. It begins with the introduction, Chapter 1, where the main idea of the thesis and the corresponding research approach are presented, together with the objectives that will be followed during the development of the work.

The following chapter, Chapter 2, introduces the historical context in which old riveted metallic bridges were built, including the observations made by the first researcher, Wöhler, who dedicated attention to the fatigue phenomena and the models developed by the researchers that followed him.

The subject of study, the rivets, its principal materials, geometrical characteristics and techniques of implementation in to metallic bridges are also presented. The fatigue phenomenon is explained and the methods and models commonly used for its interpretation, such as the stress-life method and the nominal stress method, are presented. Likewise, the codes and standards used nowadays in the construction of new structures to ensure its safety and prolong life are also addressed. And finally, a more modern approach on the behaviour of riveted connections under fatigue, developed by the researchers Taras and Grainer, is explained.

Chapter 3 describes the old metallic Portuguese bridges in study and how the analysis of their riveted connections was done. It also presents the probabilistic approach used to interpret the resulting experimental data. Furthermore, the development of the Castillo and Fernández-Canteli probabilistic model is explained. This model will be applied in the interpretation of experimental results obtained with riveted connections. The experimental data obtained by Correia (2014) and the development of the probabilistic analysis on riveted connections proposed by this work is introduced. The analysis,

interpretation and comparison of the obtained results is based on the previous method and models presented.

In Chapter 4, the focus is on the fatigue characterization of the materials extracted from old Portuguese bridges. The analysis developed is based on the experimental data collected in the work of Correia (2014). The probabilistic methods and models used in Chapter 3 are now applied to the interpretation of results and comparisons are made on the materials.

The thesis finishes with Chapter 5, with the conclusions of the work.

The Appendix contains the experimental data that generated the analysis developed on Chapter 4.

This page was intentionally left blank.

2 STATE-OF-ART

This thesis addresses the study of fatigue in metallic elements, more specifically, the fatigue on riveted connections of historical metal bridges. In this type of structures, it has been observed that the location of critical fatigue is in the riveted connections.

Fatigue is one of the main forms of damage and failure in a metal structure. Despite many studies addressing fatigue phenomena in metallic structures, this is still a subject that needs more study. Fatigue is also poorly understood in terms of formation and failure mechanism. (ASM, 2008)

2.1 Historical Point of View

Metal structures have been built since the beginning of the 19th century, mainly in the format of bridges. The use of metallic materials allowed designers to reach larger spans.

Connections are rather important elements in the construction of metallic bridges. During the 19th century and the first half of the 20th century, these connections were first achieved with the use of rivets.

The first known study on fatigue was developed in 1837, by August Wöhler, a technologist in the German railroad system. Wöhler observed that there was failure in the railroad axes after several hours of service, when these were subjected to considerably lower loads than the static load capacity of the structures. From these observations, Wöhler performed the first systematic study of fatigue with the aid of laboratory tests on fatigue under cyclical stresses (X. W. Ye, 2014). Following Wöhler, came Rankine in 1842, that argued about the fatigue strength of railway axles. Afterwards, in 1853, Morin discussed on the safe life design to be adopted in axles of horse-drawn mail coaches. In 1854, Braithwaite was the first to utilize the term “fatigue” that was presented in his paper about fatigue failures in machinery equipment and a discussion in admissible stresses for fatigue loaded components (Correia, 2014).

Between the years of 1858 and 1870, the German technologist August Wöhler, conducted many experiments in railways axles. His work led to the design and construction of the first testing machines. Wöhler noticed the influence of the stress amplitude on fatigue damage. His experimental data was presented by his successor Spangenberg. (Correia, 2014)

Spangenberg, was the one who presented the S-N curve, that is, the graphical representation of the fatigue in form of curves. (Correia, 2014)

In the period between 1870 and 1950, Coffin and Manson, were able to comprehend the cyclic plasticity of metals that is the base of low cycle fatigue. The Coffin-Manson law emphasizes the fatigue ductility exponent for experimental data. The law describes the uniaxial and cyclical load by relating the plastic amplitude to cycle number of fracture. The test based in the Coffin-Manson law will be defined by the metal composition, the temperatures conditions which it is found and the range of amplitude values that its desire to investigate (Tirbonod, 2015). In 1903 Ewing and Humfrey noticed the existence

of slip bands on surfaces of rotating-bending specimens, which promoted the first metallurgical definition on the fatigue process. (Correia, 2014)

The first large scale fatigue tests were performed between the periods of 1905 and 1920, in aircraft components. The tests were executed to improve the fatigue strength of these elements. (Correia, 2014)

In beginning the 20th century, it was observed that the repetitive loading and unloading application may cause the mechanism of fatigue, leading to nucleation of microcracks, crack growth, and consequently to complete failure of the structure (X. W. Ye, 2014).

Investigation on variable amplitude was done by Gassner and theories of damage accumulation were developed by Palmgren and Miner, leading to the linear damage accumulation theory. Forest performed the first crack propagation tests. Weibull developed the statistical methods to evaluate the strength of the material. Müller-Stock established the methodology to perform statistical evaluation on a large number of fatigue experiments. These advances took place between 1920 and 1945 (Correia, 2014).

During the years of 1945 to 1960, Coffin and Manson established the foundations of low cycle fatigue. Their work was encouraged by the aircraft industry. Still during this period, Miner's rule was vastly investigated and debated, and proposals were made to overcome the limitations of the linear damage rule. Based in Griffith works, Irwin comprehend that the stress intensity factor (K is the stress intensity factor used in fracture mechanism to predict the crack propagation and fracture strength) was the main parameter to control the static strength of a cracked body, leading him to develop the linear elastic fracture mechanics (Correia, 2014). The stress intensity factor is used in fracture mechanisms to predict the crack propagation and the fracture strength. (Jr & Raju, 1986)

Posteriorly to 1960, fracture mechanics got its development in the application to fatigue. Paris was one of the first to perceive the relation between fracture mechanics and fatigue. The association was given the name of Paris relation, and afterwards many proposals have been presented to surpass the limitation found in the Paris relation. The Paris equation relates the stress intensity with a critical crack growth when a load is applied. The fatigue crack growth under variable amplitude loading was proposed by Elber, leading to the "crack closure" concept. (Correia, 2014)

2.2 The Rivet

The rivet is composed of the rivet head (or shop head) - the rounded segment, and the rivet shank - the elongated segment. The most common rivet used in structural applications has a rounded head, as presented in Figure 1.

The main materials used to fabricate rivets were cast iron, during the periods of 1780 to 1850, wrought iron, between 1850 and 1900, and finally steel from around 1880 to nowadays. This material, or type of metal components, has specific characteristics. Cast iron is very strong when submitted to

compression stresses, but becomes brittle or weak when exposed to tensile stresses. Wrought iron is resistant when submitted to tensile strength and is also ductile in compression. Steel is a strong material, but it is not as resistant to corrosion as wrought iron (Lindenberg, 2016).

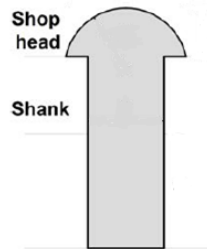


Figure 1 - Representation of a rivet (Collette Q. , 2014)

The manufacture of a rivet can be done manually or mechanically in a shop or at a job site, with the application of a hot or a cold technique, (Collette Q. , 2014). Figure 2 presents the common processes adopted in the production of rivets.

	Cast iron	Wrought steel Puddled steel	Mild steel (19th century)	Mild steel (20th century)
Produced since	1709 (Abraham Darby I.)	1784 (Henry Cort)	Blast process 1855 Bessemer steel (Henry Bessemer) 1879 Thomas steel (Sidney G. Thomas) Hearth process 1865 Siemens-Martin steel (Friedrich u. Wilhelm Siemens, Pierre u. Emile Martin)	
Produced till	today	≈ 1900	≈ 1900 Bessemer steel in steel structures ≈ 1980 Thomas steel, ≈ 1990 Siemens-Martin steel	
Producing process	Re-melting pig iron by means of coke and cleaning	1. Puddling process: Conversion of pig iron into steel by stirring in a pasty state carried out in a reverberatory furnace → puddle balls 2. Mechanical slag removal and welding together of lumps of steel by means of a steam hammer or squeezer → blooms 3. In the following years further treatment by heating and rolling in a rolling mill → muck bars	Bessemer process Air-refining process in which low-phosphorus pig iron is converted into liquid steel in the Bessemer converter consisting of an acid lining by blowing air through the molten pig iron → excess carbon and impurities, such as silicon and manganese, are oxidised → acid Bessemer steel Thomas process Same process as Bessemer process but also for high-phosphorus pig iron which is possible by a basic lining based on dolomite (Thomas converter) → basic Thomas steel Siemens-Martin process Allothermic hearth process, in which pig iron with or without steel scrap and/or iron ore is melted in the Siemens regenerative furnace → excess carbon and impurities are burnt out → basic Siemens-Martin steel	

Figure 2 - Common processes adopted in the production of rivets (Lindenberg, 2016)

In the end of 19th century, rivets were designed, firstly considering that the thickness of the plates, e , had approximately 6,3 mm but it was projected according to the needs presented by the project. The rivet shank diameter, d , was calculated based on the d/e ratio. The shank diameter was around 16,0 mm (Figure 3). (Collette, Sire, & Wouters, 2014)

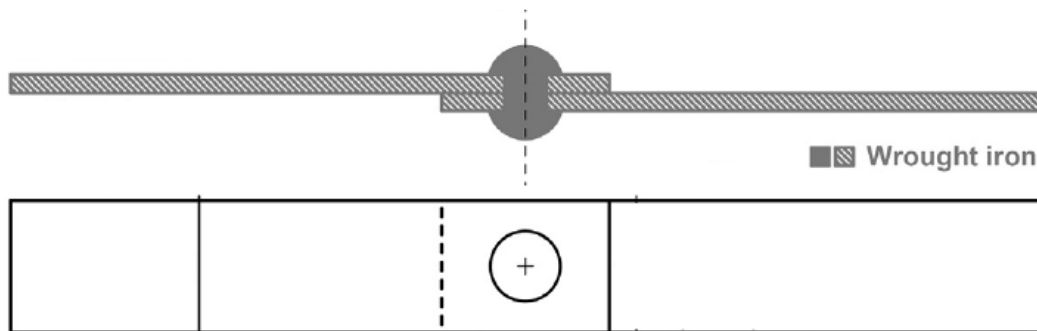


Figure 3 - Elevation and plan views of a riveted specimen (Collette, Sire, & Wouters, 2014)

Rivets can be installed with different techniques: hot-riveting or cold-riveting. The hot-riveting technique consists on installing the rivet when the metal is heated to high temperatures. This technique has introduced by the boiler market (Lindenberg, 2016). The application of the technique is done in three steps: first, a hole is made in the plates, so that all the pieces can be fastened together. After the plates are securely fastened together, holes are drilled with the correct size for the rivet installation and the rivet stoker places the rivet at a high temperature. It was not possible to know the temperature of the specimen or a method that involved time waiting to obtain the desired temperature and therefore because there was not an available method to do so. Therefore, the temperature and the time needed were not very accurate. When the rivet reaches a white-hot color and a glossy appearance or when the redness of the metal is visible, the rivets are ready for installation (Collette, Sire, & Wouters, 2014). The rivet was passed to the rivet catcher, who was responsible for positioning the hot rivet on its final place and with the help of tongs (Collette Q. , 2014). The final step was the driving of the rivet, positioning the rivet shank in the rivet hole (Figure 4). Because of the heat propagated by the rivet, the shank expands until the hole is filled, ensuring a secure fit, that is fundamental to a structure that is submitted to cyclical loading. When the rivet cools down, it shrinks and everything is hold together (Lindenberg, 2016). The group of men able to install the hot-rivets was composed by the rivet stoker, rivet passer, rivet catcher and the holder-on (Figure 5). (Collette Q. , 2014)

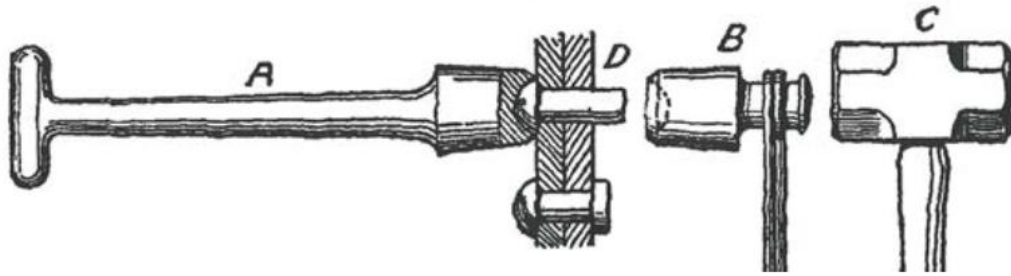


Figure 4 - Representation of the tools used to the positioning and installation of the rivets (Collette Q. , 2014)

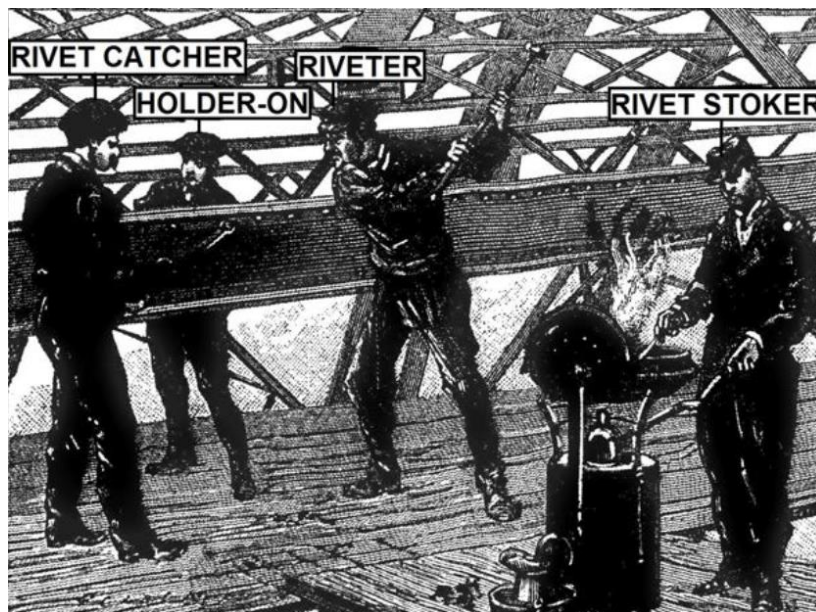


Figure 5 - Group of men responsible for the hot-riveting installation (Collette Q. , 2014)

Hot-riveting has an advantage over cold-riveting. The cold-riveting technique works by the frictional strength given by the cooling of the rivet that provides the connection with some lateral compression, clamping force, pressing the plates and rivet together (Collette Q. , 2014). The hammering of the cold rivets puts it in its final position on the structure. (Deng & Hutchinson, 1998)

Nowadays, the use of hot-riveting or cold-riveting is expensive and time consuming. That is why most rivets are substituted by bolts (Collette Q. , 2014).

2.3 The Fatigue Phenomenon

Primarily, one must understand what fatigue is. According to the Oxford English dictionary the fatigue phenomena is a weakness in metal or other materials caused by repeated variations of stress (Oxford Dictionarie, 2013). On a more scientific approach, fatigue is a physical phenomenon that occurs due to the application of varying stress that is lower than the stress required to cause failure in one

single application of stress. The phenomenon can affect any part of the structure that is subjected to cyclic loading (ASM, 2008).

The fatigue mechanism is a phenomenon not yet completely understood. To understand the mechanism of fatigue, it is necessary to consider several factors that affect fatigue life and fatigue crack growth, like the material surface quality, the residual stress and the environmental influence (X. W. Ye, 2014).

It is understood that cracks are formed due to fatigue, that is, repetitive application of loads over a long period of time and repetitive cycles (X. W. Ye, 2014). The fatigue phenomenon consists in three periods: the initiation period, the crack growth and the failure itself (Figure 6). (Lindenberg, 2016)

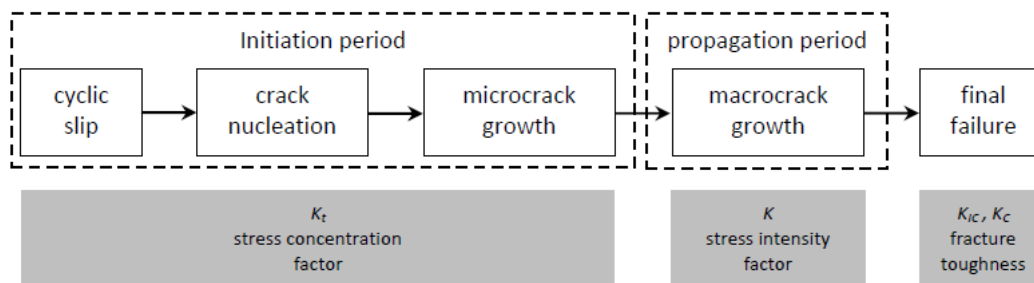


Figure 6 - Three period of the fatigue life (Correia, 2014)

Normally, fatigue begins at a geometrical discontinuity in the structure, for example a notch or rivet hole, causing a stress concentration region that is susceptible to crack initiation, hence, influencing the fatigue performance. The failure commonly happens in the region where there is tension. As a result of the stress, the growth of the crack leads to the reduction of the cross section which becomes insufficient to carry the load without failure. Usually the crack starts with a micro-crack growing to a single crack, and then a prevalent macro-crack that develops perpendicularly to the tensile stress. (Lindenberg, 2016)

The shear crack on a crystallographic slip plan (Figure 7), and the back-and-forth movement, leads to the formation of intrusions and extrusions, called as the initiation of the cracking phenomena (Stage I) (ASM, 2008) and (X. W. Ye, 2014)). The crack formation propagates from the plastic deformation to a macroscopic size crack perpendicularly to the applied load (Stage II) (X. W. Ye, 2014). Failure develops itself when the crack becomes deep enough, so that the section can no longer support the load applied (Stage III) (ASM, 2008).

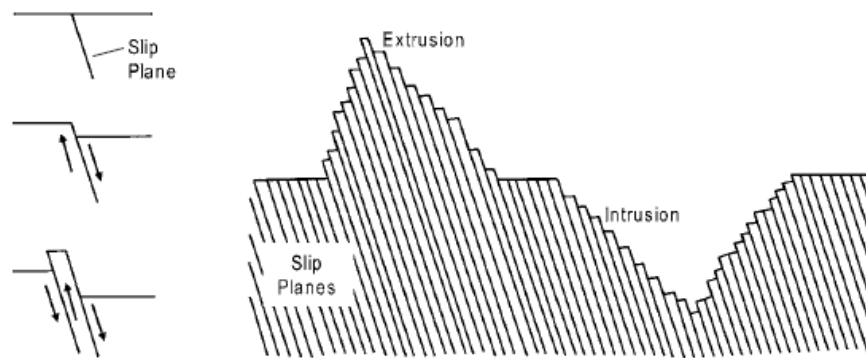


Figure 7 - Representation of the sliding movement of the slip plans (ASM, 2008)

The initiation of the crack happens mostly in steel components, during the fatigue life. Specially in the high-cycle fatigue regime, structures submitted to more than 10.000 cycles and application of elastic stress (X. W. Ye, 2014). Despite the applied stress is low, plastic deformation can occur at the crack tip. In the low-cycle fatigue (less than 10.000 cycles), the fatigue life is spent in crack propagation. (X. W. Ye, 2014). High-cycle and low-cycle fatigue methods data are normally reproduced in graphics where the stress-life is represented (ASM, 2008).

The fatigue phenomenon can be analyzed with two different approaches: the stress-life (S - N curve) method and the strain-life (ϵ - N) method.

2.4 Methods that consider the Fatigue Life

2.4.1 Stress-Life Method or S-N Curve

The stress-life method or S-N curve is used to study high-cycle fatigue and long-life prediction when the stress and the strain loads possess elastic characteristics. It is aimed to study the life of a structure and does not distinguish the beginning or the propagation of the crack. The method establishes the relation between the stress range and the number of cycles up to failure, represented in a S-N curve. The stress variation can be the difference between the maximum and the minimum stress or the stress amplitude. (X. W. Ye, 2014)

Various S-N curves are used to classify the fatigue resistance of different details based on their geometry. Each S-N curve has a category with similar fatigue strength, such as transverse butt welds, cover planted beams, longitudinal welds, etc. (Robert J. Dexter, 2013)

The categories of the curves are divided in:

- Category 1: compression and bending members, built-up members in tension; continuous connections between flange angles and web plates, or cover plates and flange;
- Category 2: joints in trusses using gusset plates;
- Category 3: tension splices with symmetrical splice plate assembly;

- Category 4a: connections of bracing elements to tension flanges of members submitted to bending;
- Category 4b: onset of cover plates in built-up bending members (Taras & Greiner, 2009)

2.4.2 Nominal Stress Method

The nominal stress method is the simplest and most commonly used method for the estimation of fatigue life in steel bridges. The method includes a global observation of the phenomenon on the structure and then in a particular segment of the structure (X. W. Ye, 2014). The nominal stress method determines the fatigue resistance and the applied load, through calculation, supported by the nominal stress near the detail (Lindenberg, 2016).

2.5 Codes related to Fatigue Calculation

There are three main codes that will be mentioned in this study:

- European Code - Eurocode 3 (EC 3), mostly used in the countries belonging to the European Union and other Europeans countries that do not belong to the Europeans Union (e.g. Macedonia, Croatia, etc.), with the exception of British countries.
- United States of America Code: ASTM, code followed and developed in the United States of America. Many countries rely on the studies developed for ASTM to develop their own national codes.
- British Code: BS, code followed by British countries.

2.5.1 Eurocode 3

The EC 3 - Part 1-9 says that fatigue should be calculated taking into account the S-N curve (previously explained in section 2.4.1), and the safe life method should be satisfactory for the structure safety without the need for regular inspection. The safe life method has to be applied in situations in which a component presents crack formation and such crack may lead to a quick structure failure or a structural component failure.

The fatigue assessments methods exhibited in EC 3 - Part 1-9 use the fatigue resistance in terms of fatigue strength curves for nominal stresses. To be able to achieve the required reliability, the EC 3 - Part 1-9 proposes two methods: the damage tolerant method and the safe-life method. The damage tolerant method recommends a good selection of materials, details and stress levels so that cracks in the material can be avoided, or if the crack is formed, the crack formation is retarded. Hence, to the safe-life method, the good selection of details and materials would result in a high enough value of fatigue life, that is at least equal to the one required for an ultimate limit state verification. The limit state of a structure is the moment when the structure no longer resists the loading and no longer fulfils the original design.

All calculations must be performed at the serviceability limit state. The calculation of the nominal stresses (direct stress or shear stress) is carried out by the calculation of the potential moment of fatigue initiation. The resultant possible stress effects in the details or connection, such as the rivets, are shown in Figure 8, Figure 9 and Figure 10. The ones not included in those figures should use the stress concentration factor (SCF). The SCF is calculated with Equations (1) and (2),

$$\gamma_{Ff} \Delta\sigma_{E,2} = k_f \times \lambda_1 \times \lambda_2 \times \lambda_i \times \dots \times \lambda_n \times \Delta\sigma (\gamma_{Ff} Q_k) \quad (1)$$

$$\gamma_{Ff} \Delta\tau_{E,2} = k_f \times \lambda_1 \times \lambda_2 \times \lambda_i \times \dots \times \lambda_n \times \Delta\tau (\gamma_{Ff} Q_k) \quad (2)$$

where,

γ_{Ff} is the partial factor for equivalent constant amplitude stress ranges $\Delta\sigma_E$, $\Delta\tau_E$ (equivalent constant amplitude stress range related to n_{max});

$\Delta\sigma_{E,2}$ and $\Delta\tau_{E,2}$ are equivalent constant amplitude stress range related to 2 million cycles;

λ_i is the damage equivalent factor;

Q_k is characteristic value of a single variable action;

k_f is the stress concentration factor to take into account the local stress magnification in relation to detail geometry not included in the reference $\Delta\sigma_R$ -N-curve or (S-N curve).

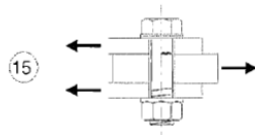
Detail category	Constructional detail	Description	Requirements
100 m=5		<u>Bolts in single or double shear</u> Thread not in the shear plane 15) - Fitted bolts - normal bolts without load reversal (bolts of grade 5.6, 8.8 or 10.9)	15) $\Delta\tau$ calculated on the shank area of the bolt.

Figure 8 - Example of plain members and mechanically fastened joints (EUROPEAN STANDARD, 2005)

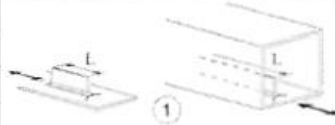




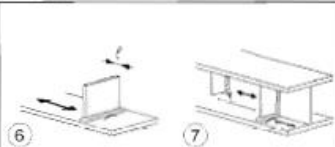
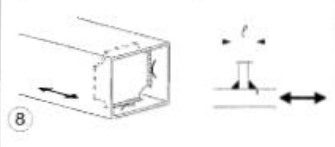
Detail category	Constructional detail	Description	Requirements
80	$L \leq 50\text{mm}$	 <p>1) The detail category varies according to the length of the attachment L.</p>	The thickness of the attachment must be less than its height. If not see Table 8.5, details 5 or 6.
71	$50 < L \leq 80\text{mm}$		
63	$80 < L \leq 100\text{mm}$		
56	$L > 100\text{mm}$		
71	$L > 100\text{mm}$ $\alpha < 45^\circ$	 <p>2) Longitudinal attachments to plate or tube.</p>	
80	$r > 150\text{mm}$	 <p>3) Longitudinal fillet welded gusset with radius transition to plate or tube; end of fillet weld reinforced (full penetration); length of reinforced weld $> r$.</p>	<u>Details 3) and 4):</u> Smooth transition radius r formed by initially machining or gas cutting the gusset plate before welding, then subsequently grinding the weld area parallel to the direction of the arrow so that the transverse weld toe is fully removed.
90	$\frac{r}{t} \geq \frac{1}{3}$ or $r > 150\text{mm}$	 <p>4) Gusset plate, welded to the edge of a plate or beam flange.</p>	
71	$\frac{1}{6} \leq \frac{r}{t} \leq \frac{1}{3}$		
50	$\frac{r}{t} < \frac{1}{6}$		
40	 <p>5) As welded, no radius transition.</p>		
80	$l \leq 50\text{mm}$	 <p>6) Welded to plate.</p>  <p>7) Vertical stiffeners welded to a beam or plate girder.</p> <p>8) Diaphragm of box girders welded to the flange or the web. May not be possible for small hollow sections. The values are also valid for ring stiffeners.</p>	<u>Details 6) and 7):</u> Ends of welds to be carefully ground to remove any undercut that may be present. 7) $\Delta\sigma$ to be calculated using principal stresses if the stiffener terminates in the web, see left side.
71	$50 < l \leq 80\text{mm}$		
80			

Figure 9 – Example of attachments and stiffeners (EUROPEAN STANDARD, 2005)

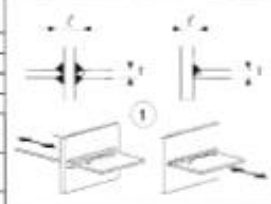
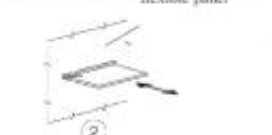

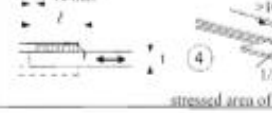







Detail category	Constructional detail		Description	Requirements
80	$t < 50$ mm	all t [mm]	 <p>Cracks in form and Tee joints.</p> <p>1) Toe failure in full penetration butt welds and all partial penetration joints.</p>	<p>1) Inspected and found free from discontinuities and misalignments outside the tolerances of EN 1090.</p> <p>2) For computing $\Delta\sigma$, use modified nominal stress.</p> <p>3) In partial penetration joints two fatigue assessments are required. Firstly, root cracking evaluated according to stresses defined in section 5, using category 36* for $\Delta\sigma_r$ and category 80 for $\Delta\sigma_t$. Secondly, toe cracking is evaluated by determining $\Delta\sigma$ in the load-carrying plate.</p>
71	$50 < t \leq 80$	all t		
63	$80 < t \leq 100$	all t		
56	$100 < t \leq 120$	all t		
56	$t > 120$	$t \leq 20$		
50	$120 < t \leq 200$	$t > 20$		
45	$200 < t \leq 300$	$t > 30$		
40	$t > 300$	$t > 50$		
As detail 1 in Table 8.5	flexible panel		 <p>2) Toe failure from edge of attachment to plate, with stress peaks at weld ends due to local plate deformations.</p>	<p>Details 1) to 3).</p> <p>The misalignment of the load-carrying plates should not exceed 15 % of the thickness of the intermediate plate.</p>
36*	 <p>3) Root failure in partial penetration Tee-butt joints or fillet welded joint and in Tee-butt weld, according to Figure 4.6 in EN 1993-1-8:2005 (5).</p>			
As detail 1 in Table 8.5	 <p>4) Fillet welded lap joint.</p> <p>stressed area of main panel: $a_{\text{along}} = 1/2$</p>		<p>4) $\Delta\sigma$ in the main plate to be calculated on the basis of area shown in the sketch.</p> <p>5) $\Delta\sigma$ to be calculated in the overlapping plates.</p>	
45*	 <p>5) Fillet welded lap joint.</p>		<p>Details 4) and 5):</p> <ul style="list-style-type: none"> -Weld terminations more than 10 mm from plate edge. -Shear cracking in the weld should be checked using detail 8). 	
56*	$L < 3$	$L \geq 3$	 <p>Cover plates in beams and plate girders.</p> <p>6) End zones of single or multiple welded cover plates, with or without transverse end weld.</p>	<p>6) If the cover plate is wider than the flange, a transverse end weld is needed. This weld should be carefully ground to remove undercut.</p> <p>The minimum length of the cover plate is 300 mm. For shorter attachments size effect see detail 1).</p>
50	$t \leq 20$	$t \leq 20$		
45	$20 < t \leq 30$	$t \leq 20$		
40	$t > 30$	$30 < t \leq 50$		
36	-	$t > 50$		
56	 <p>7) Cover plates in beams and plate girders.</p> <p>7) Transverse end weld ground flush. In addition, if $t > 20$ mm, front of plate at the end ground with a slope < 1 in 4.</p>			
80	 <p>8) Continuous fillet welds transmitting a shear flow, such as web to flange welds in plate girders.</p> <p>9) Fillet welded lap joint.</p>		<p>8) $\Delta\sigma$ to be calculated from the weld throat area.</p> <p>9) $\Delta\sigma$ to be calculated from the weld throat area considering the total length of the weld. Weld terminations more than 10 mm from the plate edge, see also 4) and 5) above.</p>	
see EN 1994-2 (90 m ³)	 <p>10) For composite application</p>		<p>10) $\Delta\sigma$ to be calculated from the nominal cross section of the stud.</p>	
71	 <p>11) Tube socket joint with 80% full penetration butt welds.</p>		<p>11) Weld toe ground. $\Delta\sigma$ computed in tube.</p>	
40	 <p>12) Tube socket joint with fillet welds.</p>		<p>12) $\Delta\sigma$ computed in tube.</p>	

Figure 10 - Example of load carrying joints (EUROPEAN STANDARD, 2005)

In the calculation of the fatigue strength, the nominal stress ranges are defined according to the corresponding S-N curve, as presented in section 2.4.1. The S-N curve corresponds to a specific category that is defined for each type of connection or detail.

For constant amplitude nominal stress ranges, the fatigue strength can be obtained with equations (3) to (6).

$$\Delta\sigma_R^m N_R = \Delta\sigma_C^m 2x10^6 \text{ with } m = 3 \text{ for } N \leq 5x10^6 \text{ observe Figure 11} \quad (3).$$

$$\Delta\tau_R^m N_R = \Delta\tau_C^m 2x10^6 \text{ with } m = 5 \text{ for } N \leq 10^8 \text{ observe Figure 12.} \quad (4)$$

$$\Delta\sigma_D = \left(\frac{2}{5}\right)^{1/3} \Delta\sigma_C = 0,737 \Delta\sigma_C \text{ observe Figure 11} \quad (5)$$

$$\Delta\tau_L = \left(\frac{2}{100}\right)^{1/5} \Delta\tau_C = 0,457 \Delta\tau_C \text{ is the cut off limit, observe Figure 11} \quad (6)$$

For nominal stress spectra with stress ranges above and below the constant amplitude fatigue limit $\Delta\sigma_D$, the fatigue strength is based on the extended fatigue strength curves, according to equations (7) to (9),

$$\Delta\sigma_R^m N_R = \Delta\sigma_C^m 2x10^6 \text{ with } m = 3 \text{ for } N \leq 5x10^6 \quad (7)$$

$$\Delta\sigma_R^m N_R = \Delta\sigma_D^m 5x10^6 \text{ with } m = 5 \text{ for } 5x10^6 \leq N \leq 10^8 \quad (8)$$

$$\Delta\sigma_L = \left(\frac{5}{100}\right)^{1/5} \Delta\sigma_D = 0,549 \Delta\sigma_D \text{ is the cut off limit, observed in Figure 11} \quad (9),$$

where,

m is the slope of fatigue strength curve.

N_R is the design life time expressed as the number of cycles related to a constant stress range.

$\Delta\sigma_D$ is the fatigue limit for constant amplitude stress range at the number of cycles N_D .

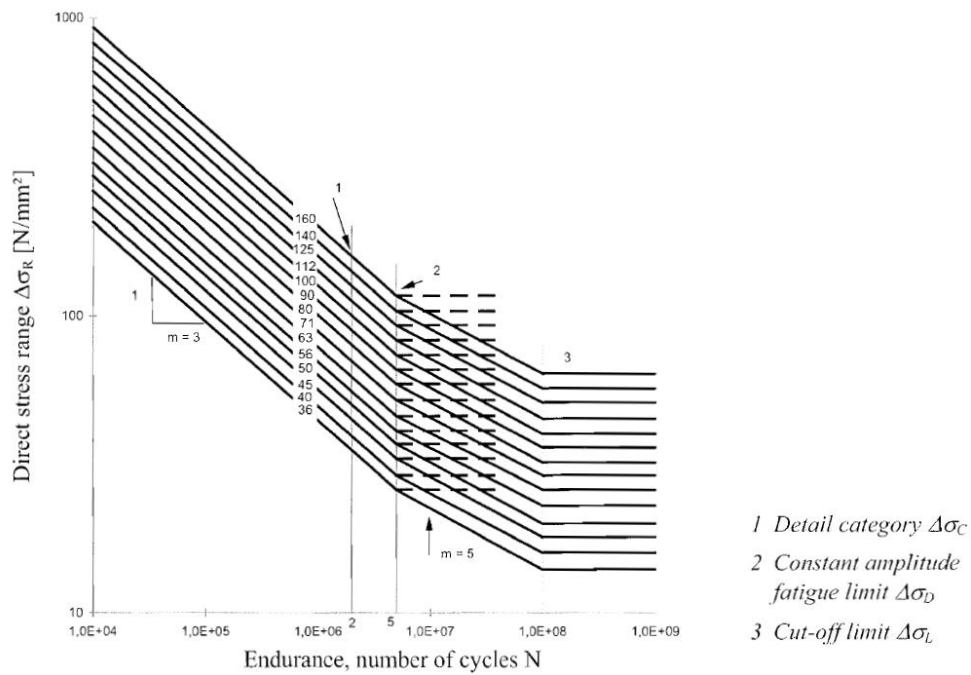


Figure 11 – Fatigue strength curves for normal stress ranges (EUROPEAN STANDARD, 2005)

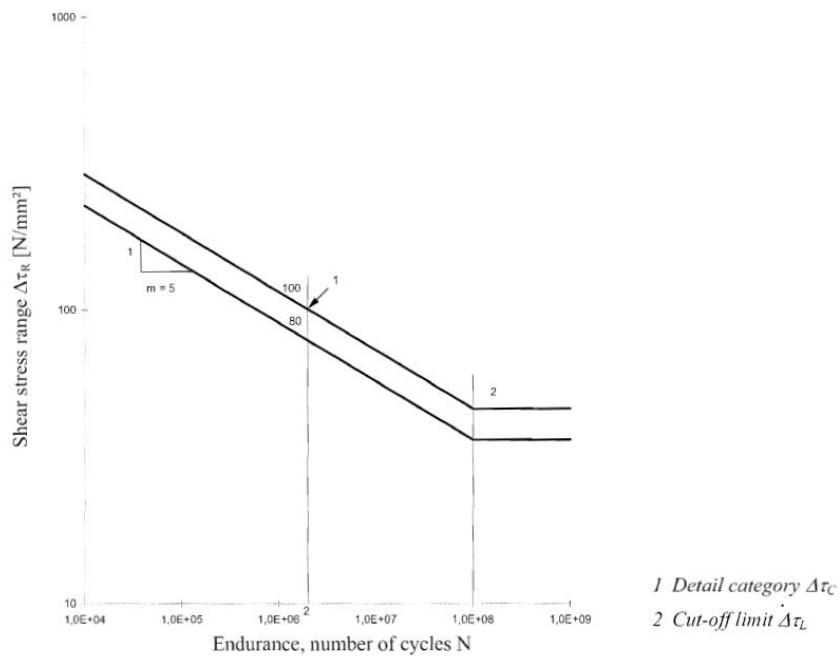


Figure 12 - Fatigue strength curve for shear stress ranges (EUROPEAN STANDARD, 2005)

Experimental tests were performed in order to establish the parameters presented in Figure 11 and Figure 12. The value of the stress range $\Delta\sigma_C$ is due to a number of cycles, N_C , that is equal to two million

cycles, and calculated at a confidence level of 75% with a 95% log N probability, by considering the standard deviation, the size of the sample and the effects of residual stress.

2.5.2 ASTM E 793 -91

The ASTM E 793-91 code considers the calculation of the S-N curve (due to the stress) and ϵ -N curve (due to strain) (Figure 13). The method in the code is applied to linearized curves. Equations (10) to (13) reflect this idea.

$$\log N = A + B(S) \quad (10)$$

or

$$\log N = A + B(\epsilon) \quad (11)$$

or

$$\log N = A + B(\log S) \quad (12)$$

or

$$\log N = A + B(\log \epsilon) \quad (13)$$

where S and ϵ can correspond to the maximum or the minimum value of the amplitude of stress or strain, in one cycle, maintained constant with a specific value of its ratio, or a constant amplitude for a specific value of an average stress or strain value, or similar information stated in appropriate independent variable. In case of uncertainty in the S and ϵ values, an equivalent value has to be adopted in the analysis. (ASTM E739-91, 2004)

In the ASTM code, the fatigue life is considered an unknown and complex distribution. Therefore, to simplify the analysis, it is assumed that the variance of log N is continue through the entire extension of the independent variable used in the test, which can be adopted as X. The independent variable can be S or ϵ , or its respective logarithmic values, depending on which one is going to produce a straight-line plot to the interest value. The log N value is utilized as the random dependent variable in the analysis, and is adopted as Y. (ASTM E739-91, 2004)

$$Y = A + BX \quad (14)$$

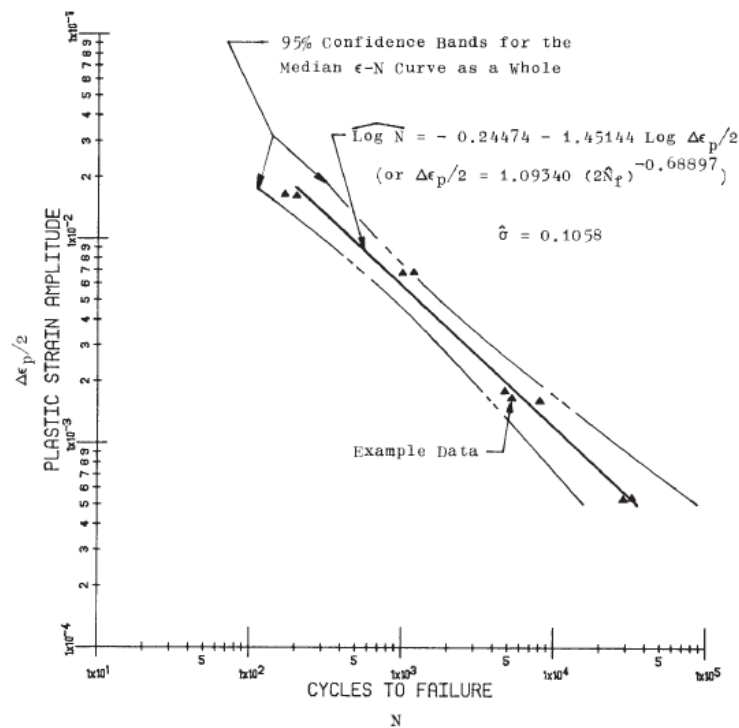


Figure 13 – Example of Fatigue Life N (Y) vs. Plastic Strain Amplitude $\Delta \epsilon/2$ (X) (ASTM E739-91, 2004)

2.5.3 British Code - BS 5400

In the British Code, BS 5400 (BRITISH STANDARD, 1980), the calculations of fatigue life are carried out by considering two methods: the assessment without damage and the assessment with damage.

In the method of assessment without damage, the value of the maximum range of stress for a specific use or design life is delimited. The method is only used in the conditions presented on Figure 14.

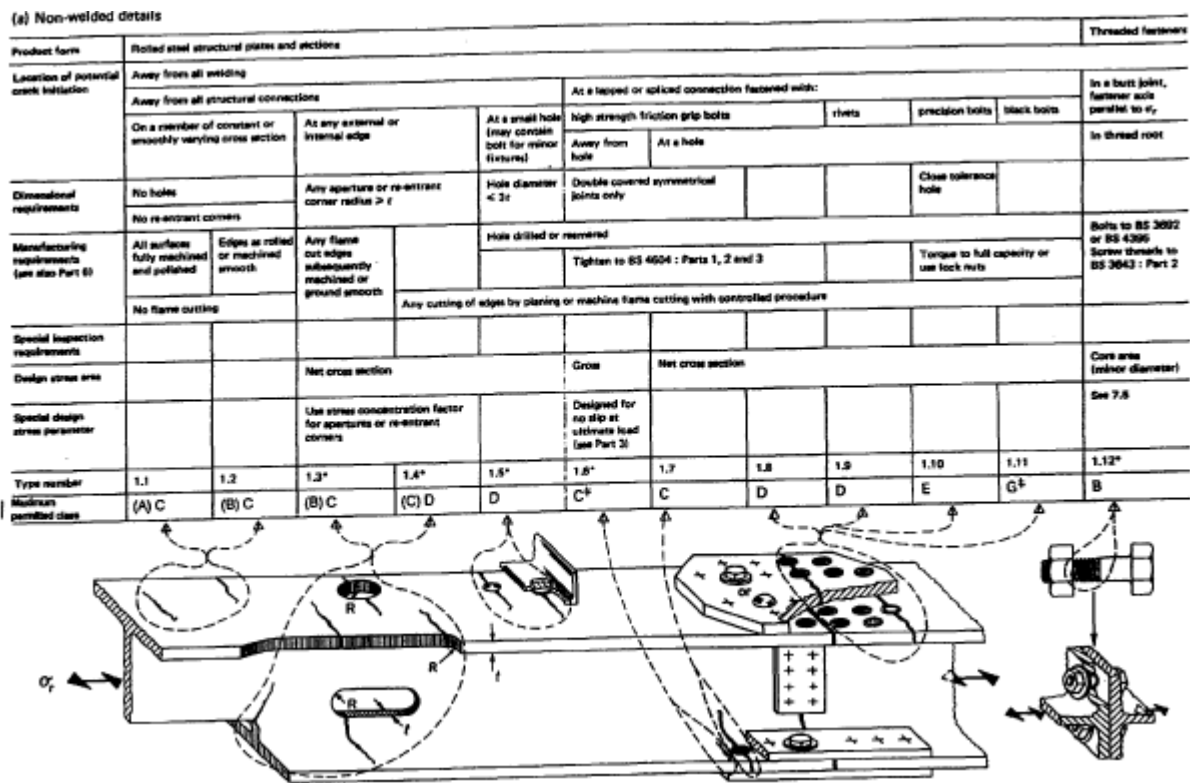


Figure 14 – Classification of non-welding components used in the calculation of fatigue life

In this code, if the effective stress is in the compressive zone for non-welded members or details, the effects of the fatigue loading can be ignored. In the assessment with damage, the Miner's theory for damage accumulation can be used in any component for which the S-N curve is known.

2.5.4 Taras and Greiner approach

The authors Taras and Greiner (Taras & Greiner, 2009) noted the lack of studies and knowledge on the fatigue behavior of riveted structures. The main issue observed by the authors was the insufficiency of recommendations in the specific case of riveted structures, as many codes are very focused in welded connections, but not in riveted connections. So, a research was developed, gathering the interests and funds of private companies. It resulted in a new interpretation of the fatigue phenomenon in rivets.

For the development of the study, the authors used test data related to fatigue that was internationally available. The classification was done according to the detail of the structure and a statistical evaluation of the collected data.

The categorization of the data helped to provide more consistent results, even for the case of common detail categories, by defining more useful assessment lines than the lower-bound ones. This

approach led the research to develop a fatigue class catalogue that could be integrated in the existing procedures reported in literature.

According to the authors, the fatigue line 71 found on the EC 3 – Part 1-9 and displayed in Figure 15, is the curve with the highest stress range for the fatigue life assessment of rivets. The results obtained showed that this S-N curve line represents a lower boundary of the tests results. The line denominated as line 100 (RL805) is applicable to rivets and connections that were produced in steel after 1900. After many tests, it was concluded that the materials were not safe when the safety factors were applied.

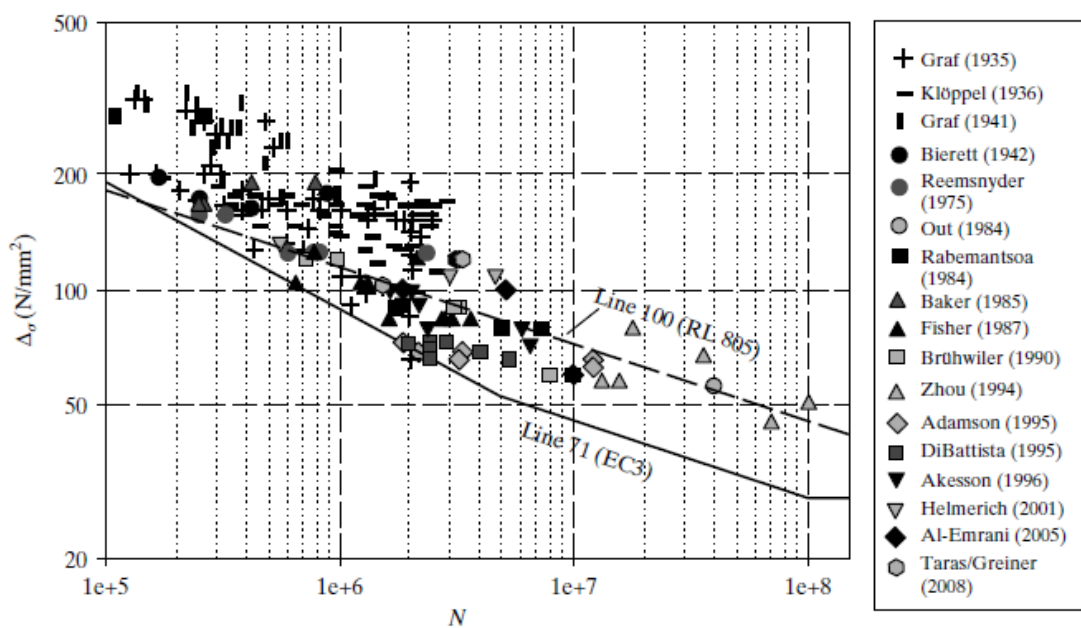


Figure 15 – S-N curve result from Taras and Greiner research (Taras & Greiner, 2009)

It was concluded that the line 71, presented on EC 3 – Part 1-9, is a good approximation to the lower bound, but not necessarily is the ideal detail to apply to a rivet component, because of its behavior in the high cycle range.

The authors also observed the non-consideration of the stress ratio (R) in the curve presented in EC 3 – Part 1-9, since such curve was designed for welded connections with high tensile residual stress. But, it is known that in non-welding connections or structure, the level of R influences the fatigue strength. After an extended research on the Eurocode and RL 805 specification of the German Federal Railways, it was observed that only a small quantity of fatigue tests was performed with the intention of relating the stress ratio and the fatigue strength. Therefore, the ratios could not be determined with absolute certainty, based on the available tests. Thus, a decision was made with the objective of a statistical evaluation, and the values given in Figure 16 were adopted.

Wrought iron and mild steel of before 1900	
$R < 0,0/R \geq -1,0$	$R \geq 0,0$
$f(R) = \frac{1 - R}{1 - 0,70 \times R}$	$f(R) = \frac{1 - R}{1 - 0,75 \times R}$
Mild steel post-1900, St37, St48, St52, etc.	
$R < 0,0/R \geq -1,0$	$R \geq 0,0$
$f(R) = \frac{1 - R}{1 - 0,40 \times R}$	$f(R) = \frac{1 - R}{1 - 0,60 \times R}$

Figure 16 - Increase or reduction of fatigue strength, as function of the stress ratio (Taras & Greiner, 2009)

To study the potential pre-damage in the specimens, components were separated in categories, and such categories were also considered in the statistical evaluation presented in Figure 15. The most important categories are the same as previously quoted in section 2.4.1: category 1 to category 4b (Figure 17).

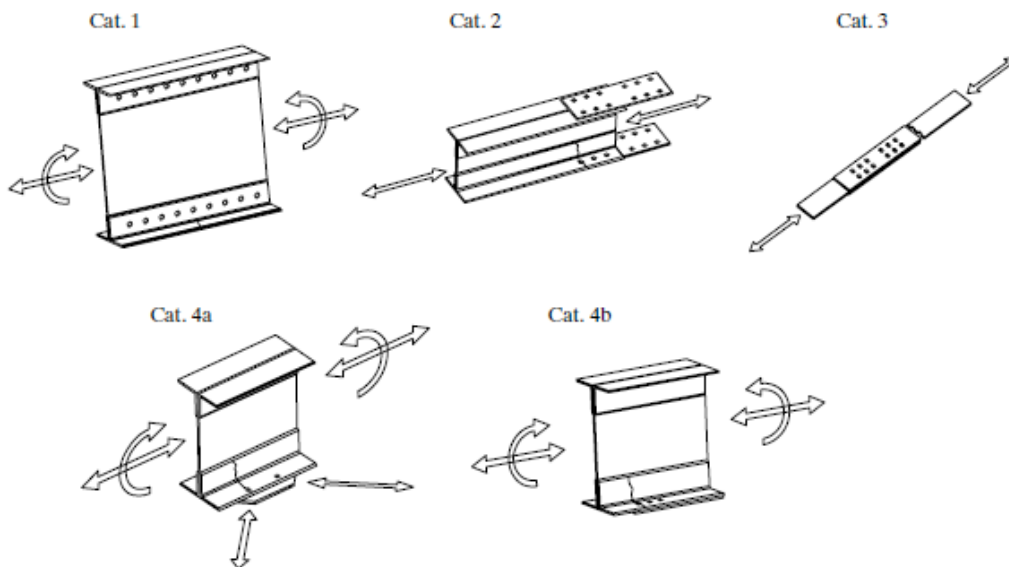


Figure 17 – Most important categories for the statistical evaluation (Taras & Greiner, 2009)

The statistical evaluation of the test data in some specimens may lead to error. In certain situations, the specimen in study was not taken to its failure, which means that means a higher number of load cycles could be achieved by the specimen. The method of maximum likelihood estimation (MLE) is applied to solve this error, where the variational maximization of parameters is used to determine the likelihood of occurrence of the data. When used to study fatigue, the method determines the S-N curve describing the most likely fatigue result.

If in the fatigue tests where failure occurs the likelihood can be explained as the ordinate of normalized probability density function (pdf). To obtain a maximization of the sum of a product, instead of utilizing the likelihood function, the authors adopted a log-likelihood function. And to be able to apply the MLE method, the authors assumed that the cumulative distribution functions follows the normal distribution.

With the analysis of the statistics methods just mentioned, Taras and Greiner were able to obtain S-N lines that were accepted by the Austrian standard ONR 24008 (Österreichisches Normungsinstitut, 2006). The proposal is summarized in a new developed fatigue class catalogue, which can be seen in Figure 18. It is common to express the normal stress range in MegaPascal (MPa) at $N = 2 \times 10^6$ load cycles. With this knowledge, the fatigue class selection, on the authors proposal, can enter as “minimum value of slip resistance” used to indirectly estimate the transmitted level of shear force transmitted by the rivet holes that transmits the pressure and through shear stress (Figure 19). The minimum value of slip resistance is normally used, because, in most cases, it is not known with which technique the rivets were implemented (hand or pneumatic hammer).

Fatigue strength (MPa)	Constructional detail	Description and examples	Remarks
$\Delta\sigma_c = 90$ (80) $m = 5$		Symmetrical joint with splice plates	The ratio $\sigma_{bearing}$ to σ_{net} must be smaller than 2
		– Middle plates in two-shear connections are to be verified with $\Delta\sigma_c = 90$	When rivets of steel grade St44 or higher were employed no corrosion protection coating must have been applied
		– $\Delta\sigma_c = 80$ applies for the splice plates themselves, so no verification is required when $2t_l > 1,12 t$	If one of these conditions is not kept, $\Delta\sigma_c = 80$ applies (70 for the gusset plates)
$\Delta\sigma_c = 85, m = 5$		Continuous connection of flange angles and web plates in built-up girders $\Delta\sigma$ at the centre of the rivet	The calculated shear force per rivet and shearing area must not exceed the minimum value of slip resistance as indicated in <i>Table 3</i>
		Continuous connection between cover plates and flange angles in built-up girders	The calculated shear force per rivet and shearing area must not exceed the minimum value of slip resistance as indicated in <i>Table 3</i>
$\Delta\sigma_c = 85, m = 5$		Latticed members under tension or compression loads	The calculated shear force per rivet and shearing area must not exceed the minimum value of slip resistance as indicated in <i>Table 3</i>
$\Delta\sigma_c = 71, m = 5$		One-shear joint with gusset plates	If the calculated shear force in the rivets is lower than the minimum value of slip resistance, $\Delta\sigma_c = 85$ can be used
$\Delta\sigma_c = 71, m = 5$	–	All cases for which normally $\Delta\sigma_c = 85$ applies if the minimum value of slip resistance in the rivet is exceeded	The calculated shear force per rivet and shearing area exceeds the minimum value of slip resistance as indicated in <i>Table 3</i>
$\Delta\sigma_c = 71, m = 5$		Area of the connection of a lateral bracing element to the tension flange of a girder	If the restraining effect of the lateral bracing element is considered during the calculation of the applied stress range $\Delta\sigma_c = 85$ can be used
$\Delta\sigma_c = 71, m = 5$		Onset of a cover plate	If the calculated shear force in the rivets is lower than the minimum value of slip resistance $\Delta\sigma_c = 85$ can be used

Figure 18 - Classification of construction details (Taras & Greiner, 2009)

Riveting technique and number of rivets in the connection	Minimum value of slip resistance per rivet shear plane (kN)
<i>Unknown technique</i> or riveting by hand or by pneumatic hammer, $n < 15$ rivets, wrought iron or mild steel rivets (St34...)	12
Riveting by pneumatic hammer, $n \geq 15$ rivets, wrought iron or mild steel rivets (St34...)	15
Riveting with bent lever, wrought iron or mild steel rivets (St34...)	25

Figure 19 - Minimum values (Taras & Greiner, 2009)

This page was intentionally left blank.

3 FATIGUE ON CONNECTING ELEMENTS

The work developed in this chapter is based on the experimental results obtained by Correia (2014). The objective of this previous work was to study the fatigue behavior in different old metallic materials and connections used in Portuguese bridges. The bridges in study are Luiz I, Fão, Pinhão, Trezói and Viana. The present chapter will focus the connection characterization and will try to define S-N fatigue curves associated with riveted connections.

3.1 The Portuguese bridges in study

The five old bridges included in this analysis were constructed between the years of 1878 and 1906. In the following map, the location of each bridge is pointed out (Figure 20).



Figure 20 - Location of the bridges in study (onestopmap, 2017)

- Luiz I bridge

Bridge Luiz I crosses the Douro River, between Porto and Gaia cities (Figure 21). It was designed by Gustave Eiffel and the construction started in 1886. The main visual aspect of this bridge is, it possesses a double deck supported by an arch, with a span of 172 meters and an arch radius of 45 meters.



Figure 21 – Luiz I bridge (author, 2017)

- Fão bridge

Fão is a roadway bridge. It crosses the Cávado River in Esposende county. It has a continuous deck with eight spans supported on masonry piers (Figure 22). The bridge was designed by Abel Maria Mota under the supervision of the French Engineer Raynau, and it was finished in 1892. (Correia, 2014) The bridge has a length of 267 meters, divided in to 8 spans with 33,5 meters each. It possesses 7 masonry piers, each with 15 meters depth. (Jesus, Silva, & Correia, 2014)



Figure 22 - Fão road bridge (Jesus, Silva, & Correia, 2014)

- Pinhão bridge

Pinhão bridge, as the name says, is located in the city of Pinhão and crosses the Douro river, linking Pinhão to São João da Pesqueira and Peso da Régua. It is a single deck arched bridge. It was designed by Gustave Eiffel and built between the years of 1903 and 1906. The bridge is composed of four spans, three spans with 68,8 meters and one with 10 meters. There is only one deck with 6 meters width, divided in one traffic lane with 4.60 meters width and two sidewalks with 0.675 meters width each. (Figure 23).



Figure 23 - Pinhão bridge (Correia, 2014)

- Viana bridge

The oldest bridge in study is the Viana bridge, usually called the Eiffel Bridge (Figure 24). As the names indicates, the bridge was designed by Gustave Eiffel and is located in Viana do Castelo. More precisely, it crosses the Lima river, between the cities of Darque and Viana do Castelo. It was inaugurated in 1878. The bridge serves as roadway and railway. It is 6 m wide and possess 573 meters of extension, with continuous deck and divided in nine spans.



Figure 24 - Viana bridge (Correia, 2014)

- Trezói bridge

The Trezói railway bridge was inaugurated in the year of 1956. It is the youngest bridge in study. The bridge deck is composed of three spans and possess a total length of 126 meters. It is a young bridge, when compared to the other bridges analyzed in this thesis. It is known that the material used in its construction is steel (Figure 25) (Correia, 2014).



Figure 25 - Trezói railway bridge (Correia, 2014)

3.2 Probabilistic models directed to fatigue

To study the lifetime of bridges, it is recommended to use probabilistic models. The use of a deterministic approach may lead to a metallic structure or connection where the required safety levels are not met. Many factors can influence the fatigue results, such as, the material variability. To achieve

adequate safety levels on structural details on mechanical components that present a diffused pattern on experimental results, a simplified analysis provides more comprehensive results if the probabilistic approach to fatigue is applied (Correia, 2014).

3.2.1 Global interpretation of probabilistic models

A concern when considering a probabilistic approach to fatigue phenomenon is the dispersion of the resulting data on the S-N curve. It is possible to observe in Figure 26, while the dispersion of the stress amplitude decreases the fatigue life increases. (Correia, 2014)

For an engineering approach of the results, it is recommended to use a normalized approximation of the results. This normalization is obtained by performing a linear regression analysis on the logarithm of the number of cycles to failure ($\log N_f$) versus the logarithm of the stress amplitude ($\log \sigma_a$) of the results. Next, it is possible to determine a mean S-N curve with the standard deviation, admitting a LogNormal distribution for the number of cycles, given the stress range. Hence, safety margins are established on the design curve method. The design curve is derived by changing the average strain-life curve in logarithm coordinates two or three times the standard deviation. This is the recommendation on the existing codes EC3, ASTM 739 and BS5400 (items 2.5.12.5.2 and 2.5.3). (Correia, 2014)

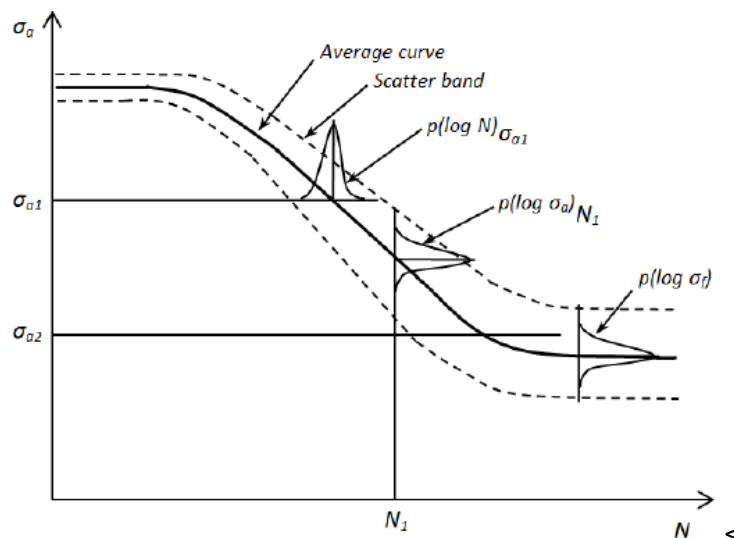


Figure 26 – Distribution band in a S-N curve (Correia, 2014)

3.2.2 Probabilistic fatigue damage

To describe the different sources of uncertainty that appear in the prediction procedures, it is necessary to use probabilistic fatigue models. Many of the models normally used have a deterministic base. The application of a model with deterministic base subsequently requires additional statistical argument to be able to establish safety margins. Therefore, assumptions on the statistical distribution are implied. In order to perform reliability analyses, fatigue resistance must be established in an

appropriate probabilistic format. As a result, failure prediction and risk analysis in fatigue are not capable to support probabilistic fatigue models. (Correia, 2014)

The basic probabilistic model given by Castillo and Fernández-Canteli accounts the S-N curve and the ϵ -N curve, by assuming simple variables, i.e. stress range and strain amplitudes drive the fatigue damage variables. This makes it possible to compare the stress or fatigue data given by the loading conditions and using a hyperbolic field derived from Weibull or Gumbel distribution (Figure 27) (Correia, 2014).

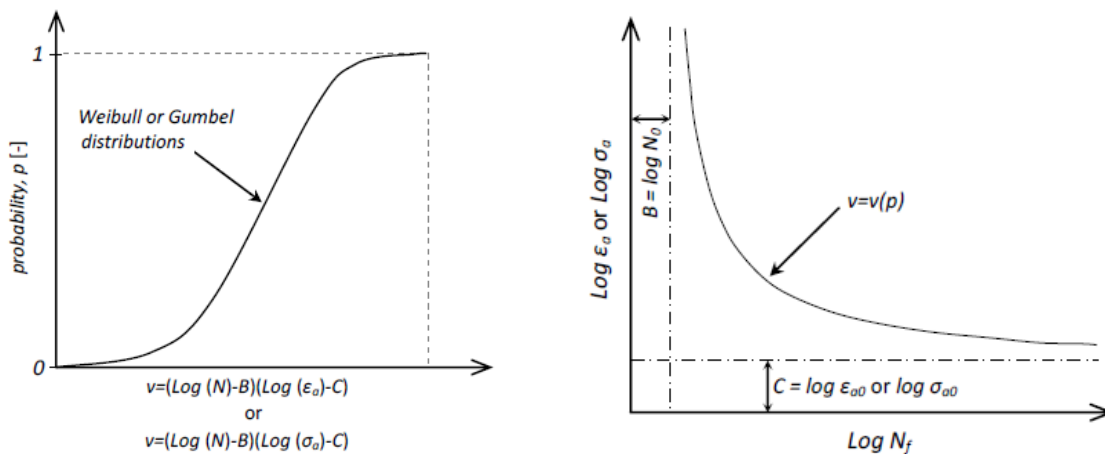


Figure 27 – Representation of the probabilistic curves (Correia, 2014)

To analyse the mean stress effect on S-N curve, Castillo and Fernández-Canteli propose an analytical approach, but the resulting probabilistic model involves the use of a large quantity of parameters that require a complicated identification procedure (Correia, 2014) The large use of parameters can have a computational and time cost, involving the use of computers that are capable of processing such data.

3.2.3 Castillo and Fernández-Canteli probabilistic model

In the model developed by Castillo and Fernández-Canteli, the use of two simple damage variables is proposed, in order to describe the probabilistic stress and strain fields, the uniaxial stress and the strain amplitudes. In the graphic represented in Figure 28, the $p - \epsilon_a - N$ Weibull field defined by percentile curves that have hyperbolic shapes with two main asymptotes can be observed. The horizontal asymptote represents the fatigue limit and the vertical one stands for the limit value of lifetime, i.e. limiting the number of cycles. (Correia, 2014)

The probabilistic S-N curves/fields are presented in Figure 28. The curves represent the percentile curves which correspond to the probability of failure equal to $p=0,01$; $p=0,05$; $p=0,50$ and $p=0,95$ (1%, 5%, 50% and 95%). The parameters of the obtained S-N curve, using the Castillo and Fernández-Canteli

method, are achieved with the percentile curve compared to the probabilities of failure of 5%. (Mayorga, et al., 2017).

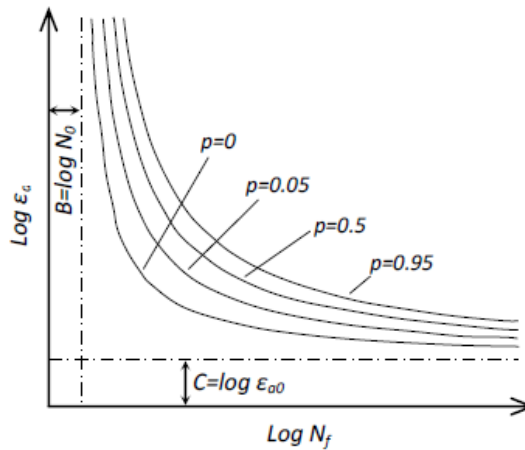


Figure 28 – Probabilistic representation of $\varepsilon_a - N$ field (Correia, 2014)

3.3 Study of the riveted connections

The riveted connections, were studied by Correia (2014), according to the Portuguese code (NP 10002-1 Standard) and submitted to monotonic tensile tests. Round specimens were used, machined from the original structural element, which was extracted from the designated bridge and tested (Figure 29). The dimensions of the specimens are listed in

Table 1. (Correia, 2014)



Figure 29 - example of round specimens put in to submitted to monotonic tensile test (Correia, 2014)

Table 1 - The dimension of the round specimens submitted to monotonic tensile test (Correia, 2014)

Bridge	Section	Diameter (mm)	Cross-Section (mm ²)
Fão	Diagonal	6,0	28,27
Luiz I	Diagonal	6,0	28,27
	Diagonal	8,0	50,27
Pinhão	Diagonal	5,0	19,63
	Bracing	8,0	50,27
Trezói	Bracing	8,0	50,27
	Viaduct	4,0	12,57
Viana	Viaduct	5,0	19,63
	Viaduct	6,0	28,27

Several monotonic tests were performed by Correia, involving the study of the tensile strength (f_u), ultimate tensile strength (f_y), elongation at fracture (A) and reduction of the cross-section at its failure (Z). As a result, the statistic values of: mean, standard deviation and coefficient of variation were obtained for each bridge material. (Correia, 2014)

The results of the analyses reveal that the material from Viana bridge had the lowest ductility properties. Instead, Pinhão bridge material presented a high ductility, and Trezói bridge presented the highest strength properties combined with high ductility. Remembering that Pinhão it is the youngest bridge in the group under study, at that at the time of construction the steel production was evolving in a fast way, therefore the material present in the bridge is similar to the ones used in the construction of new metallic bridges. (Correia, 2014)

Metallographic analysis of the materials, optical microscope observation and chemical composition were also performed. In the optical microscope observation, it was found that the compose of ferrite matrix is common in all the specimens. The presence of perlite in addition with the ferrite matrix was found in Pinhão bridge and in Trezói bridge materials. However, this test has showed the density is

higher in centennial materials, by having this characteristic the ductility of the material is limiting and increasing the dispersion of the mechanical properties. (Correia, 2014)

With the chemical composition test, it was possible to observe that the lowest sulphur and phosphorus content was found in the material from the Trezói bridge. Its main material is the ferritic steel with low presence of carbon, thus it should present a ferrite matrix. But the sample from Luiz I bridge presented a higher presence of carbon, silicone and manganese, which is coherent with the characteristics of puddled iron. (Correia, 2014)

3.3.1 Probabilistic study of riveted connection

The following data was obtained by Correia (2014) in his research and the resulting graphics were built with the help of the software ProFatigue®, developed in the University of Oviedo, Spain; within the Excel Office environment. The software ProFatigue® is a resourceful tool for the derivation of probabilistic S-N and ϵ -N curves or fields by utilizing experimental fatigue data. The software estimates the involved parameters presents in the regression probabilistic Weibull fatigue model. (Fernández-Canteli, Przybille, Nogal, Aenlle, & Castillo, 2014)

The aim of the work is to obtain the necessary parameters to accomplish the proposed statistical comparisons. Through the use of the program ProFatigue® the graphics following the method Weibull were obtained. And from these removed the shortcomings of the necessary counters for the future calculations with the standards E739, EC3, method the Taras and Greiner; and Castillo and Fernández-Canteli. (Mayorga, et al., 2017)

The main intention in this section is to compare the results obtained through the various methods previously described and codes available to analyze the behavior of the riveted connections in bridges. This approach is applied to the bridges previously mentioned. The analysis is made according to the type of connection that the bridges present, either double shear or single shear.

3.3.1.1 Riveted connections from Viana bridge

To study the riveted connections from Viana bridge, specimens were extracted from the longitudinal direction of the member taken from bridge. The bridge presents double shear riveted connections that were cut out for analysis (Figure 30). A sum of 14 specimens were tested and submitted to a stress R-ratio of 0,1 (Figure 16) and frequency (f) between 5,0 and 7,5 Hz. All results are collected in

Table 2 (Correia, An Integral Probabilistic Approach for Fatigue Lifetime Prediction of Mechanical and Structural Components, 2014).

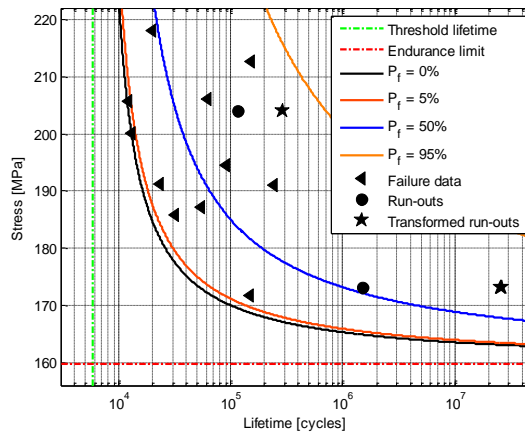


Figure 30 - Photos of the specimens with double shear riveted connections, cut from Viana bridge (Correia, 2014)

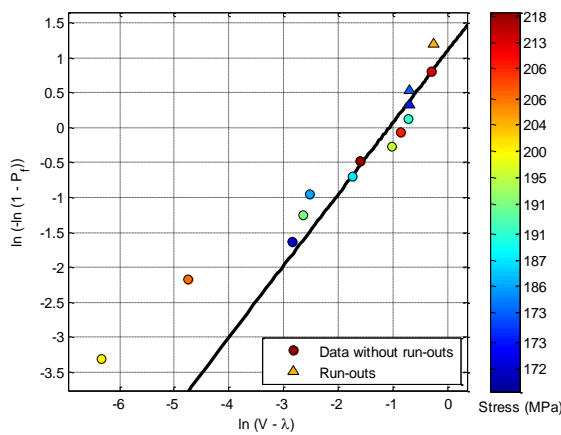
Table 2 - Results from Viana bridge stress test on connections (Correia, 2014)

Specimens	N cycles	$\Delta\sigma$ norm (MPa)	Area (mm ²)	f (Hz)
V1	1513265	173,10	300,40	5,0
V2	1500331	173,13	300,40	7,5
V3	240383	190,97	300,40	7,5
V4	149378	171,79	300,40	7,5
V5	61456	206,04	300,40	5,0
V6	149879	212,63	300,40	5,0
V7	19768	218,10	300,40	5,0
V8	12195	205,71	300,40	5,0
V9	31954	185,82	300,40	5,0
V10	53638	187,21	300,40	5,0
V11	114510	204,03	300,40	5,0
V12	23196	191,26	300,40	5,0
V13	91069	194,56	300,40	5,0
V14	12950	200,11	300,40	5,0

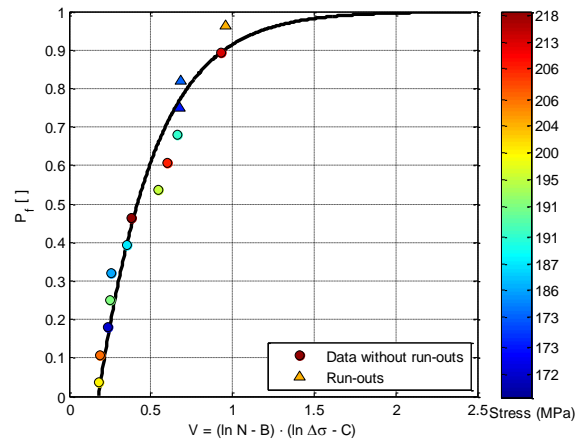
In Figure 31 **Error! Reference source not found.** it can be observed an alternative to the study of the local approach to fatigue, which is based on local or notch stress or strain. And frequently used to determine the fatigue crack initiation.



(a)



(b)



(c)

Figure 31 - (a) S-N Curve of Viana bridge riveted connections obtained with ProFatigue® software;

(b) Probabilistic paper of Viana bridge riveted connections; (c) Weibull distribution of Viana bridge riveted connections

With the graphics presented in Figure 31 it was possible to obtain the parameters presented in Table 3 which will be used in the comparison included on section 3.4.1. The parameters obtained are: β , the shape parameter of the Weibull model, B, the linear regression parameter (related to the lifetime), C, the material constant (related to endurance limit) and λ , the threshold parameter of the Weibull model.

Table 3 - Estimated parameters on the connections of Viana bridge

β	B	C	Δ	λ
1,03	8,67	5,07	0,34	0,18
	(5828 cycles)	(159,67MPa)		

3.3.1.2 Riveted connections from Fão bridge

The Fão bridge also presents a double shear type connection (Figure 32). A total of 15 specimens were tested and submitted to a stress R-ratio equal to 0,0 and frequencies between 2,5 and 10,0 Hz. The results can be observed in Table 4. (Correia, 2014)

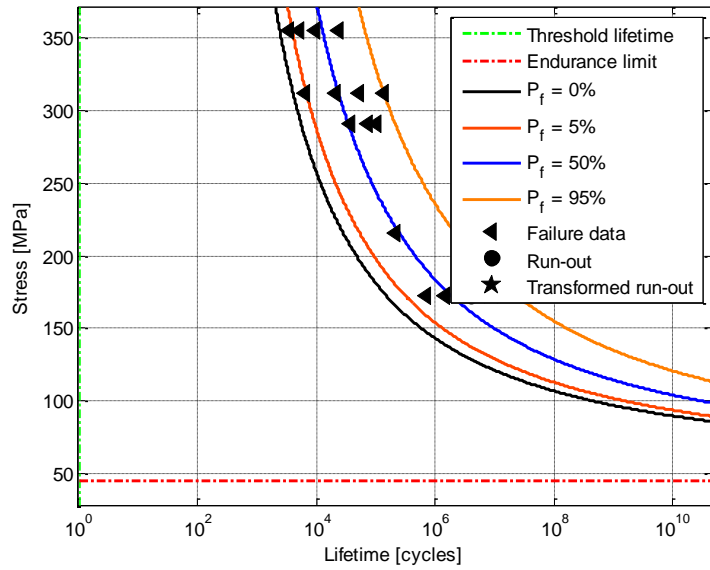


Figure 32 – Illustration of the Luiz I bridge connection, before testing (Correia, 2014)

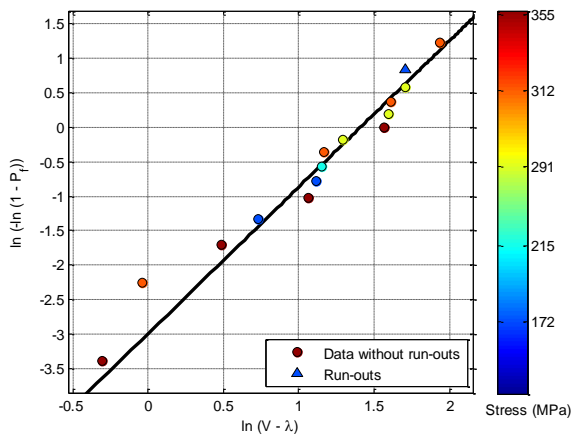
Table 4 – Results from Fão bridge stress test on connections (Correia, An Integral Probabilistic Approach for Fatigue Lifetime Prediction of Mechanical and Structural Components, 2014)

Specimens	N cycles	$\Delta\sigma$ norm (MPa)	Area (mm ²)	f (Hz)
FA1	9744	355,47	162,3	2,5
FA2	5285	355,47	162,3	2,5
FA3	24357	355,47	162,3	2,5
FA4	3458	355,47	162,3	5,0
FA5	141330	312,38	162,3	2,5
FA6	52879	312,38	162,3	5,0
FA7	6644	312,38	162,3	5,0
FA8	21050	312,38	162,3	5,0
FA9	38242	290,84	162,3	5,0
FA10	103809	290,84	162,3	5,0
FA11	75749	290,84	162,3	5,0
FA12	210995	215,44	162,3	5,0
FA13	699161	172,35	162,3	5,0
FA14	4000000	172,35	162,3	10,0
FA15	1439414	172,35	162,3	5,0

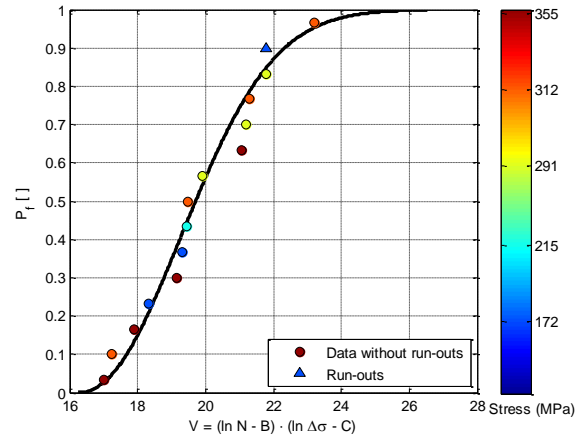
Figure 33, represent the study of the local approach (explained in item 3.3.1.1) of the double shear of Fão bridge.



(a)



(b)



(c)

Figure 33 – (a) S-N Curve of Fão bridge riveted connections obtained with the ProFatigue® software ; (b) - Probabilistic paper of Fão bridge riveted connections; Weibull distribution on Fão bridge riveted connections

With the graphics presented in Figure 33, it was possible to calculate the parameters included in Table 5 which will be used in the comparison presented in section 3.4.1.

Table 5 - Estimated parameters on the connections of Fão bridge

β	B	C	Δ	λ
2,12	0	3,79	4,10	16,26
	(1 cycle)	(44,14 MPa)		

3.3.1.3 Riveted connections from Trezói bridge

The riveted joints of the Trezói bridge possess single shear (Figure 34). A sum of 7 specimens were studied and tested with a R-ratio of 0,1 and frequencies between 4,0 and 10,0 Hz. All results can be observed in Table 6. (Correia, 2014)

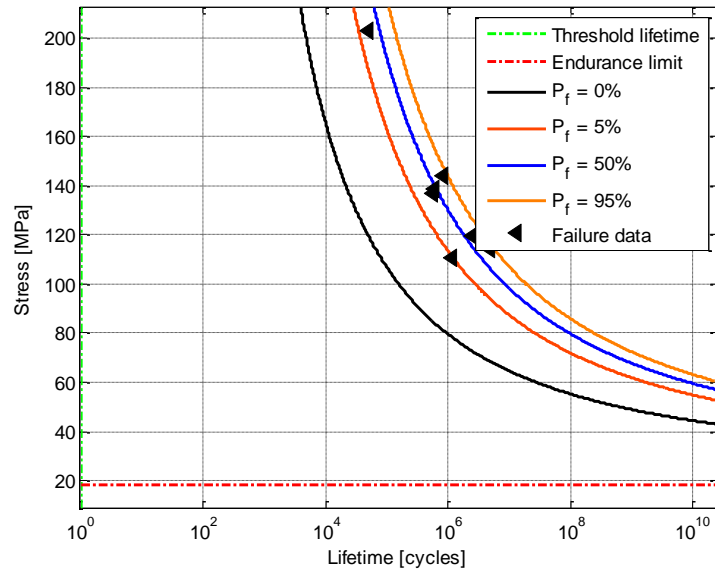


Figure 34 - Photo of the specimens from Trezói bridge (Correia, 2014)

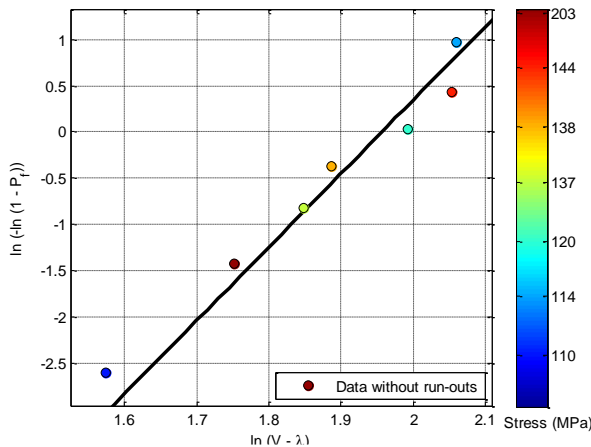
Table 6 – Results from Trezói bridge stress test connections (Correia, An Integral Probabilistic Approach for Fatigue Lifetime Prediction of Mechanical and Structural Components, 2014)

Specimens	N cycles	$\Delta\sigma$ norm (MPa)	Area (mm ²)	f (Hz)
F1	50771	203,17	280,8	4,0
F2	846982	143,88	280,8	6,0
F3	605387	138,45	280,8	6,0
F4	566467	137,18	280,8	10,0
F5	2518224	119,80	280,8	10,0
F6	4901965	114,20	280,8	8,0
F7	1202674	110,47	280,8	10,0

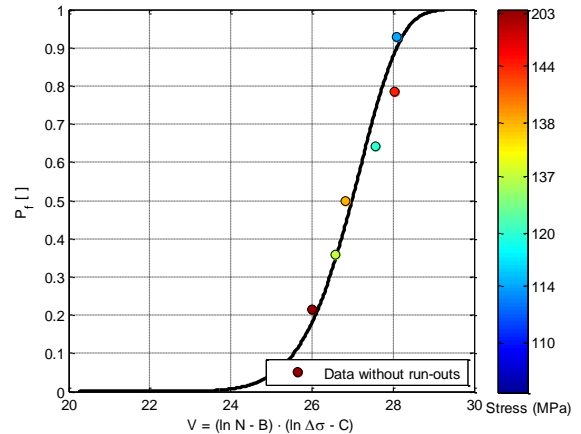
Also in Figure 35 it can be observed the study of the local approach (explained in item 3.3.1.1) of the single shear of Trezói bridge.



(a)



(b)



(c)

Figure 35 – (a) S-N Curve of Trezói bridge riveted connections obtained with the ProFatigue® software, (b) Probabilistic paper of Trezói bridge of the riveted connections, (c) Weibull distribution Trezói bridge of the riveted connections

With the graphics presented above it was possible to obtain the constants presented in the

Table 7 which will be used to the following run-out study to the comparison on the item 3.4.1.

Table 7 - Estimated parameters on the connections of Trezói bridge

β	B	C	Δ	λ
7,93	0,0 (1 cycle)	2,92 (18,45 MPa)	7,08	20,23

3.3.1.4 Riveted connections from Luiz I bridge

The Luiz I bridge possess a single shear riveted connection (Figure 36). With a total of 7 specimens studded and tested with a R-ratio of 0,1 and frequencies between 6,0 and 8,0Hz. All results can be observed in the Table 8 (Correia, 2014).

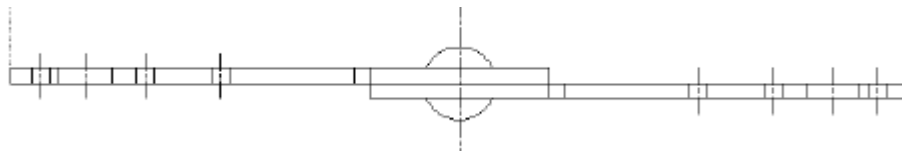
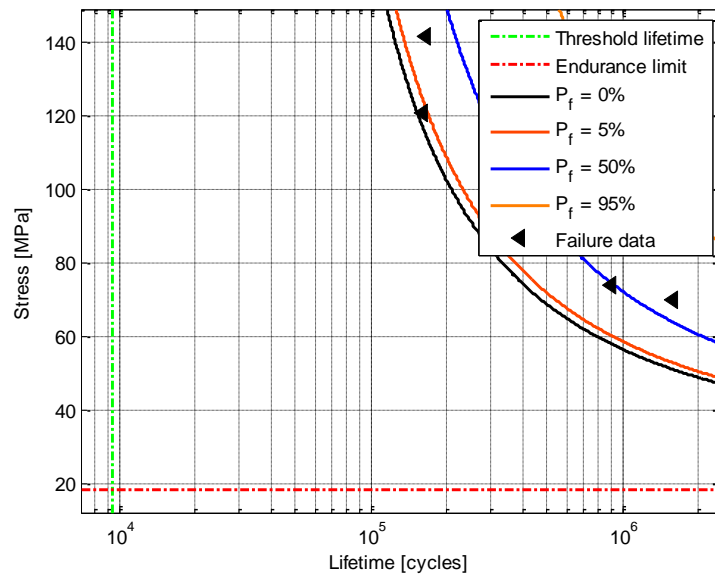


Figure 36 - Representation of the Luiz I bridge connection

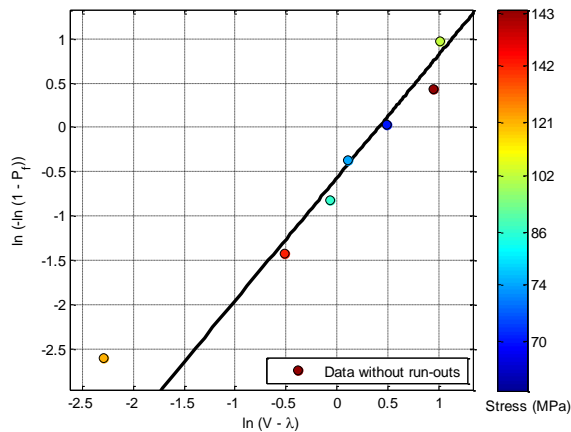
Table 8 - Results from Luiz I bridge stress test connections (Correia, 2014)

Specimens	N cycles	$\Delta\sigma$ norm (MPa)	Area (mm ²)	f (Hz)
S5R1	164985	141,50	210,00	8,0
S5R2	426259	142,60	210,00	6,0
S5R3	161801	120,60	210,00	7,0
S5R4	999453	101,80	210,00	7,0
S5R5	514569	86,00	210,00	7,0
S5R6	1586560	70,00	210,00	8,0
S5R7	904586	73,80	210,00	8,0

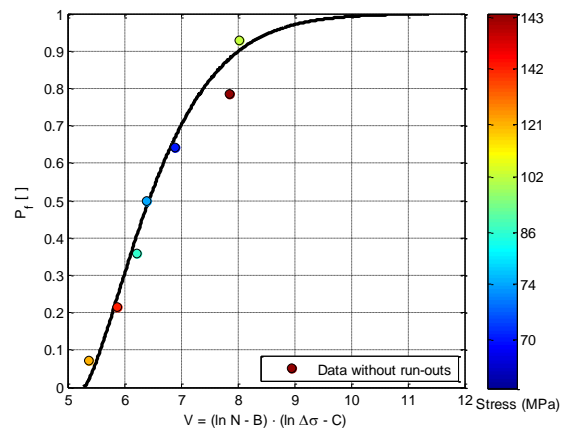
The Figure 37 it is shown the study of the local approach (explained in item 3.3.1.1) of the double shear of Luiz I bridge.



(a)



(b)



(c)

Figure 37 – (a) S-N Curve of Luiz I bridge riveted connections obtained with the ProFatigue® software, (b) Probabilistic paper of Luiz I bridge of the riveted connections, (c) Weibull distribution Luiz I bridge of the riveted connections

With the graphics presented above it was possible to obtain the constants presented in the which will be used to the following study to the comparison on the item 3.4.1.

Table 9 - Estimated parameters on the connections of Luiz I bridge

β	B	C	Δ	λ
1,39	9,14 (9359 cycles)	2,90 (18,25 MPa)	1,50	5,28

3.3.1.5 Riveted connections from Pinhão bridge

The Pinhão bridge also has a single shear riveted connection (Figure 38). In this bridge were extracted 7 specimens tested and submitted under a stress R-ratio equal to 0,1 and frequency of 6,0 Hz. All results can be observed in the Table 10. (Correia, 2014)

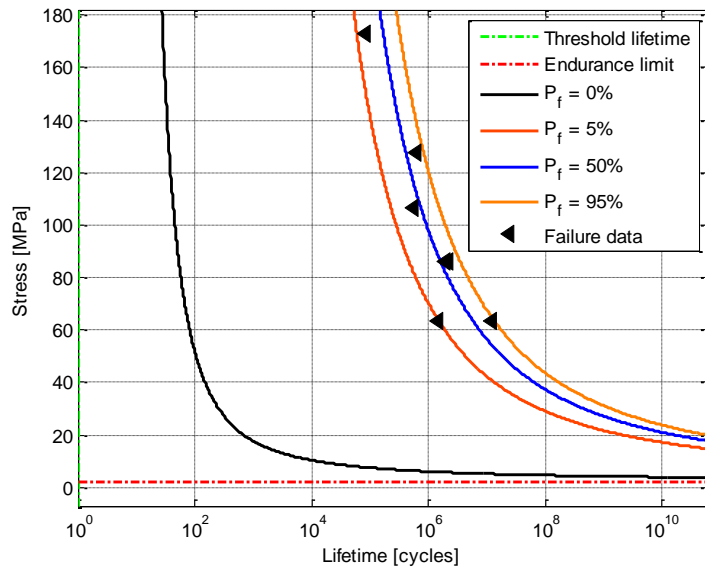


Figure 38 - Illustration of the specimens from Pinhão bridge

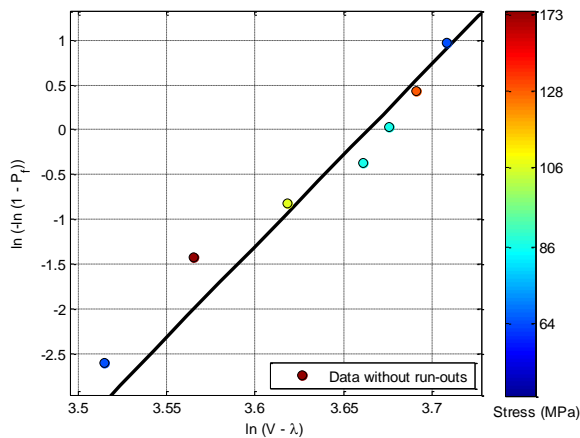
Table 10 – Results from Pinhão bridge stress test connections (Correia, 2014)

Specimens	N cycles	$\Delta\sigma$ norm (MPa)	Area (mm ²)	f (Hz)
CF1	86140	172,96	269,3	6,0
CF2	635172	127,51	269,3	6,0
CF3	574452	106,47	269,3	6,0
CF4	1922024	85,87	269,3	6,0
CF5	2243676	85,87	269,3	6,0
CF6	1450789	63,54	269,3	6,0
CF7	12000000	63,54	269,3	6,0

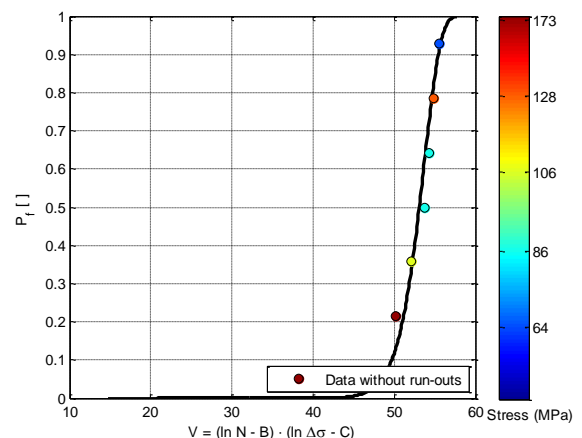
In the Figure 39 it can be seen the study of the local approach (explained in item 3.3.1.1) of the double shear of Pinhão bridge.



(a)



(b)



(c)

Figure 39 – (a) S-N Curve of Pinhão bridge riveted connections obtained with the ProFatigue® software, (b) Probabilistic paper of Pinhão bridge of the riveted connections, (c) Weibull distribution Pinhão bridge of the riveted connections

With the graphics presented in Figure 39 it was possible to obtain the parameters presented in

Table 11 which will be used in the comparison developed in section 3.4.1.

Table 11 - Estimated parameters on the connections of Pinhão bridge

β	B	C	Δ	λ
20,23	0	0,74	39,02	14,78
	(1 cycle)	(2,10 MPa)		

3.4 Results of the connections elements

The results obtained were divided in double shear and single shear riveted connections.

3.4.1 Proposed S-N curves for double shear and single shear riveted connections

The main objective of this work is to observe the behaviour of the riveted connections when submitted to 10^4 load cycles (Figure 40 and Figure 41), since this interval is not covered by the existing standards. To obtain the desired results the riveted connections are submitted to high-cycles of loading to obtain the fatigue phenomena.

As mentioned before, Fão and Viana bridges possess riveted connections with double shear. Figure 40 presents a comparison between the methods of the S-N curve, EC3 – Part 1-9 and Taras and Grainer proposal curve (sections 2.4.1, 2.5.1 and 2.5.4).

The results are compared to category 71 curve proposed in Eurocode 3 – Part 1-9, where m corresponds to the parameter related to the curve in a logarithm representation. The stress range at the value of 2×10^6 cycles gives the normalization of the curve. The curve may also defined by other gradient values: $m = 3$, as recommended by the Eurocode 3 – Part 1-9, $m = 5$ as suggested by Taras & Grainer and $m = 10$, as proposed by the S-N curve.

When comparing the three methods, it can be observed that the Taras and Grainer proposal curve is the one that adjusts better to the the data measured in the experimental tests performed.

The other curves, Eurocode 3 and the S-N proposed curve cannot be the best adaptable curve, due to its linearized boundaries method. In both cases simplified calculations are made which can cause errors. Since these methods consider in their study the materials.

The same comparison was done to the bridges which possess connection with single shear (Trezói bridge, Luiz I bridge and Pinhão bridge). In the single shear (Figure 41) study the curve is defined by three changes in the gradient, from $m = 3$ as recommended by EC3 to $m = 5$ as suggested by Taras and Grainer to $m = 5,5$ as proposed by the S-N curve.

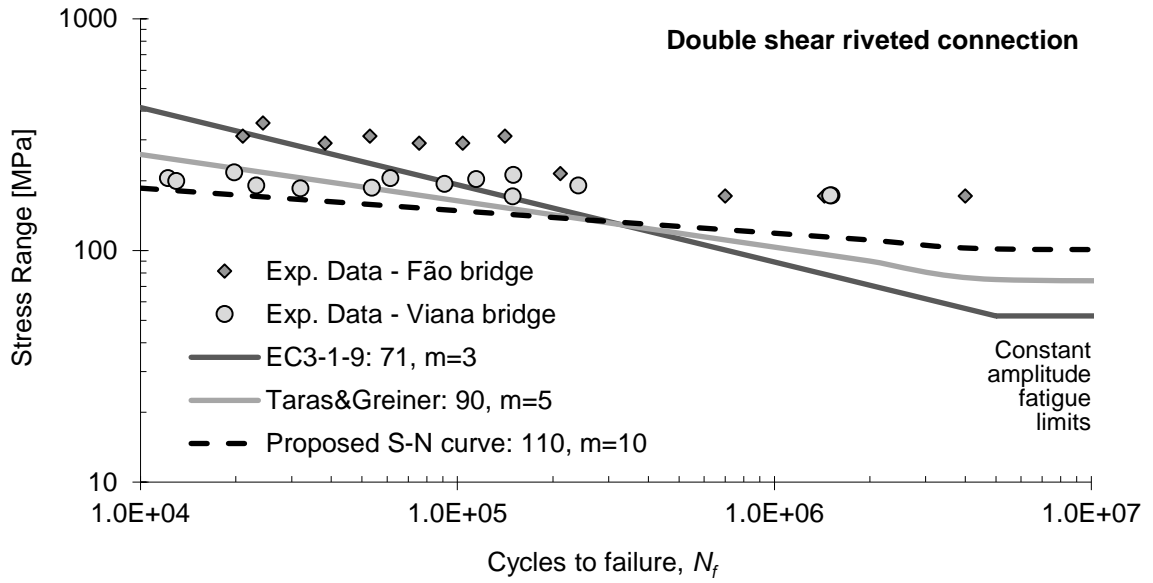


Figure 40 - Curves for double shear riveted connections

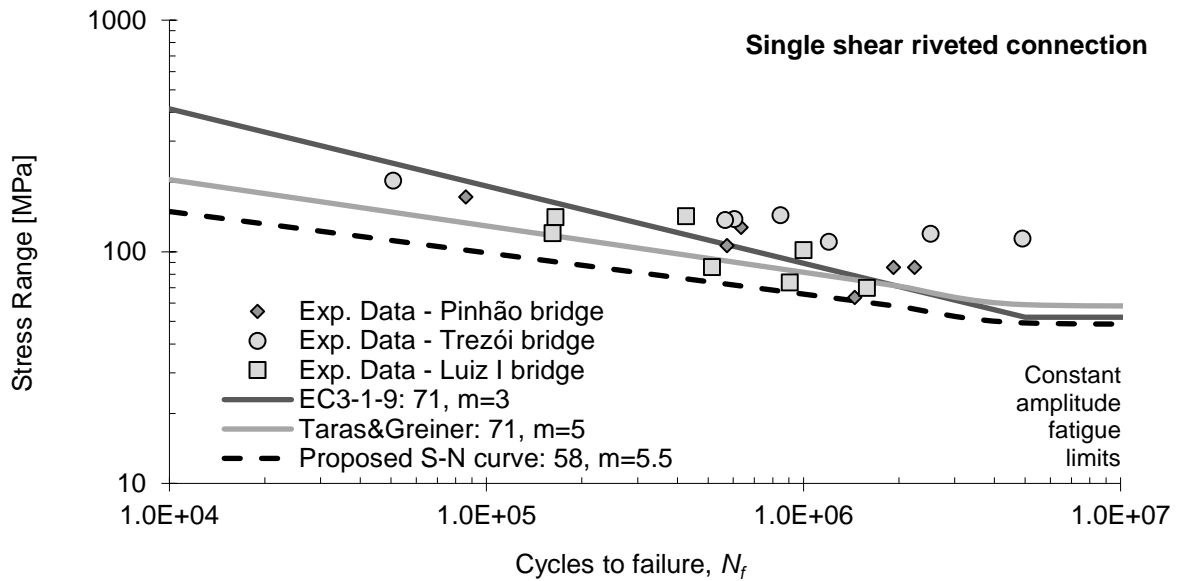


Figure 41 - Curves for single shear riveted connections

3.4.2 Statistical analysis based on comparison between ASTM E 739-91 and Castillo and Fernández-Canteli model

As observed before in section 3.2.3, the parameters of the probabilistic S-N curve according to the Castillo and Fernández-Canteli model are obtained from the curve where the probability of failure is 5%. On the other way, the ASTM E739-91 approach is very similar to the proposal associated with category 71 curve of Eurocode 3, where the gradient $m = 3$ is used.

The fatigue limit obtained through the Castillo and Fernández-Canteli model was applied on double shear rivets (Figure 42) and single shear rivets (Figure 43). In both cases, it can be observed that the approach made by the Castillo and Fernández-Canteli model is better fitted to the evolution of the fatigue life.

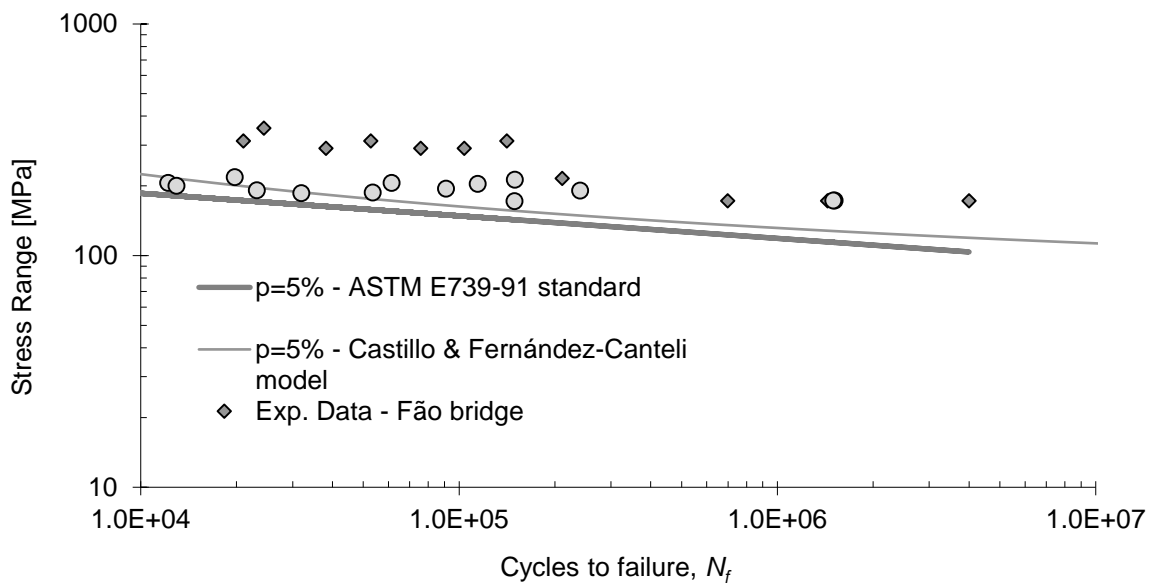


Figure 42 – Statistical analysis on the results obtained with double shear specimens

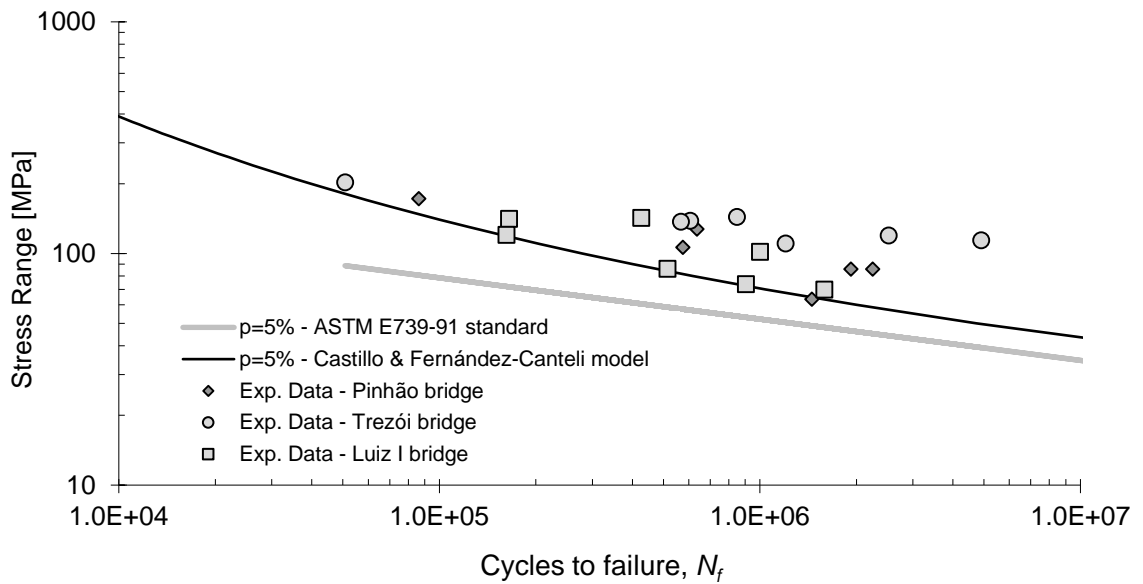


Figure 43 – Statistical analysis on the results obtained with single shear specimens

3.4.3 Statistical Analysis based on Castillo and Fernández-Canteli model

In this approach presented in this section it can be observed the good behavior of the connections, due to the behavior of the results are contained within the zone between the 5% curve and the 95% curve. The results are close to the 50% curve, the mean value, also shows the good behavior of the specimens to the fatigue (Figure 44 and Figure 45).

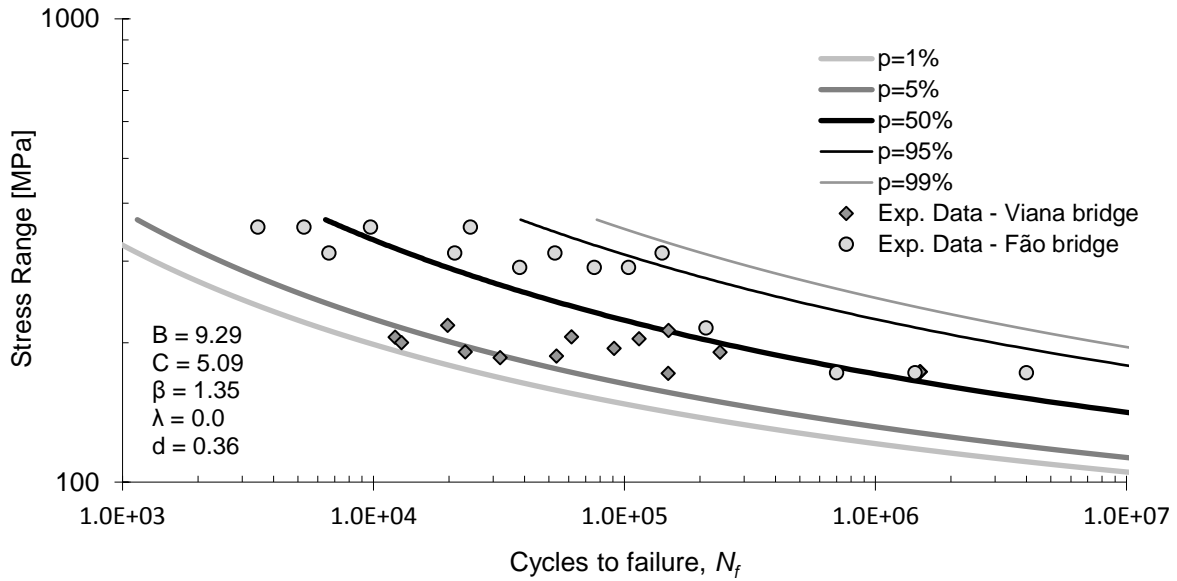


Figure 44 - Statistical Analysis based on the Castillo & Fernández-Canteli model, applied to double shear

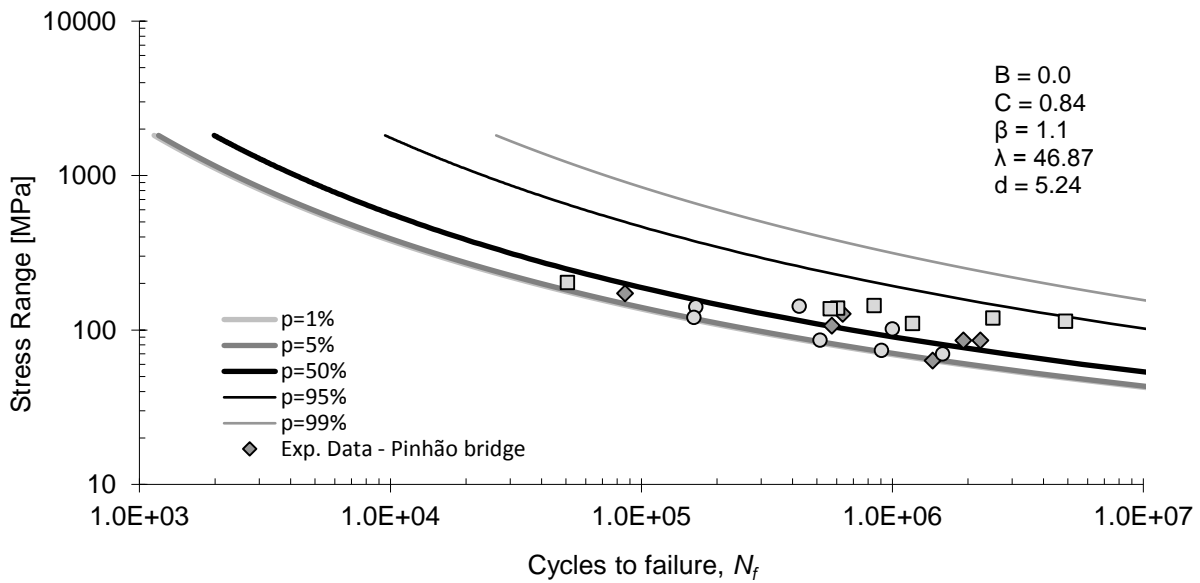


Figure 45 - Statistical Analysis based on the Castillo & Fernández-Canteli model, applied to single shear

4 FATIGUE CHARACTERIZATION OF THE MATERIAL

The material used in the construction of bridges and its connections, must possess the property of resisting external loading without presenting failure. Even more on structures submitted to low stress concentrations, such as the riveted connections. (Lindenberg, 2016)

This chapter addresses the strain-life fatigue data obtained from materials collected in old metallic bridges. The strain-life fatigue was obtained in smooth specimens that were machined from the ordinals material removed from the bridges (Figure 46, Figure 47 and Figure 48), that can be used to evaluate the crack initiation, in the scope of a local approach analysis on fatigue. (Jesus, Silva, & Correia, 2014)

The ASTM E606 Standard was followed, in order to obtain the smooth specimens. The specimens were shaped into rectangular cross sections with the sample of the Fão bridge, Luiz I bridge, Trezói bridge and Viana bridge. The choice of rectangular section specimens instead of circular section specimens was made due to the fact that the specimens withdrawals from the bridges were small. The dimensions of the specimens were varied for each material, since the material thicknesses were not constant. A base length of 12,5 mm specimens was adopted for Viana and Luiz I bridges. A base length of 25 mm was adopted for some specimens of Viana bridge and specimens from Trezói and Fão bridges. The preference given to rectangular cross-sections (d), instead of circular ones, was due to the dimensions of the structural elements extracted from the bridges, as the reduced thicknesses did not allow the preparation of round specimens. The dimensions of the specimens can be observed in Table 12. (Correia, 2014)

Several specimens were tested for stress, strain and SWT with a strain ratio equals to 0 or -1 (section 2.5.4, Figure 16), in order to characterize the elastoplastic behavior of the material and fatigue resistance.

Table 12 – Nominal dimensions of specimens used in fatigue test (Correia, 2014)

Bridge	Nº. of specimens	W (mm)	T (mm)	L (mm)	L1 (mm)	R (mm)	H (mm)
Fão	35	30,0	7,5	26,0	200,0	12,5	8,0
Luiz I	15	20,0	5,0	15,0	150,0	10,0	6,0
Trezói	10	30,0	7,5	26,0	200,0	12,5	8,0
Viana	12	22,0	6,0	20,0	150,0	15,0	7,0
	15	20,0	5,0	15,0	150,0	10,0	6,0

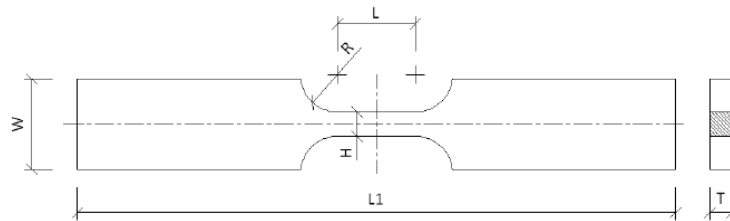


Figure 46 – Geometry of the specimen used in the fatigue tests (Correia, 2014)



Figure 47 – Example of specimens of material extracted from Fão bridge used (Correia, 2014)

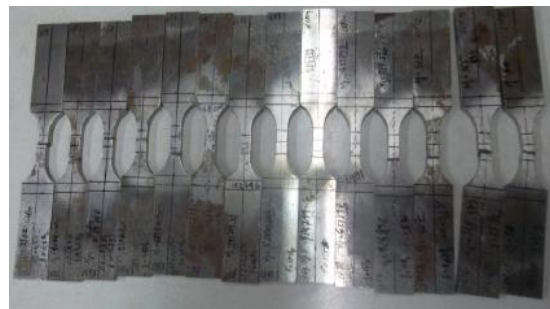


Figure 48 - Example of specimens of material extracted from the Viana bridge (Correia, 2014)

The experimental tests were performed on 27 specimens of Viana bridge, 15 specimens of Luiz I bridge, 10 specimens of Trezói bridge and 32 specimens of Fão bridge. The tests with the strain ratio equals to -1 (section 2.5.4, Figure 16) were performed on Viana, Luiz I and Trezói bridge specimens and 14 specimens of Fão bridge. The remaining 18 specimens of Fão bridge were tested with a strain ratio equal to 0.

The elastoplastic behavior and the models that are based its calculation, are used to predict the fatigue strength or resistance, to ensure the fatigue life. The models are based on the assumption of an elastic linear behavior. (Correia, 2008)

The limit fatigue stress of the material is a function of the main stress, which the material is submitted. And it is presented in a S-N curve, previously explained in the section 2.4.1. (Correia, 2008)

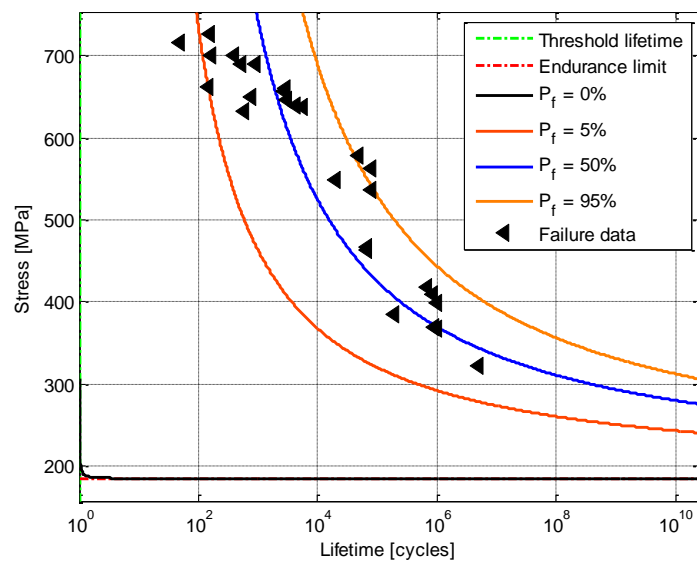
4.1 Stress-life test

The stress-life method relays on the stress amplitude to evaluate the number of cycles to failure. The method is normally used for high cycle fatigue. In low cycle fatigue the stress-life relation becomes nonlinear. (Correia, 2014)

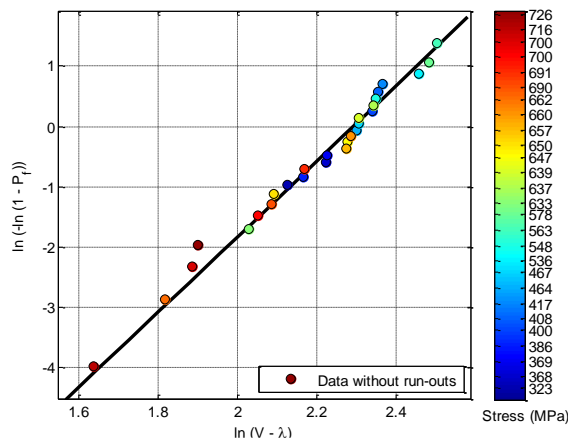
4.1.1 Stress test on Viana bridge material - Strain ratio equal 0

Figure 49 shows the results on the fatigue life of Viana bridge specimens following the log-normal distribution and the log-normal distribution parameters (i.e. the logarithmic values and standard deviation of fatigue lives at each equivalent stress amplitude). (Xiulin Zheng, 2005)

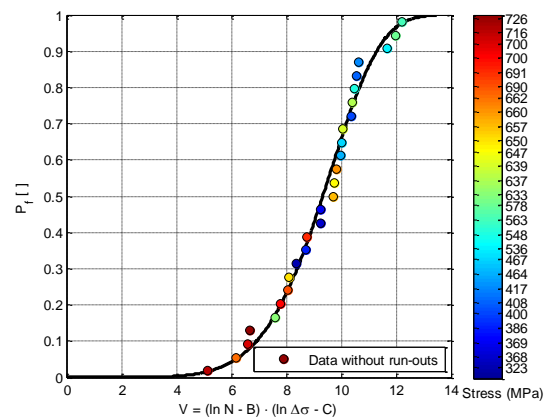
The following graphics Figure 49 where drawn considering the data presented in Appendix A - Table 31. All the graphics in the present section were developed with the software ProFatigue®.



(a)



(b)



(c)

Figure 49 – (a) S-N Curve of Viana bridge material stress test ($R_{\epsilon}=-1$), (b) Probabilistic paper of the material behavior of Viana bridge; stress test ($R_{\epsilon}=-1$), (c) Weibull distribution Viana bridge material; stress test ($R_{\epsilon}=-1$)

In the study of the stress-life and the following strain-life (item 4.2) and SWT-life (item 4.3) the tables (Table 13) with the constants β , B, C, Δ and λ represents the normalizing process explained in section 3.3.1.1. The parameters obtained are: β , the shape parameter of the Weibull model, B, the linear regression parameter (related to the lifetime), C, the material constant (related to endurance limit) and λ , the threshold parameter of the Weibull model.

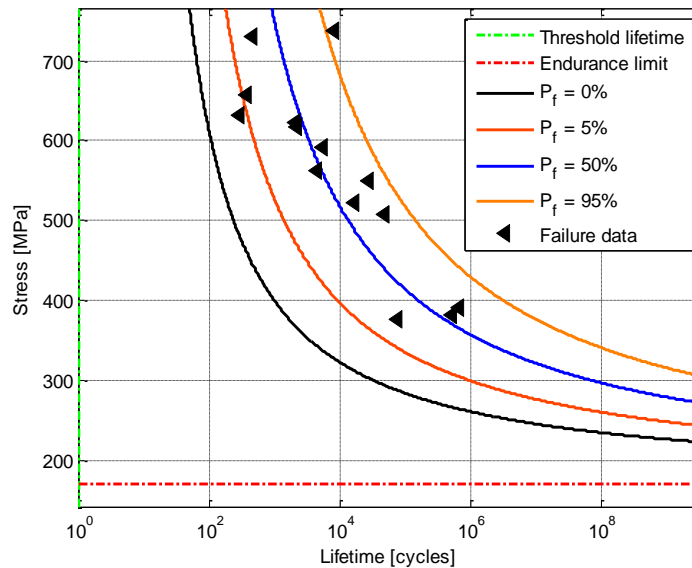
Table 13 - Material parameters estimated from the stress test results of Viana bridge

β	B	C	Δ	λ
6,4	0	-7,99	9,26	5,59
(1 cycle)				

4.1.2 Stress test on Fão bridge material

4.1.2.1 Study carried out with strain ratio equal 0

The graphics included in Figure 50 where obtained with the data presented in the Appendix A - Table 32.



(a)

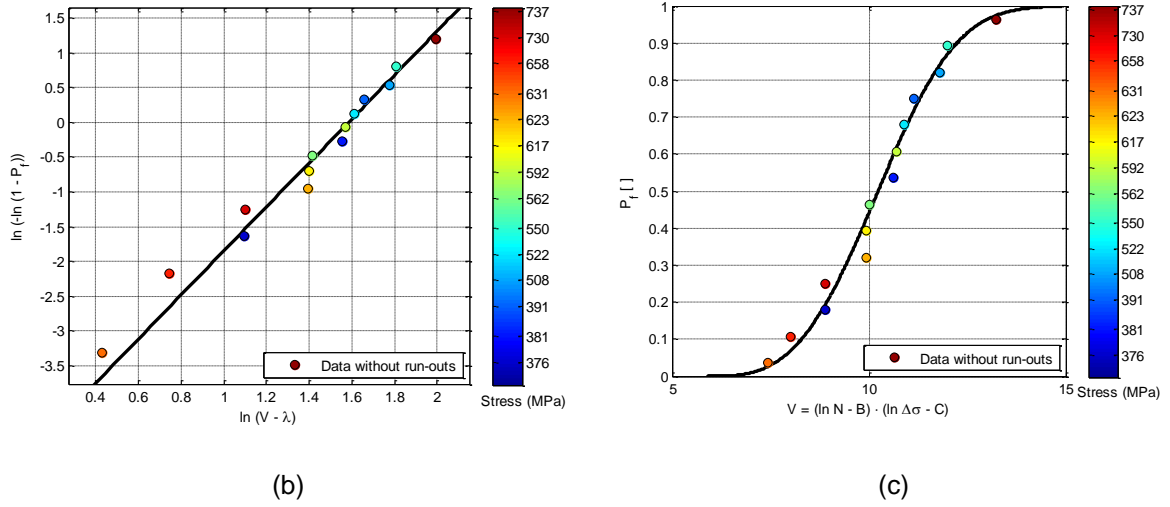


Figure 50 – (a) S-N Curve of Fão bridge material stress test ($R_{\epsilon} = 0$), (b) - Probabilistic paper of the material behavior of Fão bridge; stress test ($R_{\epsilon} = 0$), (c) Weibull material distribution on Fão bridge; stress test ($R_{\epsilon} = 0$)

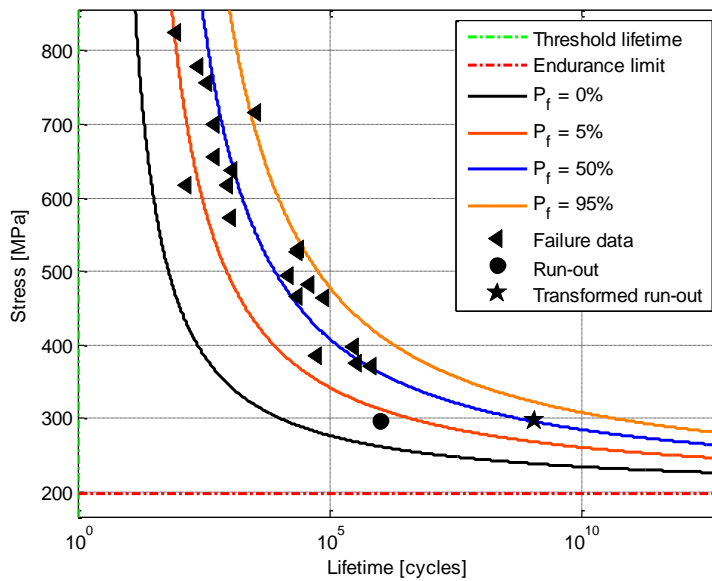
With the graphics presented in Figure 50 it was possible to calculate the parameters included in Table 14 which will be used in the comparison presented in section 4.4.

Table 14 - Material parameters estimated from the stress test results of Fão bridge ($R_{\epsilon} = 0$)

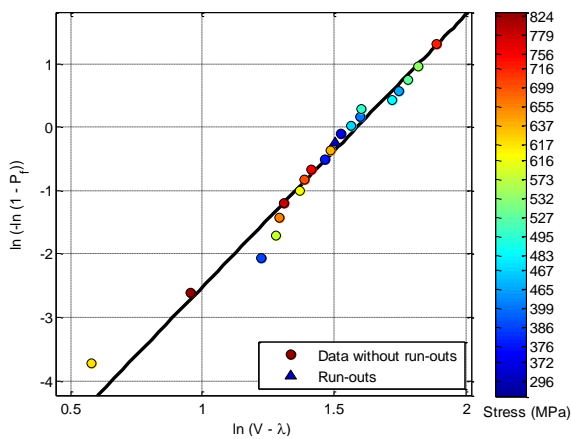
β	B	C	Δ	λ
3,17	0	5,14	4,87	5,89
	(1 cycle)	(170,36 MPa)		

4.1.2.2 Study carried out with strain ratio equal -1

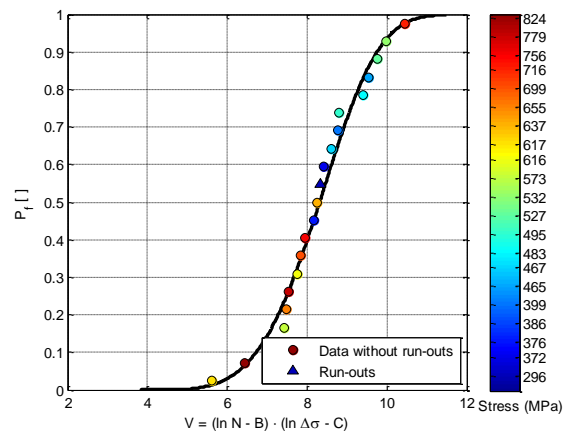
The graphics included in Figure 51 **Error! Reference source not found.** where obtained with the data presented in the Appendix A - Table 33.



(a)



(b)



(c)

Figure 51 – (a) S-N Curve of Fão bridge material stress test ($R_\varepsilon=-1$), (b) Probabilistic paper of the material behavior of Fão bridge; stress test ($R_\varepsilon=-1$), (c) Weibull material distribution on Fão bridge; stress test ($R_\varepsilon=-1$)

With the graphics presented in Figure 51 it was possible to calculate the parameters included in

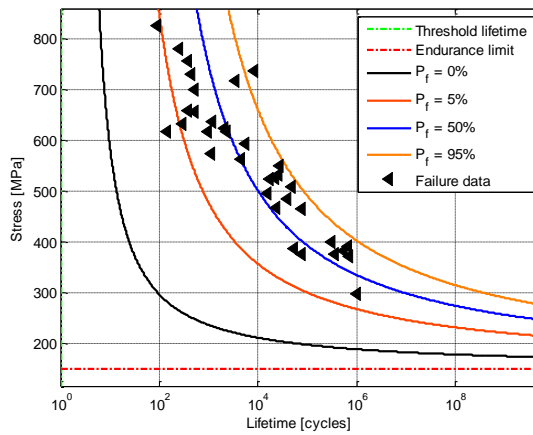
Table 15 which will be used in the comparison presented in section 4.4.

Table 15 - Material parameters estimated from the stress test results of Fão bridge ($R_e = -1$)

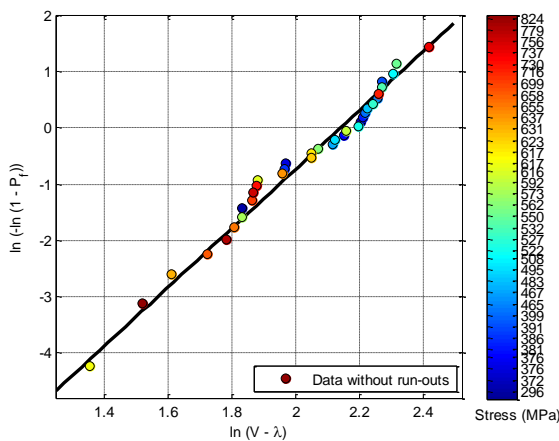
β	B	C	Δ	λ
4,31	0	5,29	4,88	3,83
	(1 cycle)	(198,85 MPa)		

4.1.2.3 Study carried out with strain ratio equal 0 and -1

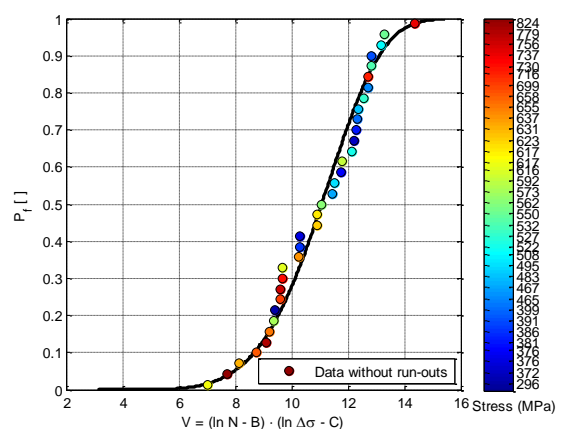
The graphics included in Figure 52 were obtained from the data presented in the Appendix A - Table 34



(a)



(b)



(c)

Figure 52 – (a) S-N Curve of Fão bridge material stress test ($R_\epsilon=0$ and $R_\epsilon=-1$), (b) Probabilistic paper of the material behavior of Fão bridge; stress test ($R_\epsilon=0$ and $R_\epsilon=-1$), (c) Weibull material distribution on Fão bridge; stress test ($R_\epsilon=0$ and $R_\epsilon=-1$)

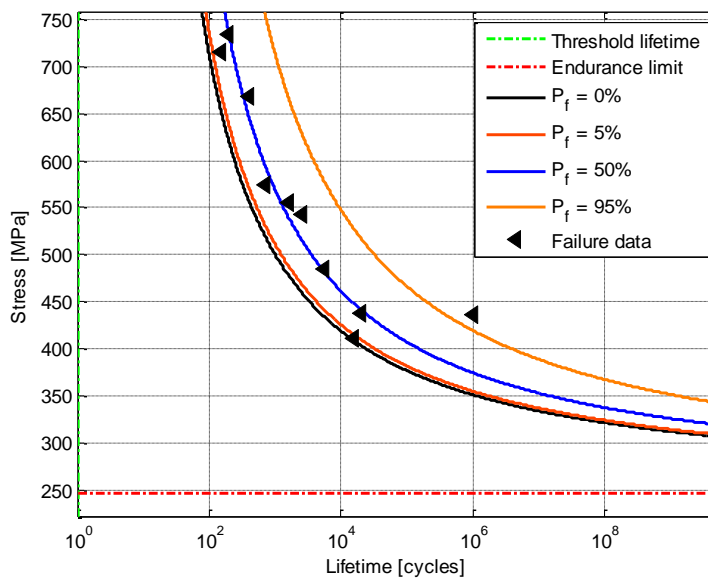
With the graphics presented in Figure 52 it was possible to calculate the parameters included in Table 16 which will be used in the comparison presented in section 4.4.

Table 16 - Material parameters estimated from the stress test results of Fão bridge ($R_\epsilon=0$ and $R_\epsilon=-1$)

β	B	C	Δ	λ
5,25	0	5,01	8,51	3,13
	(1 cycle)	(150,23 MPa)		

4.1.3 Analysis on the material behavior of Trezói bridge through stress test - strain ratio equal -1

The graphics included in Figure 53 **Error! Reference source not found.** where obtained from the data presented in the Appendix A - Table 35



(a)

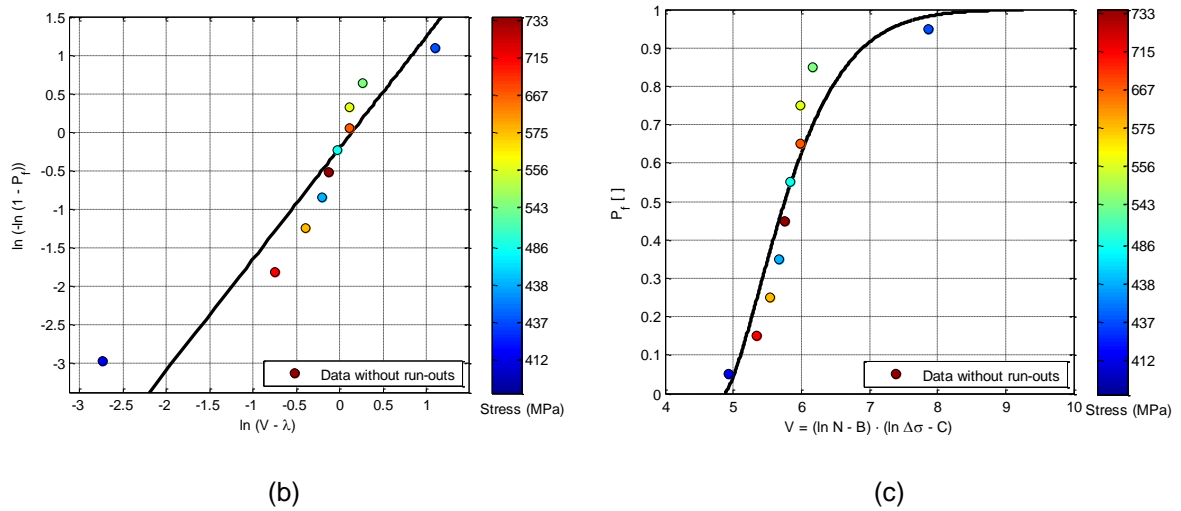


Figure 53 – (a) S-N Curve of Trezói bridge material stress test ($R_{\epsilon}=-1$), (b) Probabilistic paper of the material behavior of Trezói bridge; stress test ($R_{\epsilon}=-1$), (c) Weibull material distribution on Trezói bridge; stress test ($R_{\epsilon}=-1$)

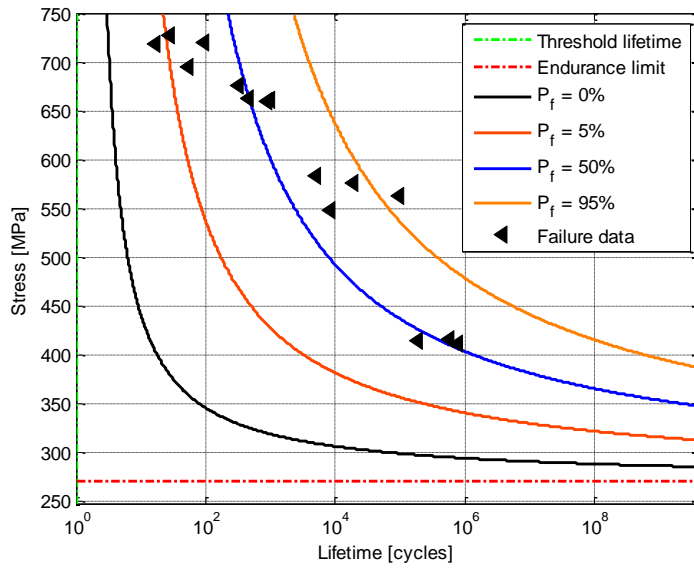
With the graphics presented in Figure 53 **Error! Reference source not found.** it was possible to calculate the parameters included in Table 17 which will be used in the comparison presented in section 4.4

Table 17 - Material parameters estimated from the stress test results of Trezói bridge ($R_{\epsilon} = -1$)

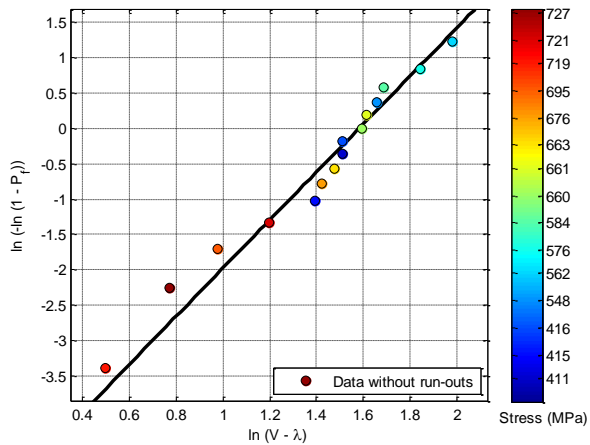
β	B	C	Δ	λ
1,45	0	5,51	1,15	4,87
	(1 cycle)	(247,41 MPa)		

4.1.4 Analysis on the material behavior of Luiz I bridge through stress test - strain ratio equal -1

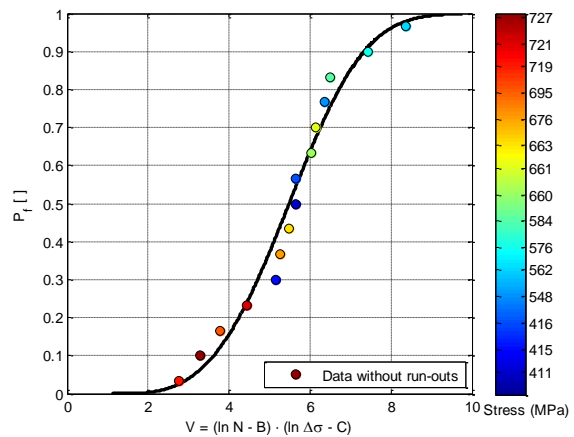
The graphics included in Figure 54 where obtained from the data presented in the Appendix A - Table 36



(a)



(b)



(c)

Figure 54 – (a) S-N Curve of Luiz I bridge material stress test ($R_{\varepsilon}=-1$), (b) Probabilistic paper of the material behavior of Luiz I bridge; stress test ($R_{\varepsilon}=-1$), (c) Weibull material distribution of Luiz I bridge, stress test ($R_{\varepsilon}=-1$)

With the graphics presented in Figure 54 **Error! Reference source not found.** it was possible to the parameters included in Table 18 which will be used in the comparison presented in section 4.4.

Table 18 - Material parameters estimated from the stress test results of Luiz I bridge ($R_{\varepsilon}= -1$)

β	B	C	Δ	λ
3,39	0	5,60	4,86	1,12
	(1 cycle)	(271,48 MPa)		

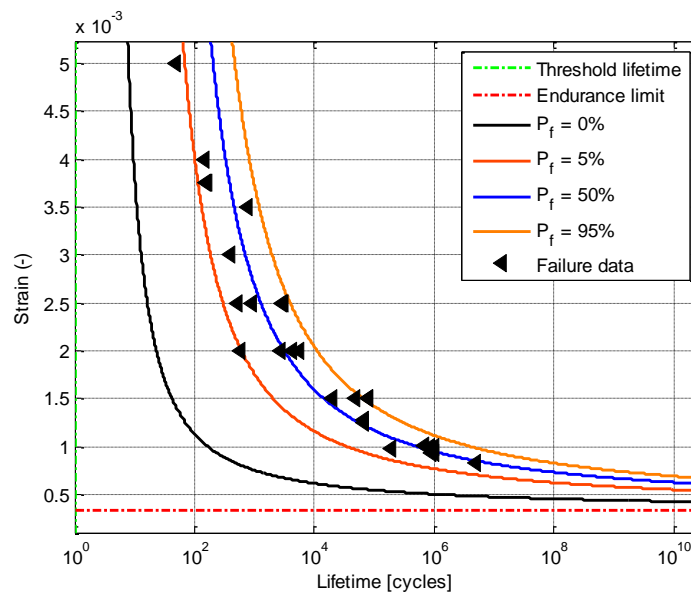
4.2 Strain-life test

The strain-life method is applied to the calculation of fatigue crack initiation for the crack growth investigation by computing the number of cycles that are necessary to initiate a macro-crack. The relations of the type of strain-life can also account for the effects of elastic and plastic deformations.

All the graphics in the present section were developed with the software ProFatigue®.

4.2.1 Material behavior Viana bridge through strain test - Study carried out with strain ratio equal -1

The graphics included in Figure 55 were obtained from the data presented in the Appendix A - Table 37



(a)

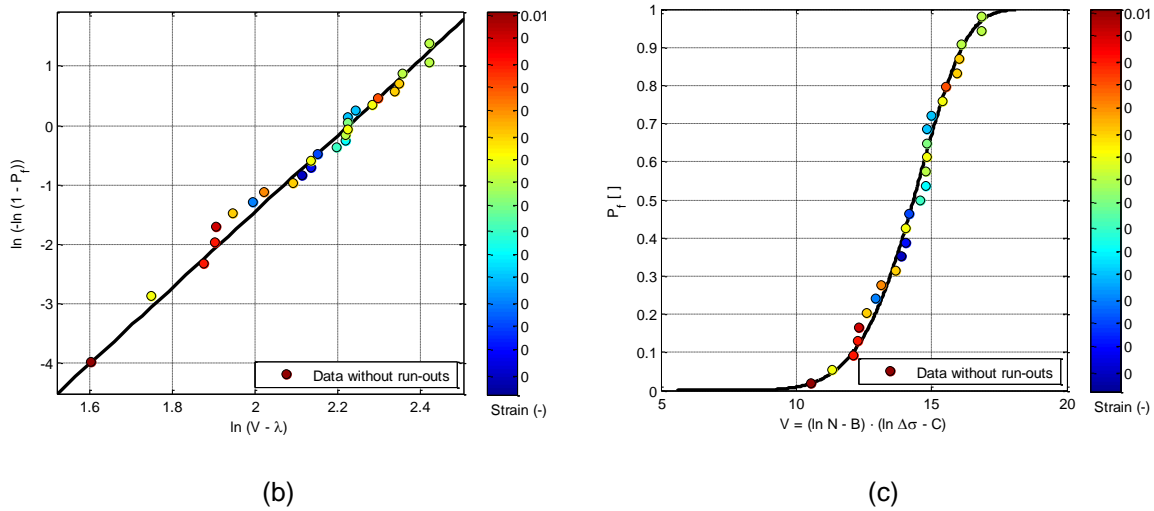


Figure 55 – (a) S-N Curve of Viana bridge material strain test ($R_{\epsilon}=-1$), (b) Probabilistic paper of the material behavior of Viana bridge; strain test ($R_{\epsilon}=-1$), (c) Weibull material distribution of Viana bridge, strain test ($R_{\epsilon}=-1$)

With the graphics presented in Figure 55 it was possible to calculate the parameters included in Table 19 which will be used in the comparison presented in section 4.4.

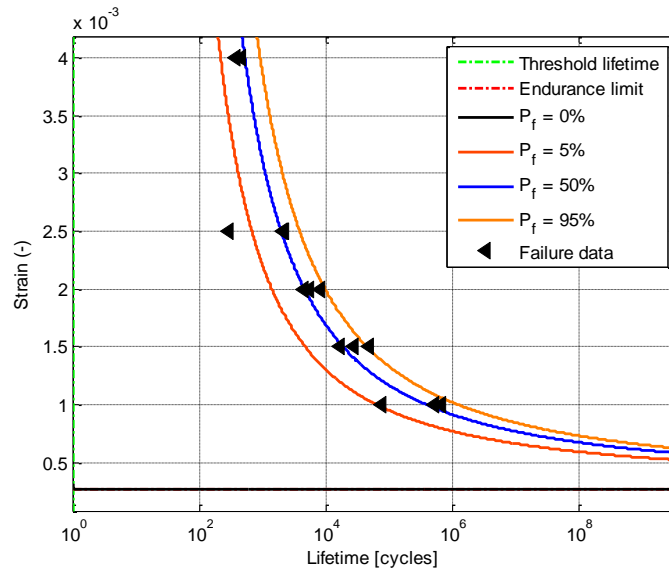
Table 19 - Estimated material parameters to stain test for Viana's bridge ($R_{\epsilon} = -1$)

β	B	C	Δ	λ
6,40	0	-7,99	9,26	5,59
	(1 cycle)	(0,0MPa)		

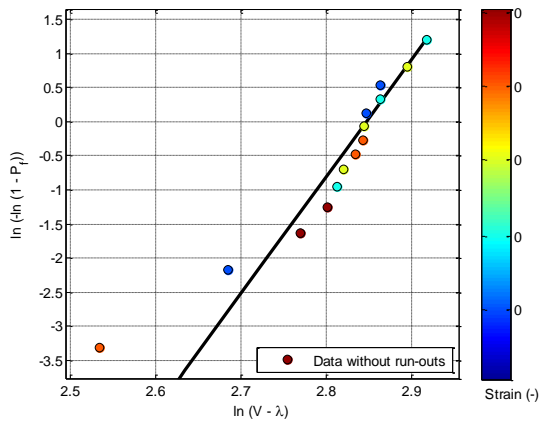
4.2.2 Analysis on the material behavior of Fão bridge through strain test

4.2.2.1 Study carried out with strain ratio equal 0

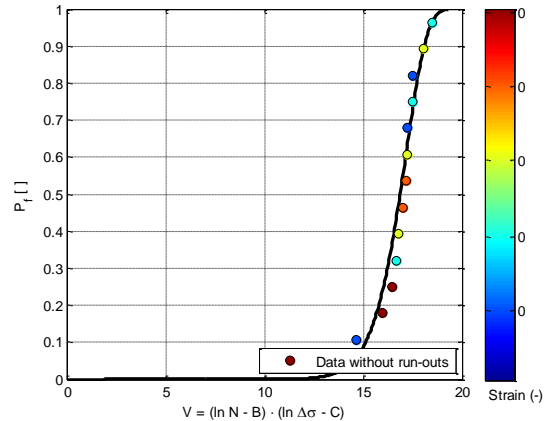
The graphics included in Figure 56 where obtained from the data presented in the Appendix A - Table 38



(a)



(b)



(c)

Figure 56 – (a) S-N Curve of Fão bridge material strain test ($R_\epsilon=0$), (b) Probabilistic paper of the material behavior of Fão bridge; strain test ($R_\epsilon=0$), (c) Weibull material distribution of Fão bridge, strain test ($R_\epsilon=0$)

With the graphics presented in Figure 56 it was possible to calculate the parameters included in

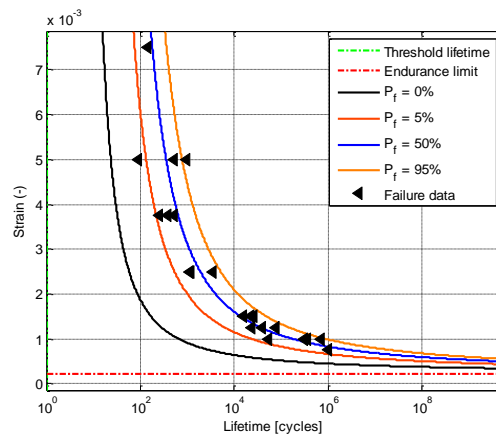
Table 20 which will be used in the comparison presented in section 4.4.

Table 20 - Material parameters estimated from the stress test results of Fão bridge ($R_\sigma = 0$)

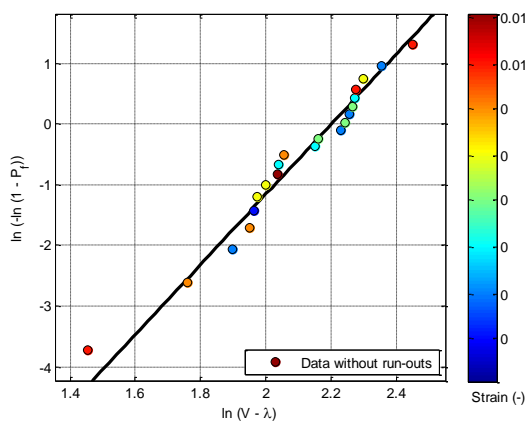
β	B	C	Δ	λ
17,20	0	-8,21	17,23	0,0
	(1 cycle)	(0,0MPa)		

4.2.2.2 Study carried out with strain ratio equal -1

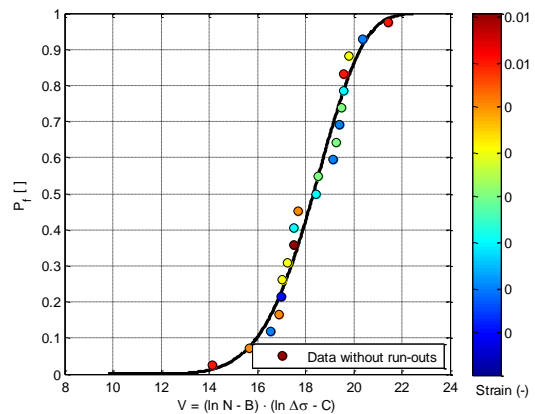
To following graphics Figure 57 where obtain through the data presented in the Appendix A - Table 39



(a)



(b)



(c)

Figure 57 – (a) Curve of Fão bridge material strain test ($R_\epsilon=-1$), (b) Probabilistic paper of the material behavior of Fão bridge; strain test ($R_\epsilon=-1$), (c) Weibull material distribution of Fão bridge, strain test ($R_\epsilon=-1$)

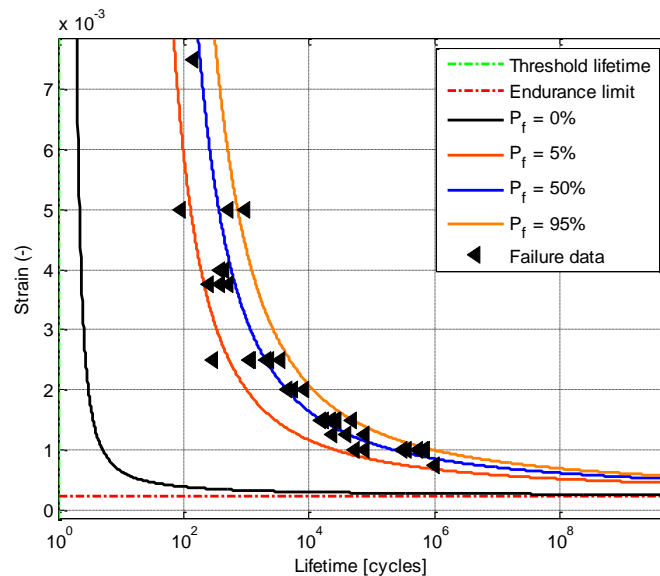
With the graphics presented in Figure 57 it was possible to calculate the parameters included in Table 21 which will be used in the comparison presented in section 4.4.

Table 21 - Material parameters estimated from the stress test results of Fão bridge ($R_\epsilon = -1$)

β	B	C	Δ	λ
5,79	0	-8,21	9,02	9,86
	(1 cycle)	(0,0MPa)		

4.2.2.3 Study carried out with strain ratio equal 0 and -1

To graphics included in Figure 58 where obtained through the data presented in the Appendix A - Table 40



(a)

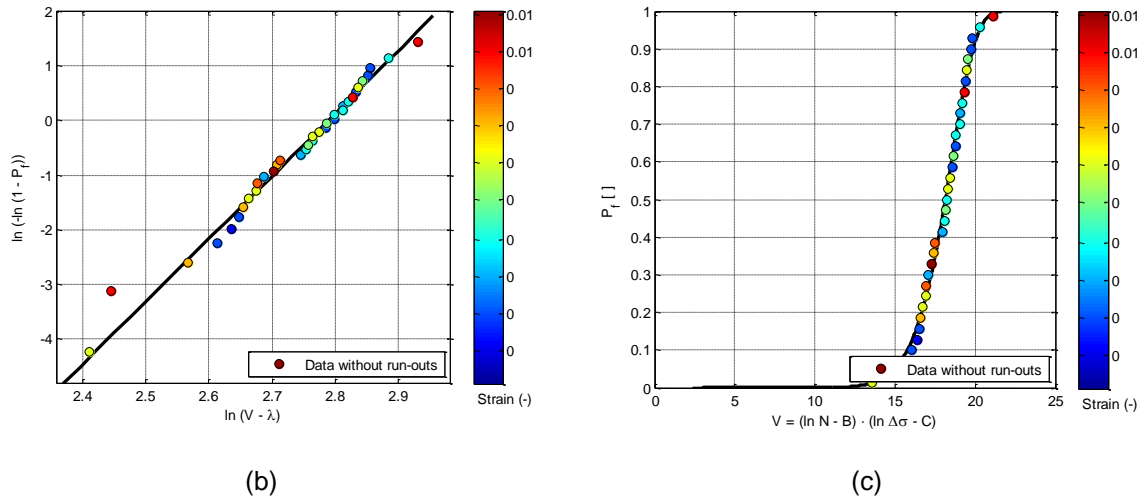


Figure 58 – (a) S-N Curve of Fão bridge material strain test ($R_\varepsilon=0$ and $R_\varepsilon=-1$), (b) Probabilistic paper of the material behavior of Fão bridge; strain test ($R_\varepsilon=0$ and $R_\varepsilon=-1$), (c) Weibull material distribution of Fão bridge, strain test ($R_\varepsilon=0$ and $R_\varepsilon=-1$)

With the graphics presented in Figure 58 **Error! Reference source not found.** it was possible to calculate the parameters included in Table 22 which will be used in the comparison presented in section 4.4.

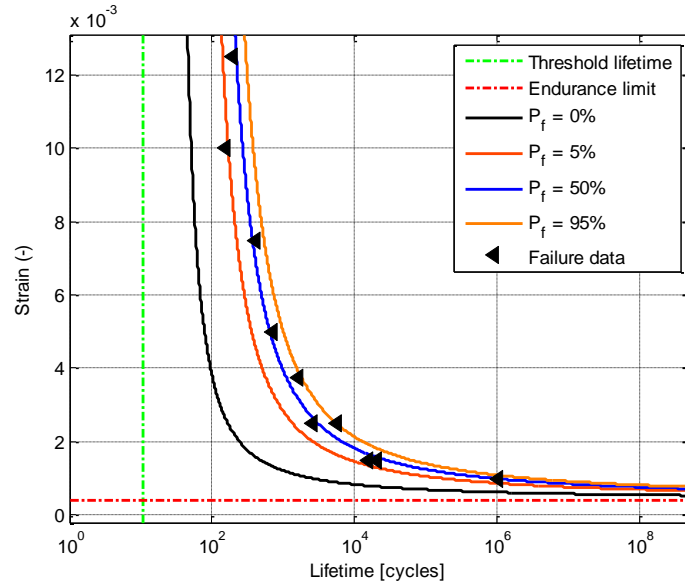
Table 22 - Material parameters estimated from the stress test results of Fão bridge ($R_\varepsilon=0$ and $R_\varepsilon=-1$)

β	B	C	Δ	λ
11,52	0	-8,38	16,25	2,40
	(1 cycle)	(0,0MPa)		

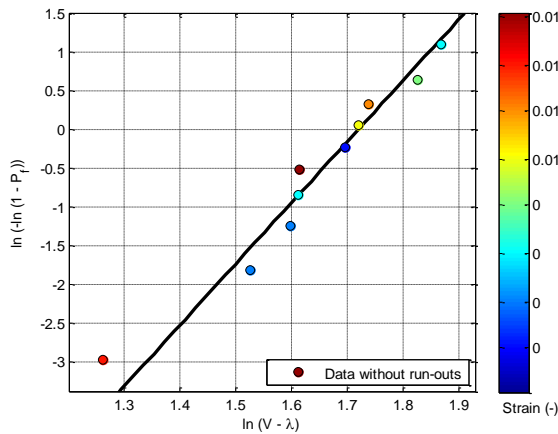
4.2.3 Analysis on the material behavior of Trezói bridge through strain test - strain ratio equal -1

The graphics included in Figure 59 were obtained from the data presented in the Appendix A -

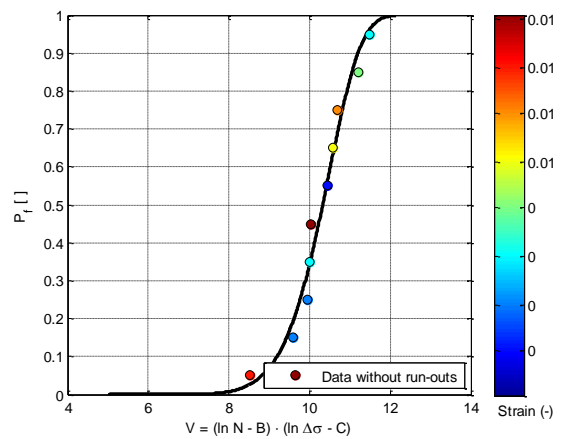
Table 41



(a)



(b)



(c)

Figure 59 – (a) S-N Curve of Trezói bridge material strain test ($R_{\varepsilon}=-1$), (b) Probabilistic paper of the material behavior of Trezói bridge; strain test ($R_{\varepsilon}=-1$), (c) Weibull material distribution of Trezói bridge, strain test ($R_{\varepsilon}=-1$)

With the graphics presented in Figure 59 it was possible to calculate the parameters included in

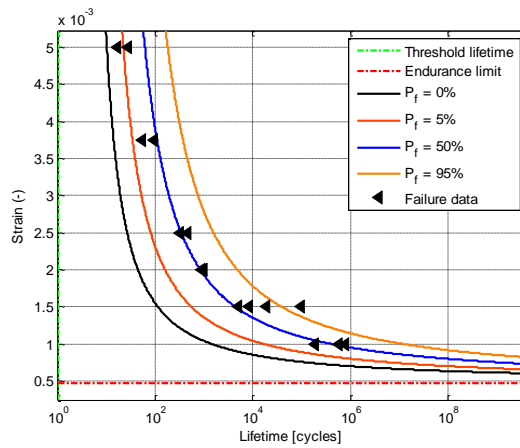
Table 23 which will be used in the comparison presented in section 4.4.

Table 23 - Material parameters estimated from the stress test results of Trezói bridge ($R_\epsilon=-1$)

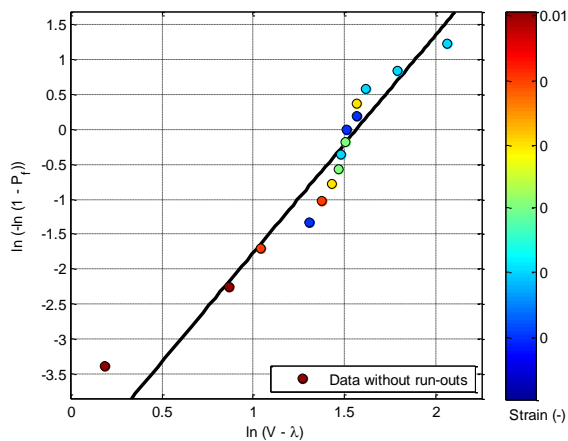
β	B	C	Δ	λ
7,90	2,38	-7,82	5,58	5,0
	(10 cycle)	(0,0MPa)		

4.2.4 Analysis on the material behavior Luiz I bridge through strain test - strain ratio equal -1

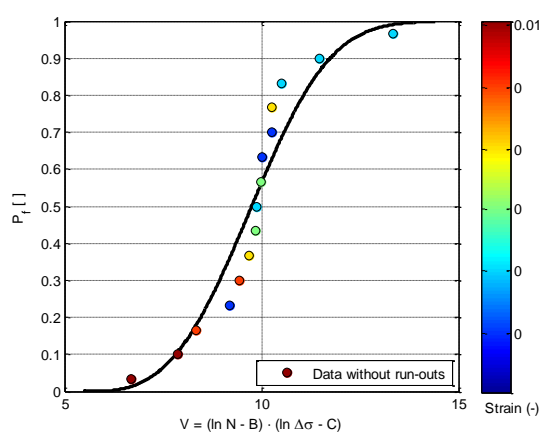
The graphics included in Figure 60 **Error! Reference source not found.** where obtained from the data presented in the Appendix A - Table 42



(a)



(b)



(c)

Figure 60 – (a) S-N Curve of Luiz I bridge material strain test ($R_\epsilon=-1$), (b) Probabilistic paper of the material behavior of Luiz I bridge; strain test ($R_\epsilon=-1$), (c) Weibull material distribution of Luiz I bridge, strain test ($R_\epsilon=-1$)

With the graphics presented in Figure 60 it was possible to calculate the parameters included in Table 24 which will be used in the comparison presented in section 4.4.

Table 24 - Material parameters estimated from the stress test results of Luiz I bridge ($R_\epsilon=-1$)

β	B	C	Δ	λ
3,12	0,0	-7,66	4,78	5,50
	(1 cycle)	(0,0MPa)		

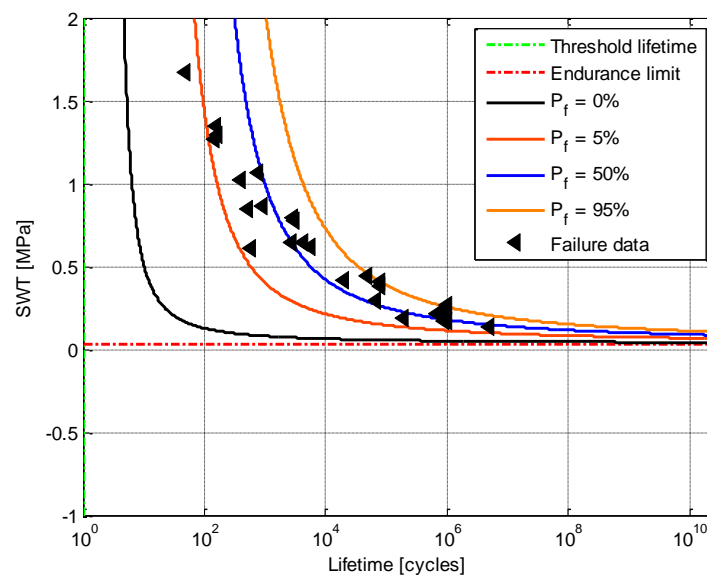
4.3 Smith – Watson – Topper - life test (SWT)

The Smith-Watson-Topper model is a deterministic model and it is utilized to demonstrate the average fatigue behavior of the bridge materials as showed in the available data.

All the graphics presented in the current section were developed with the software ProFatigue®.

4.3.1 Analysis on the material behavior Viana bridge through SWT test - strain ratio equal -1

The graphics included in Figure 61 were obtained from the data presented in the Appendix A - Table 43



(a)

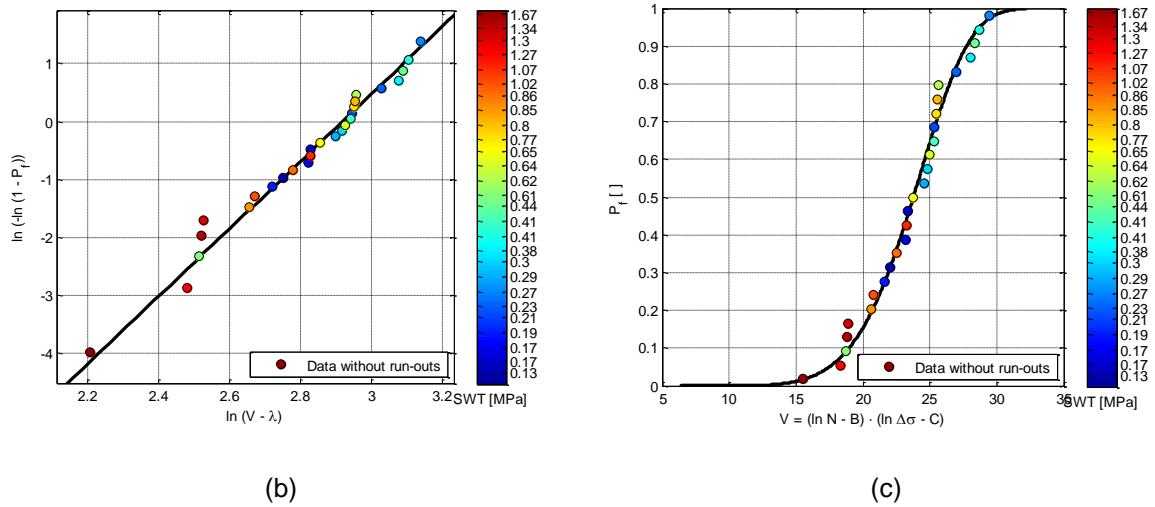


Figure 61 – (a) S-N Curve of Viana bridge material SWT test ($R_{\epsilon}=-1$), (b) Probabilistic paper of the material behavior of Viana bridge; SWT test ($R_{\epsilon}=-1$), (c) Weibull material distribution of Viana bridge, SWT test ($R_{\epsilon}=-1$)

With the graphics presented in Figure 61 it was possible to calculate the parameters included in Table 25 which will be used in the comparison presented in section 4.4.

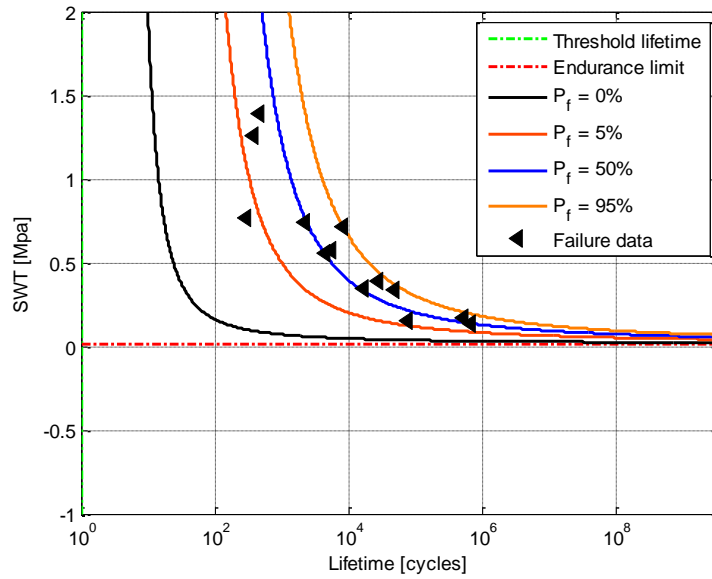
Table 25 - Material parameters estimated from the SWT test of Viana bridge ($R_{\epsilon}=-1$)

β	B	C	Δ	λ
5,38	0,0	-3,44	18,51	6,39
	(1 cycle)	(0,03MPa)		

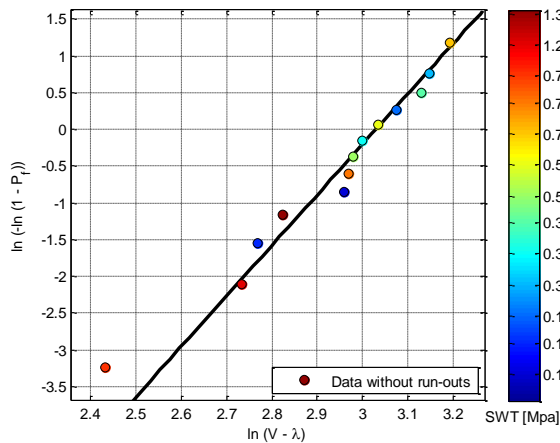
4.3.2 Analysis on the material behavior Viana bridge through SWT test

4.3.2.1 Study carried out with strain ratio equal 0

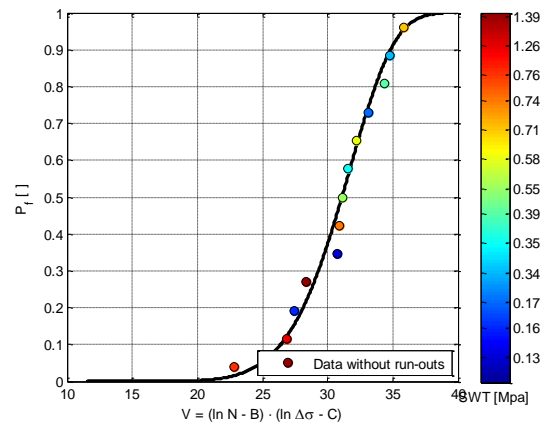
The graphics included in Figure 62 were obtained from the data presented in the Appendix A - Table 44



(a)



(b)



(c)

Figure 62 – (a) S-N Curve of Fão bridge material SWT test ($R_\epsilon=0$), (b) - Probabilistic paper of the material behavior of Fão bridge; SWT test ($R_\epsilon=0$), (c) Weibull material distribution of Fão bridge, SWT test ($R_\epsilon=0$)

With the graphics presented in Figure 62 it was possible to calculate the parameters included in

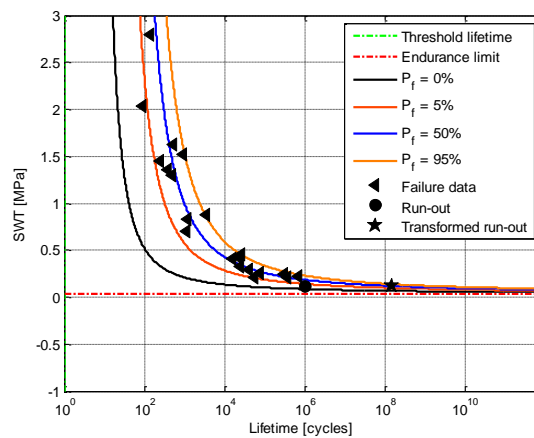
Table 26 which will be used in the comparison presented in section 4.4.

Table 26 - Material parameters estimated from the SWT test of Fão bridge ($R_\epsilon=0$)

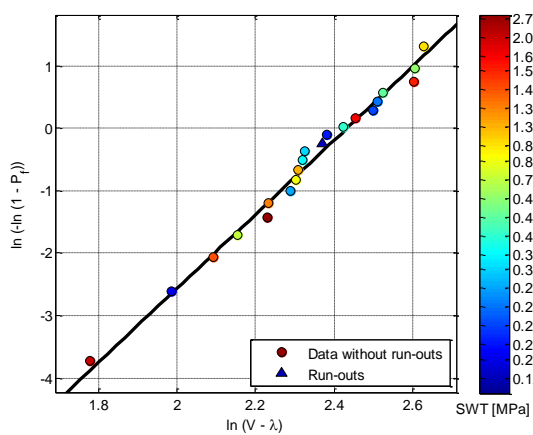
β	B	C	Δ	λ
6,88	0,0	-4,30	20,69	11,47
	(1 cycle)	(0,01MPa)		

4.3.2.2 Study carried out with strain ratio equal -1

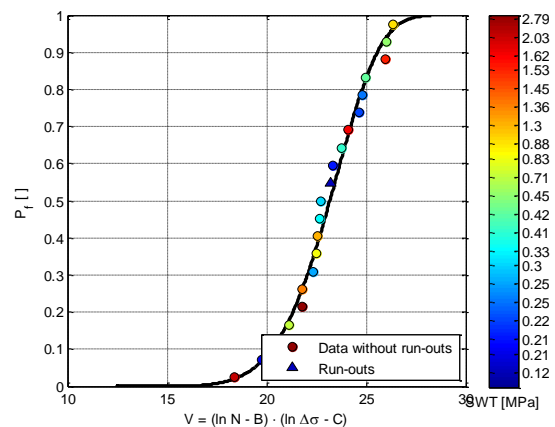
The graphics included in Figure 63 where obtained from the data presented in the Appendix A - Table 45



(a)



(b)



(c)

Figure 63 – (a) S-N Curve of Fão bridge, based on material SWT test ($R_\epsilon=-1$), (b) Probabilistic paper of the material behavior of Fão bridge; SWT test ($R_\epsilon=-1$), (c) Weibull material distribution on Fão bridge1, SWT test ($R_\epsilon=-1$)

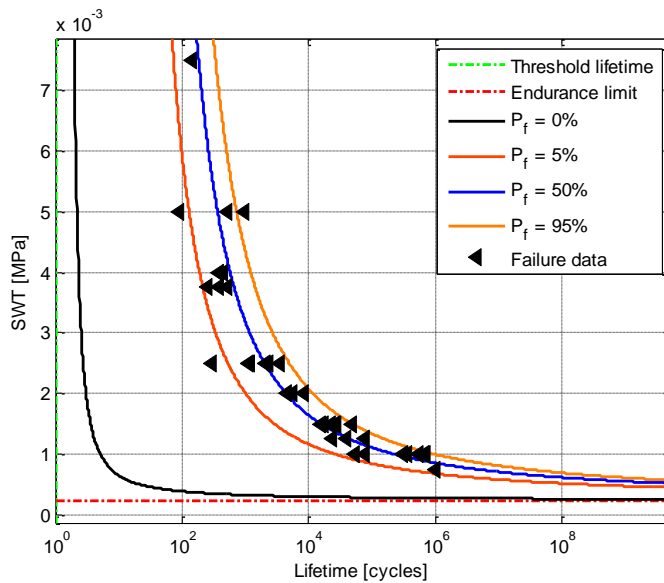
With the graphics presented in Figure 63 it was possible to calculate the parameters included in Table 27 which will be used in the comparison presented in section 4.4.

Table 27 - Material parameters estimated from the SWT test of Fão bridge ($R_\epsilon=-1$)

β	B	C	Δ	λ
5,95	0,0	-3,36	11,37	12,49
	(1 cycle)	(0,03MPa)		

4.3.2.3 Study carried out with strain ratio equal 0 and -1

The graphics included in Figure 64 where obtained from the data presented in the Appendix A - Table 46



(a)

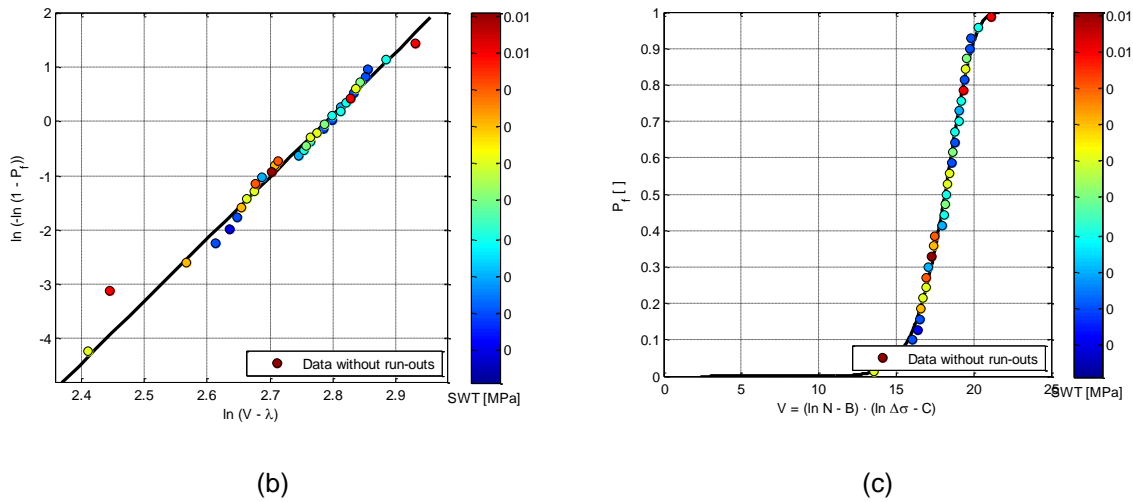


Figure 64 – (a) S-N Curve of Fão bridge, based on material SWT test ($R_\epsilon=0$ and $R_\epsilon=-1$), (b) Probabilistic paper of the material behavior of Fão bridge; SWT test ($R_\epsilon=0$ and $R_\epsilon=-1$), Weibull material distribution on Fão bridge, SWT test ($R_\epsilon=0$ and $R_\epsilon=-1$)

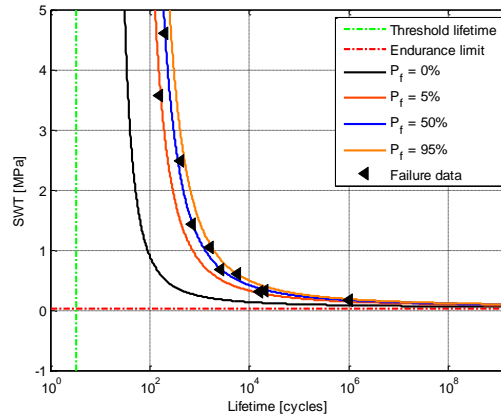
With the graphics presented in Figure 64 it was possible to calculate the parameters included in Table 28 which will be used in the comparison presented in section 4.4.

Table 28 - Material parameters estimated from the SWT test of Fão bridge ($R_\epsilon=0$ and $R_\epsilon=-1$)

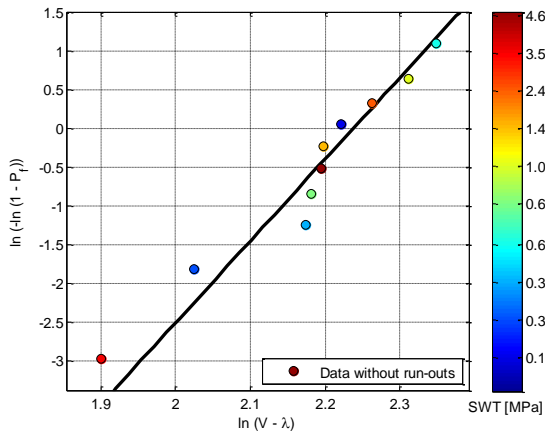
β	B	C	Δ	λ
11,52	0,0	-8,38	16,25	2,40
	(1 cycle)	(0,0MPa)		

4.3.3 Analysis on the material behavior of Trezói bridge through SWT test - strain ratio equal - 1

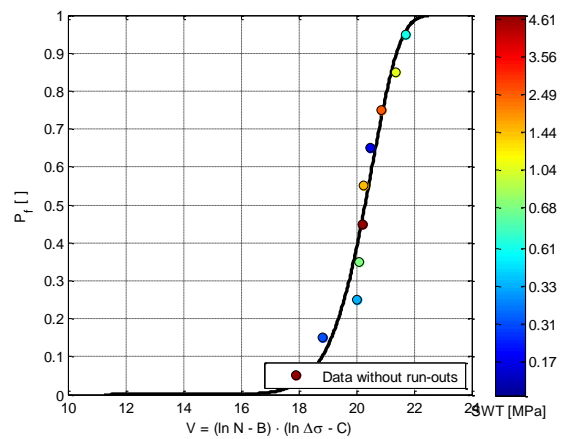
The graphics included in Figure 65 were obtained from the data presented in the Appendix A - Table 47



(a)



(b)



(c)

Figure 65 – (a) S-N Curve of Trezói's bridge, based on material SWT test ($R_{\epsilon}=-1$), (b) Probabilistic paper of the material behavior of Trezói bridge; SWT test ($R_{\epsilon}=-1$), (c) Weibull material distribution Trezói bridge, SWT test ($R_{\epsilon}=-1$)

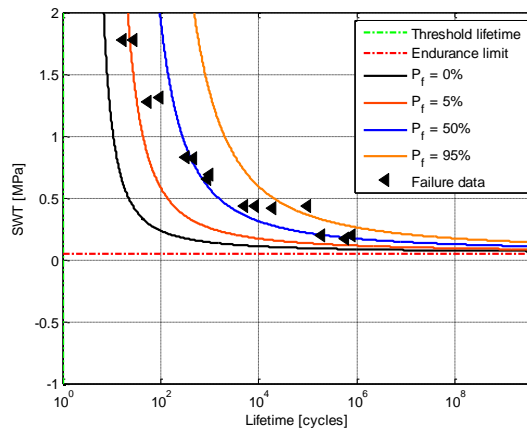
With the graphics presented in Figure 65 it was possible to calculate the parameters included in Table 29 which will be used in the comparison presented in section 4.4.

Table 29 - Material parameters estimated from the SWT test of Trezói bridge ($R_{\epsilon}=-1$)

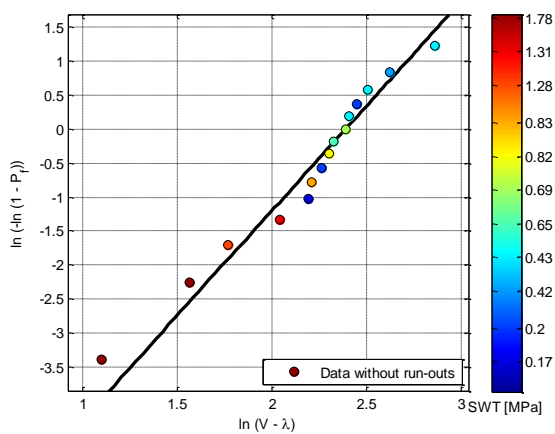
β	B	C	Δ	λ
10,52	1,19	-3,40	9,37	11,25
	(3 cycle)	(0,03MPa)		

4.3.4 Analysis on the material behavior of Luiz I bridge through SWT test - strain ratio equal - 1

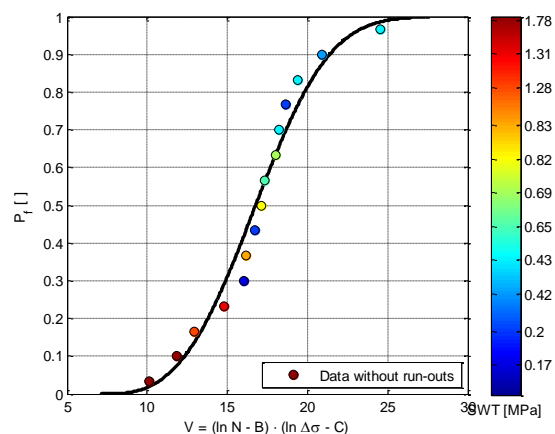
The graphics included in Figure 66 were obtained from the data presented in the Appendix A - Table 48



(a)



(b)



(c)

Figure 66 – (a) S-N Curve of Luiz I bridge, based on material SWT test ($R_\varepsilon=-1$), (b) Probabilistic paper of the material behavior of Luiz I bridge; SWT test ($R_\varepsilon=-1$), (c) Weibull material distribution on Luiz I bridge, SWT test ($R_\varepsilon=-1$)

With the graphics presented in Figure 66 it was possible to calculate the parameters included in

Table 30 which will be used in the comparison presented in section 4.4.

Table 30 - Material parameters estimated from the SWT test of Trezói bridge ($R_\epsilon=-1$)

β	B	C	Δ	λ
3,07	0,0	-2,98	10,90	7,09
	(1 cycle)	(0,05MPa)		

4.4 Comparison of the experimental data

In this section, the data obtained with the study of the local approach involving the parameters of stress range, strain amplitude and SWT, corresponding with the lifetime of each bridge material, are compared in order to demonstrate the accuracy of the probabilistic approach.

4.4.1 Statistical analysis based on ASTM E739-91 standard

The results obtained with the comparison following the statistical analysis based on the ASTM E739-91 standard possess a good behaviour, because the mean experimental data is contained in the band between $p=5\%$ and $p=95\%$. That occurs with all three types of fatigue parameters as observed in Figure 67, Figure 68 and Figure 69.

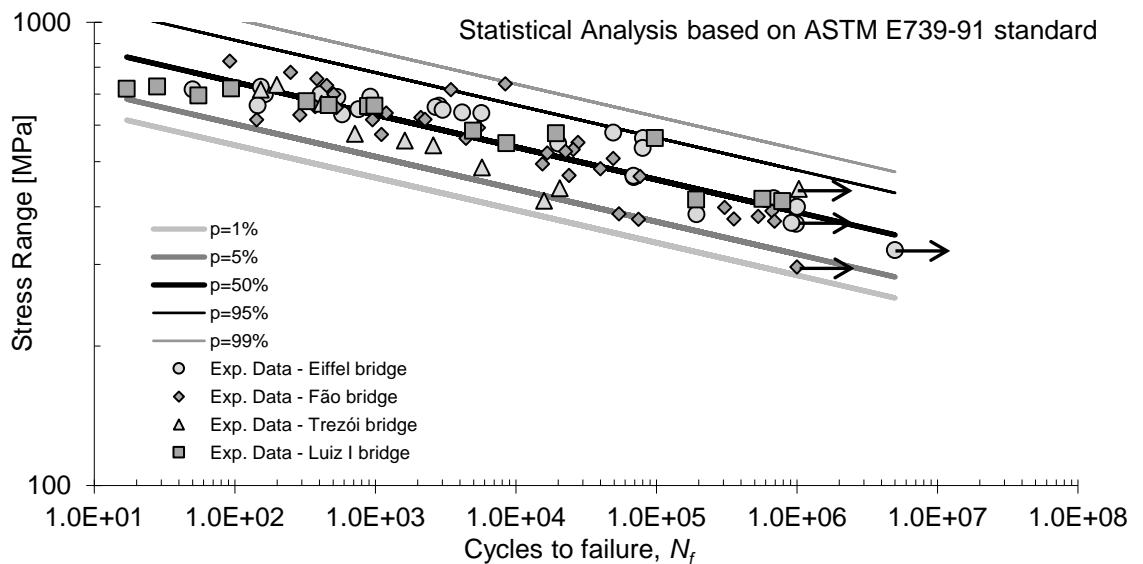


Figure 67 – Statistical analysis on the stress-life of all bridge materials

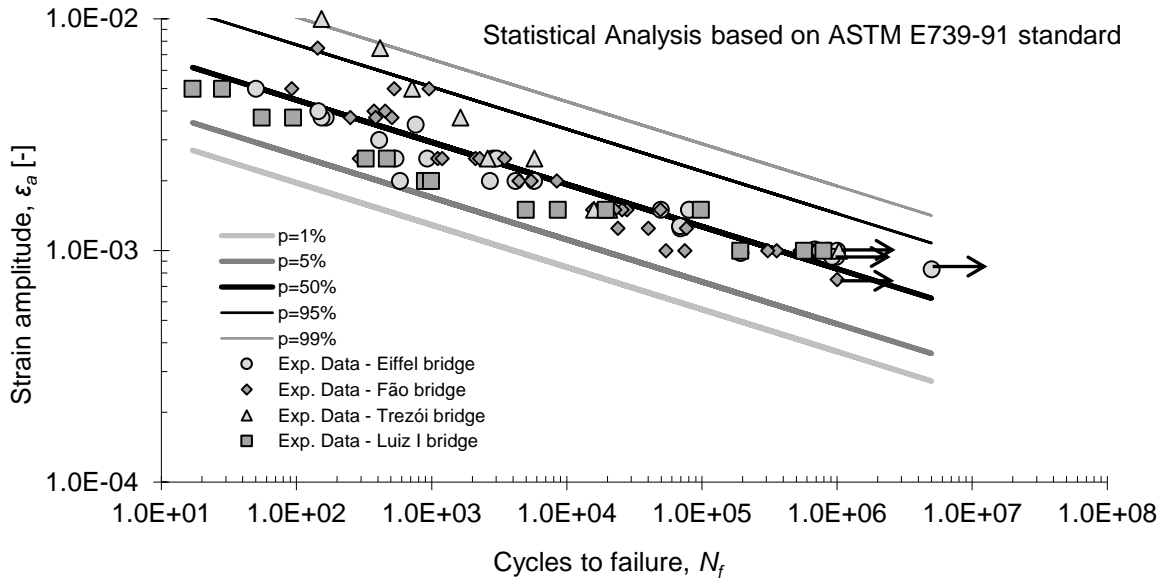


Figure 68 - Statistical analysis on the strain-life of all bridge materials

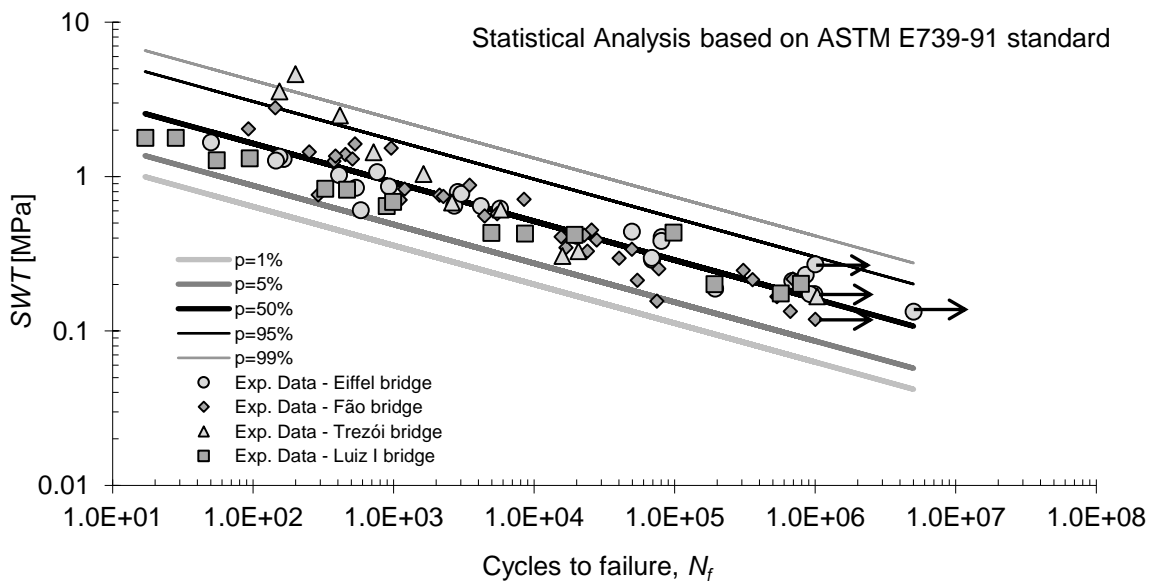


Figure 69 - Statistical analysis on the SWT-life of all bridge materials

4.5 Results from the fatigue damage parameters

As explained in section 2.4.1 the S-N curve is used to calculate the long-life time prediction of the material. The graphics included in Figure 70, Figure 71 and Figure 72 are used to express the influence of the mean stress on the fatigue limit, as well as the fatigue strength for a prescribed fatigue life. The obtained data results appear to possess good behavior, since the experimental data is mostly located above the proposed line (it can be observed in the graphics as the solid black line), hence the involved parameters stress, strain and SWT. Thus, it can be concluded that the material exhibits elastoplastic behavior (section 4).

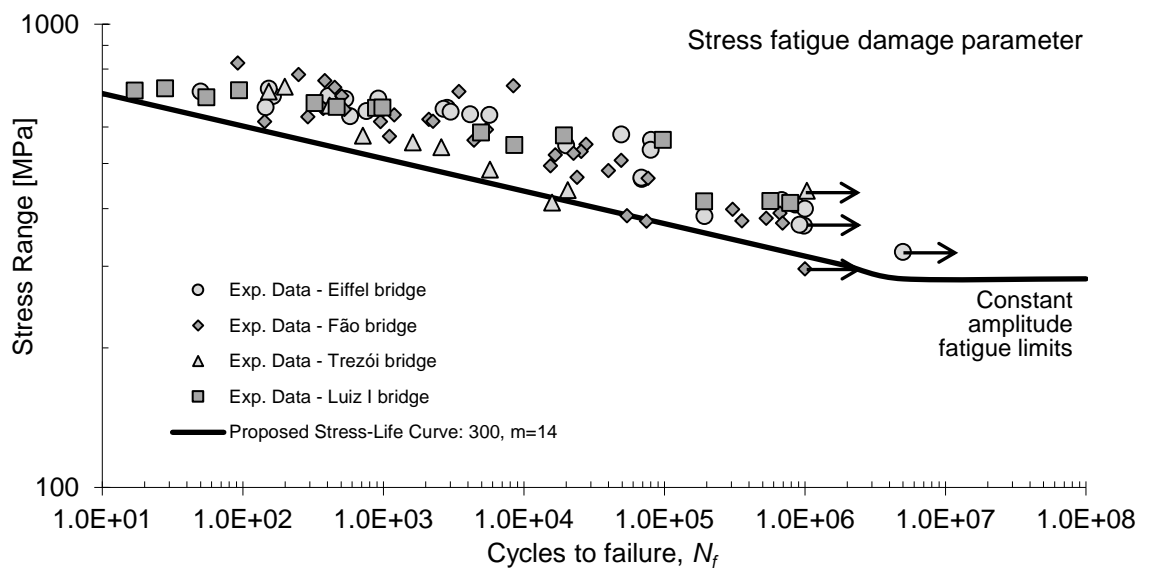


Figure 70 – Stress-life fatigue damage of all bridge materials

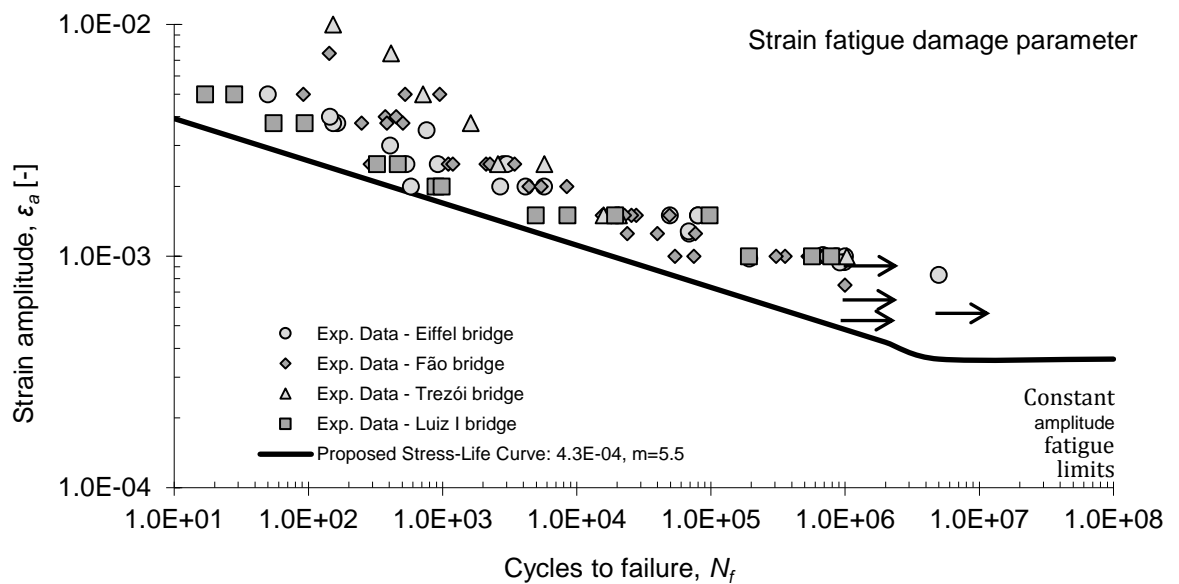


Figure 71 - Strain-life fatigue damage of all bridge materials

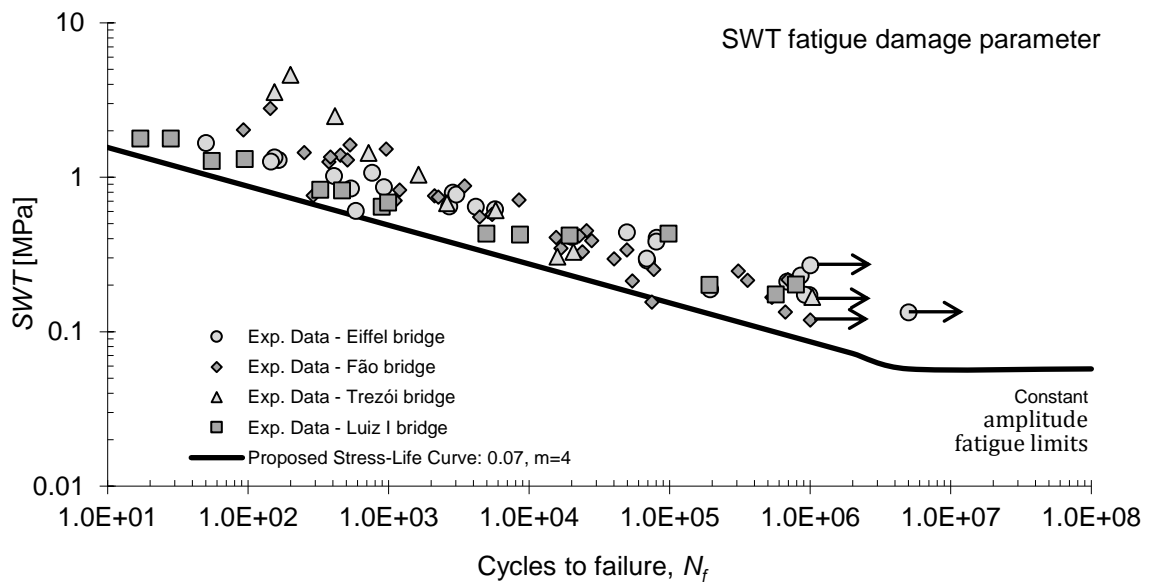


Figure 72 - SWT-life fatigue damage of all bridge materials

5 FINAL REMARKS

Fatigue failures are a concern for steel bridges due to the likelihood of the steel to deteriorate under variable stresses, being recognised as the major cause of failure in metallic bridges. Residual life calculations of existing bridges in operation should take into account fatigue as a progressive damaging mechanism. A consistent residual life prediction should be based on actual fatigue data from bridge members being assessed.

To carry out an assessment of the remaining fatigue life of old steel bridges and crane structures, critical structural details have to be identified and categorized. Surfaces and connection defects are more susceptible to fatigue failure or fatigue crack than interior defects. In the present study, the evaluation and determination of the fatigue phenomena is based on the data collected in experimental tests performed on specimens collected from old metallic bridges, in Portugal. Since it was not practicable to test a full-scale specimen member or component of the bridge in laboratory, mathematical methodologies were applied to the results obtained in small scale specimens. A probabilistic approach was chosen to analyze the results obtained and derive fatigue curves for the assessment of structural details and materials.

The first step was concentrated in collecting all experimental data available, and to study the theories, methods and approaches related to fatigue on riveted connections. Since the main goal of the thesis is aimed at historical heritage structures, a special focus was put old riveted connections and materials. Many codes and standards have a section related to the subject of fatigue in metallic connections, but none of the most relevant codes deals directly with fatigue in riveted connections.

The main codes and standards are the Eurocode 3, BS 5400 – British code and AASHTO – North American Standard. The studies in which these codes are based are related to steel structures, but the material used on many of these old bridges is puddled iron. Therefore, it was considered necessary to study the more modern approach developed by Taras and Grainer, and the probabilistic approach proposed by Castillo and Fernández-Canteli.

The following steps involved the preparation and validation of a probabilistic approach on the fatigue phenomena of riveted connections. The study developed is based on experimental data obtained in experimental tests performed in specimens collected from old Portuguese metallic bridges (Correia, 2014). Subsequently, with the assistance of the software ProFatigue®, a local approach study on riveted connections data was developed, considering double and single shear connections. This specific software follows the mathematical method known as Weibull distribution, providing results as the S-N curve, a probabilistic curve, the curve which represents the Weibull distribution and the parameters obtained from the resulting graphics. These steps were also followed to study the material obtained from the collected specimens.

Afterwards, it was possible to study the behavior of fatigue in the connection in a global approach and compare the different models and methods. As a result of this work, the following conclusions are proposed:

- In the study of the proposed S-N curves for double shear and single shear riveted connections, it was observed by comparing the curves proposed by the Eurocode 3 – Part 1-9, the S-N theoretical proposed curve and the Taras and Greiner proposed curve, that the specimens presented a good behaviour when submitted to the fatigue cycles. The curve that better represents the behaviour of the connection is the one proposed by Taras and Grainer;
- In the statistical analysis based on comparison between ASTM E 739-91 and Castillo and Fernández-Canteli model for double shear and single shear riveted connections, it can be noticed that the best results fitted to the evolution of the fatigue life is the one given by the Castillo and Fernández-Canteli model.
- In the approach presented in the statistical analysis based on Castillo and Fernández-Canteli model for double shear and single shear riveted connections it is observed the good behavior of the connections, because both results are contained within the zone between the 5% curve and the 95% curve. The results are close to the 50% curve, the mean value, also shows the good behavior of the specimens to the fatigue.
- To the statistical analysis based on ASTM E739-91 standard aimed at the material behavior, it presents good behavior when the experimental data from the different bridges are compared when submitted to the stress range, strain amplitude and SWT. In the all resulting graphics the data is contained within the zone between the 5% curve and the 95% curve. And results are close to the 50% curve, the mean value, also shows the good behavior of the specimens to the fatigue.
- To the final study of the fatigue damage parameters, which is applied the S-N curve to evaluate the life-time of the material. The results obtained for when the material is submitted to stress range, strain amplitude and SWT shows the material from the different bridges present elastoplastic behavior. That is the material resists the fatigue strength.

5.1 Future developments

The following step is the proposal of the study of the fatigue numerical analysis of double and single shear riveted connections based on full range fatigue curve. And the development to S-N curves specifically aimed towards the old and new rivet connection.

REFERENCES

- ASM, I. (2008). Fatigue. In *Elements of Metallurgy and Engineering Alloys* (pp. 243-264). Materials Park, Ohio, USA.
- ASTM E739-91. (2004). (Reapproved 2004). *Standard Practice for Statistical Analysis of Linear or Linearized Stress-Life (S-N) and Strain-Life (e-N) Fatigue Data*, pp. 1-7.
- Bates, W. (1991). *Historical Structural Steelwork Handbook*. London: The British Constructional Steelwork Association Limited.
- BRITISH STANDARD. (1980). BS 5400. *Steel, Concrete and Composite Bridges. Part 10: Code of Practice for Fatigue*, pp. 1-78.
- Bussell, M. (1997). *Appraisal of Existing Iron and Steel Structures*. The Steel Construction Institute. Berkshire : The Steel Construction Institute.
- Calvert, E. (2013). *How the industrial revolution changed Britain's architecture*. Dissertation, VIA University College, School of Technology and Business, Horsens, Denmark.
- Castillo, E., López-Aenlle, M., Ramos, A., Fernández-Canteli, A., Kieselbach, R., & Esslinger, V. (2005). Specimen length effect on parameter estimation in modelling fatigue strength by Weibull distribution. *International Journal of Fatigue*, 1047-1058.
- Collette, Q. (2014, June). Riveted Connections in Historical Metal Structures (1840-1940). Hot-driven rivets: technology, design and experiments. pp. 1-266.
- Collette, Q., Sire, S., & Wouters, I. (2014). Lap Shear Tests on Repaired Wrought-Iron Riveted Connections. *Engineering Structures*, pp. 1-12.
- Correia, J. A. (2008, 12). Desenvolvimento de modelos de previsão da vida à fadiga de ligações rebitadas. 6-23.
- Correia, J. A. (2014). An Integral Probabilistic Approach for Fatigue Lifetime Prediction of Mechanical and Structural Components. pp. 48-382.
- Custodio, J. (n.d.). *A Máquina a Vapor de Soure - um património industrial da Fundação Belmiro de Azevedo*. (A. G. Oliveira, M. Magalhaes, & J. Custodio, Eds.) SONAE Imobiliaria, S.A.
- Deng, X., & Hutchinson, J. W. (1998). The Clamping Stress in a Cold-Driven Rivet. *Pergamon Press*, 683-694.
- European Committee for Standardization. (1991). Eurocode 1: Actions on structures. Brussels.
- EUROPEAN STANDARD. (2005). EN 1993-1-9 : 2005. *Eurocode 3: Design of steel structures - Part 1-9: Fatigue*, pp. 1-37.

- Fernández-Canteli, A., Przybille, C., Nogal, M., Aenlle, M. L., & Castillo, E. (2014). ProFatigue: A software program for probabilistic assessment of experimental fatigue data sets. *Procedia Engineering* 74, 236-241.
- GSA. (1998, 3). Cast Iron: Characteristics, Uses and Problems. *Outdoor Sculpture Manual - Center for Public Buildings*.
- Jesus, A. M., Silva, A. L., & Correia, J. A. (2014, October 22). Fatigue of riveted and bolted joints made of puddle iron - An experimental approach. *Journal of Constructional Steel Research*, pp. 81-91.
- Jr, J. C., & Raju, I. S. (1986). *Computational Methods in the Mechanics of Fracture*. Hampton, U.S.A.: Elsevier Science Publishers B.V.
- Krause, D. (1969). *Gray Iron- A Unique Engineering Material*. Iron Casting Research Institute, Philadelphia.
- Lindenberg, R. J. (2016, June 08). Fatigue and Strength Behaviour of Existing Riveted Steel Structures: A Case Study of The Waalbrug (Nijmegen). pp. 13-58.
- Mayorga, L. G., Stéphane Sire, J. A., Jesus, A. M., Calos Rebelo, A. F.-C., Ragueneau, M., & Plu, B. (2017, May 26). Statistical evaluation of fatigue strength of double shear riveted connections and crack growth rates of materials from old bridges. *Engineering Fracture Mechanics*, pp. 1-17.
- Mechanical Properties of Gray Iron - Hardness*. (2010). Retrieved June 5, 2015, from Atlas Foundry Company: www.atlasfdry.com/grayiron-hardness.htm
- onestopmap*. (2017, July 05). Retrieved from <https://www.onestopmap.com/>
- Österreichisches Normungsinstitut. (2006, 12). ONR 24008. *Bewertung der Tragfähigkeit bestehender Eisenbahn- und Straßenbrücken*.
- Oxford Dictionarie. (2013). *Definition of fatigue in English*. *Oxford Dictionaries Online*. Retrieved 04 20, 2017, from <https://en.oxforddictionaries.com/definition/fatigue>
- Proceq SA. (n.d.). *Metal Hardness Tester - Equotip Bambino 2*. Retrieved June 1, 2015, from proceq: www.proceq.com/nondestructivetestequipment/metal-testing/hardness-testing/equotip-bambino-2.html
- Robert J. Dexter, J. M. (2013, March). Manual for Repair and Retrofit of Fatigue Cracks in Steel Bridges. *FHWA-IF-13- 020, University of Minnesota, Department of Civil Engineering*, pp. 9-18.
- Rondal, J., & Rasmussen, K. J. (2004). On the strength of cast iron columns. *Journal of Constructional Steel Research* 60.

- Taras, A., & Greiner, R. (2009). Development and Application of a Fatigue Class Catalogue for Riveted Bridge Components. pp. 1-13.
- Tirbonod, B. (2015). A fixed point in the Coffin–Manson law. *International Journal of Fatigue* 81, 143-147.
- U.S. General Services Administration. (1998, March). Wrought Iron: Characteristics, Uses and Problems. *Historic Preservation - Technical Procedures*.
- Verhoef, A. P. (Ed.). (1999). Problems and Possibilities - Cast Iron, Wrought Iron, Steel. *International Congress on Urban Heritage and Building Maintenance*. Delft: Office Faculty of Architecture Delft University of Technology.
- X. W. Ye, Y. H. (2014). A State-of-the-Art Review on Fatigue Life Assessment of. *Mathematical Problems in Engineering* - Article ID 956473, pp. 1-13.
- Xiulin Zheng, J. W. (2005). On the prediction of P–S–N curves of 45 steel notched elements and probability distribution of fatigue life under variable amplitude loading from tensile properties. *International Journal of Fatigue*, 601-609.

This page was intentionally left blank.

APPENDIX A: TABLES OF THE DATA OF THE RIVETED CONNECTION

1 RESULTS OBTAINED FOR THE MATERIALS SUBMITTED TO STRESS

Table 31 – Results obtained from Correia’s research; Viana bridge stress test ($R_e=-1$); (Correia, 2014)

Specimens	N_f cycles	$\Delta\sigma$ (Mpa)	Area (mm ²)	f (Hz)
LCF-viana-050-01	2845	660,37	37,84	0,800
LCF-viana-050-02	922	691,09	37,96	0,800
LCF-viana-050-03	537	690,36	38,52	0,800
LCF-viana-040-01	2684	656,79	38,08	1,000
LCF-viana-040-02	581	632,79	38,34	1,000
LCF-viana-040-03	5697	637,38	38,68	1,000
LCF-viana-030-01	80281	562,65	38,19	1,333
LCF-viana-030-02	49460	578,36	37,86	1,333
LCF-viana-020-01	854096	408,38	37,92	2,000
LCF-viana-020-02	1000000	399,58	38,04	2,000
LCF-viana-075-01	164	700,35	38,40	0,533
LCF-viana-075-02	153	726,31	38,48	0,533
LCF_050_01	3012	646,98	30,0608	0,800
LCF_040_01	4154	639,10	31,0236	1,000
LCF_030_01	80120	535,88	29,6946	1,333
LCF_030_02	20010	548,05	30,5893	1,333
LCF_025_01	68911	463,72	30,2202	1,600
LCF_007_01	68502	466,70	29,988	15,000
LCF_006_01	192794	385,58	31,1121	15,000
LCF_005_01	5000000	322,59	31,0097	15,000
LCF_0055_01	984799	367,51	29,8758	15,000
LCF_006_02	684114	417,24	28,763	15,000
LCF_0055_02	914896	369,31	29,766	15,000
LCF_060_01	407	700,21	29,5715	0,667
LCF_070_01	759	649,86	29,841	0,571
LCF_080_01	145	661,91	30,4776	0,500
LCF_100_01	50	716,16	28,782	0,400

Table 32 - Results obtained from Correia's research; Fão bridge stress test ($R_e=0$); (Correia, 2014)

Specimens	N_f cycles	$\Delta\sigma$ (Mpa)	Area (mm ²)	f (Hz)
LCF-e020-01	4416	561,79	43,86	1,00
LCF-e020-02	5433	591,80	44,59	1,00
LCF-e020-03	8420	736,84	34,98	1,00
LCF-e015-01	49300	507,97	37,31	1,33
LCF-e015-02	16788	522,47	38,60	1,33
LCF-e015-03	27731	550,33	41,72	1,33
LCF-e040-01	374	657,58	34,79	0,50
LCF-e040-02	452	730,47	37,94	0,50
LCF_e025-01	290	631,26	43,38	0,80
LCF-e025-02	2108	623,48	38,77	0,80
LCF-e025-03	2254	617,30	38,90	0,80
LCF-e010-01	530604	381,34	43,37	2,00
LCF-e010-02	663962	391,23	43,23	2,00
LCF-e010-03	74549	375,88	38,44	2,00

Table 33 – Results obtained from Correia's research; Fão bridge stress test ($R_{\varepsilon}=-1$); (Correia, 2014)

Specimens	N_f cycles	$\Delta\sigma$ (Mpa)	Area (mm ²)	f (Hz)
LCF-150-01	143	616,59	38,52	0,267
LCF-100-01	92	824,48	39,14	0,400
LCF-100-02	955	616,37	40,51	0,400
LCF-100-03	528	654,92	41,87	0,400
LCF-075-01	384	755,61	36,98	0,533
LCF-075-02	250	779,19	37,80	0,533
LCF-075-03	507	699,42	42,92	0,533
LCF-050-01	1106	572,95	42,68	0,800
LCF-050-02	3454	715,77	38,32	0,800
LCF-050-03	1195	636,91	36,73	0,800
LCF-030-01	25560	531,51	37,20	1,333
LCF-030-02	22618	526,50	41,03	1,333
LCF-030-03	15517	494,96	40,33	1,333
LCF-025-01	23878	467,02	40,33	1,600
LCF-025-02	76677	464,76	40,07	1,600
LCF-025-03	39998	483,21	41,38	1,600
LCF-020-01	692177	372,07	38,60	5,000
LCF-020-02	357127	376,46	40,97	5,000
LCF-020-03	54116	385,79	33,68	5,000
LCF-020-04	306129	398,56	44,19	5,000
LCF-015-01	1000000	296,46	35,06	5,000

Table 34 – Results obtained from Correia’s research; Fão bridge stress test ($R_{\varepsilon}=0$ and $R_{\varepsilon}=-1$);
(Correia, 2014)

Specimens	N_f cycles	$\Delta\sigma$ (Mpa)	Area (mm ²)	f (Hz)
LCF-e020-01	4416	561,79	43,86	1,00
LCF-e020-02	5433	591,80	44,59	1,00
LCF-e020-03	8420	736,84	34,98	1,00
LCF-e015-01	49300	507,97	37,31	1,33
LCF-e015-02	16788	522,47	38,60	1,33
LCF-e015-03	27731	550,33	41,72	1,33
LCF-e040-01	374	657,58	34,79	0,50
LCF-e040-02	452	730,47	37,94	0,50
LCF_e025-01	290	631,26	43,38	0,80
LCF-e025-02	2108	623,48	38,77	0,80
LCF-e025-03	2254	617,30	38,90	0,80
LCF-e010-01	530604	381,34	43,37	2,00
LCF-e010-02	663962	391,23	43,23	2,00
LCF-e010-03	74549	375,88	38,44	2,00
LCF-150-01	143	616,59	38,52	0,267
LCF-100-01	92	824,48	39,14	0,400
LCF-100-02	955	616,37	40,51	0,400
LCF-100-03	528	654,92	41,87	0,400
LCF-075-01	384	755,61	36,98	0,533
LCF-075-02	250	779,19	37,80	0,533
LCF-075-03	507	699,42	42,92	0,533
LCF-050-01	1106	572,95	42,68	0,800
LCF-050-02	3454	715,77	38,32	0,800
LCF-050-03	1195	636,91	36,73	0,800
LCF-030-01	25560	531,51	37,20	1,333
LCF-030-02	22618	526,50	41,03	1,333
LCF-030-03	15517	494,96	40,33	1,333
LCF-025-01	23878	467,02	40,33	1,600
LCF-025-02	76677	464,76	40,07	1,600
LCF-025-03	39998	483,21	41,38	1,600
LCF-020-01	692177	372,07	38,60	5,000
LCF-020-02	357127	376,46	40,97	5,000
LCF-020-03	54116	385,79	33,68	5,000
LCF-020-04	306129	398,56	44,19	5,000
LCF-015-01	1000000	296,46	35,06	5,000

Table 35 - Results obtained from Correia's research; Trezói bridge stress test ($R_\varepsilon=-1$); (Correia, 2014)

Specimens	N _f cycles	$\Delta\sigma$ (Mpa)	Area (mm ²)	f (Hz)
LCF1	716	574,60	59,04	0,400
LCF2	1626	555,80	59,47	0,533
LCF3	5749	485,80	59,70	0,800
LCF4	20596	438,20	60,52	1,333
LCF5	1031126	436,80	61,07	2,000
LCF6	15852	412,00	60,44	1,333
LCF7	2586	542,80	59,50	0,800
LCF8	414	667,40	60,78	0,267
LCF9	153	715,40	60,32	0,200
LCF10	199	733,00	62,01	0,160

Table 36 - Results obtained from Correia's research; Luiz I bridge stress test ($R_\varepsilon=-1$); (Correia, 2014)

Specimens	N _f cycles	$\Delta\sigma$ (Mpa)	Area (mm ²)	f (Hz)
LCF-Luiz1A-050-01	17	718,98	33,41	0,400
LCF-Luiz1B-050-02	28	726,64	33,51	0,400
LCF-Luiz1C-0375-01	55	695,47	33,39	0,533
LCF-Luiz1D-0375-02	94	720,63	33,46	0,533
LCF-Luiz1E-025-01	325	675,60	33,26	0,800
LCF-Luiz1F-025-02	465	662,99	33,41	0,800
LCF-Luiz1G-020-01	888	659,87	33,41	1,000
LCF-Luiz1H-020-02	987	660,51	33,31	1,000
LCF-Luiz1I-015-01	4950	583,58	33,61	1,333
LCF-Luiz1J-015-02	97775	562,44	33,23	1,333
LCF-Luiz1K-015-03	8551	548,43	33,28	1,333
LCF-Luiz1L-015-04	19332	575,90	33,21	1,333
LCF-Luiz1M-010-01	788684	411,24	33,49	5,000
LCF-Luiz1N-010-02	191591	414,69	33,57	5,000
LCF-Luiz1O-010-03	567651	415,58	33,38	5,000

2 RESULTS OBTAINED FOR THE MATERIALS SUBMITTED TO STRAIN

Table 37 - Results obtained from Correia's research; Viana bridge strain test ($R_\varepsilon=-1$); (Correia, 2014)

Specimens	Nr cycles	$\Delta\xi/2$ (Mpa)	Area (mm ²)	f (Hz)
LCF-viana-050-01	2845	0,00250	37,84	0,800
LCF-viana-050-02	922	0,00250	37,96	0,800
LCF-viana-050-03	537	0,00250	38,52	0,800
LCF-viana-040-01	2684	0,00200	38,08	1,000
LCF-viana-040-02	581	0,00200	38,34	1,000
LCF-viana-040-03	5697	0,00200	38,68	1,000
LCF-viana-030-01	80281	0,00150	38,19	1,333
LCF-viana-030-02	49460	0,00150	37,86	1,333
LCF-viana-020-01	854096	0,00100	37,92	2,000
LCF-viana-020-02	1000000	0,00100	38,04	2,000
LCF-viana-075-01	164	0,00375	38,40	0,533
LCF-viana-075-02	153	0,00375	38,48	0,533
LCF_050_01	3012	0,00250	30,0608	0,800
LCF_040_01	4154	0,00200	31,0236	1,000
LCF_030_01	80120	0,00150	29,6946	1,333
LCF_030_02	20010	0,00150	30,5893	1,333
LCF_025_01	68911	0,00125	30,2202	1,600
LCF_007_01	68502	0,00128	29,988	15,000
LCF_006_01	192794	0,00098	31,1121	15,000
LCF_005_01	5000000	0,00083	31,0097	15,000
LCF_0055_01	984799	0,00094	29,8758	15,000
LCF_006_02	684114	0,00101	28,763	15,000
LCF_0055_02	914896	0,00094	29,766	15,000
LCF_060_01	407	0,00300	29,5715	0,667
LCF_070_01	759	0,00350	29,841	0,571
LCF_080_01	145	0,00400	30,4776	0,500
LCF_100_01	50	0,00500	28,782	0,400

Table 38 - Results obtained from Correia's research; Fão bridge strain test ($R_\varepsilon=0$); (Correia, 2014)

Specimens	N_f cycles	$\Delta\xi/2$ (Mpa)	Area (mm ²)	f (Hz)
LCF-e020-01	4416	0,00200	43,86	1,00
LCF-e020-02	5433	0,00200	44,59	1,00
LCF-e020-03	8420	0,00200	34,98	1,00
LCF-e015-01	49300	0,00150	37,31	1,33
LCF-e015-02	16788	0,00150	38,60	1,33
LCF-e015-03	27731	0,00150	41,72	1,33
LCF-e040-01	374	0,00400	34,79	0,50
LCF-e040-02	452	0,00400	37,94	0,50
LCF_e025-01	290	0,00250	43,38	0,80
LCF-e025-02	2108	0,00250	38,77	0,80
LCF-e025-03	2254	0,00250	38,90	0,80
LCF-e010-01	530604	0,00100	43,37	2,00
LCF-e010-02	663962	0,00100	43,23	2,00
LCF-e010-03	74549	0,00100	38,44	2,00

Table 39 - Results obtained from Correia's research; Fão bridge strain test ($R_\varepsilon=-1$); (Correia, 2014)

Specimens	N_f cycles	$\Delta\xi/2$ (Mpa)	Area (mm ²)	f (Hz)
LCF-150-01	143	0,00750	38,52	0,267
LCF-100-01	92	0,00500	39,14	0,400
LCF-100-02	955	0,00500	40,51	0,400
LCF-100-03	528	0,00500	41,87	0,400
LCF-075-01	384	0,00375	36,98	0,533
LCF-075-02	250	0,00375	37,80	0,533
LCF-075-03	507	0,00375	42,92	0,533
LCF-050-01	1106	0,00250	42,68	0,800
LCF-050-02	3454	0,00250	38,32	0,800
LCF-050-03	1195	0,00250	36,73	0,800
LCF-030-01	25560	0,00150	37,20	1,333
LCF-030-02	22618	0,00150	41,03	1,333
LCF-030-03	15517	0,00150	40,33	1,333
LCF-025-01	23878	0,00125	40,33	1,600
LCF-025-02	76677	0,00125	40,07	1,600
LCF-025-03	39998	0,00125	41,38	1,600
LCF-020-01	692177	0,00100	38,60	5,000
LCF-020-02	357127	0,00100	40,97	5,000
LCF-020-03	54116	0,00100	33,68	5,000
LCF-020-04	306129	0,00100	44,19	5,000
LCF-015-01	1000000	0,00075	35,06	5,000

Table 40 - Results obtained from Correia's research; Fão bridge strain test ($R_\varepsilon=0$ and $R_\varepsilon=-1$); (Correia, 2014)

Specimens	N_f cycles	$\Delta\xi/2$ (Mpa)	Area (mm ²)	f (Hz)
LCF-e020-01	4416	0,00200	43,86	1,00
LCF-e020-02	5433	0,00200	44,59	1,00
LCF-e020-03	8420	0,00200	34,98	1,00
LCF-e015-01	49300	0,00150	37,31	1,33
LCF-e015-02	16788	0,00150	38,60	1,33
LCF-e015-03	27731	0,00150	41,72	1,33
LCF-e040-01	374	0,00400	34,79	0,50
LCF-e040-02	452	0,00400	37,94	0,50
LCF_e025-01	290	0,00250	43,38	0,80
LCF-e025-02	2108	0,00250	38,77	0,80
LCF-e025-03	2254	0,00250	38,90	0,80
LCF-e010-01	530604	0,00100	43,37	2,00
LCF-e010-02	663962	0,00100	43,23	2,00
LCF-e010-03	74549	0,00100	38,44	2,00
LCF-150-01	143	0,00750	38,52	0,267
LCF-100-01	92	0,00500	39,14	0,400
LCF-100-02	955	0,00500	40,51	0,400
LCF-100-03	528	0,00500	41,87	0,400
LCF-075-01	384	0,00375	36,98	0,533
LCF-075-02	250	0,00375	37,80	0,533
LCF-075-03	507	0,00375	42,92	0,533
LCF-050-01	1106	0,00250	42,68	0,800
LCF-050-02	3454	0,00250	38,32	0,800
LCF-050-03	1195	0,00250	36,73	0,800
LCF-030-01	25560	0,00150	37,20	1,333
LCF-030-02	22618	0,00150	41,03	1,333
LCF-030-03	15517	0,00150	40,33	1,333
LCF-025-01	23878	0,00125	40,33	1,600
LCF-025-02	76677	0,00125	40,07	1,600
LCF-025-03	39998	0,00125	41,38	1,600
LCF-020-01	692177	0,00100	38,60	5,000
LCF-020-02	357127	0,00100	40,97	5,000
LCF-020-03	54116	0,00100	33,68	5,000
LCF-020-04	306129	0,00100	44,19	5,000
LCF-015-01	1000000	0,00075	35,06	5,000

Table 41 - Results obtained from Correia's research; Trezói bridge strain test ($R_e=-1$); (Correia, 2014)

Specimens	Nr cycles	$\Delta\xi/2$ (Mpa)	Area (mm ²)	f (Hz)
LCF1	716	0,00500	59,04	0,400
LCF2	1626	0,00375	59,47	0,533
LCF3	5749	0,00250	59,70	0,800
LCF4	20596	0,00150	60,52	1,333
LCF5	1031126	0,00100	61,07	2,000
LCF6	15852	0,00150	60,44	1,333
LCF7	2586	0,00250	59,50	0,800
LCF8	414	0,00750	60,78	0,267
LCF9	153	0,01000	60,32	0,200
LCF10	199	0,01250	62,01	0,160

Table 42 - Results obtained from Correia's research; Luiz I bridge strain test ($R_e=-1$); (Correia, 2014)

Specimens	Nr cycles	$\Delta\xi/2$ (Mpa)	Area (mm ²)	f (Hz)
LCF-Luiz1A-050-01	17	0,00500	33,41	0,400
LCF-Luiz1B-050-02	28	0,00500	33,51	0,400
LCF-Luiz1C-0375-01	55	0,00375	33,39	0,533
LCF-Luiz1D-0375-02	94	0,00375	33,46	0,533
LCF-Luiz1E-025-01	325	0,00250	33,26	0,800
LCF-Luiz1F-025-02	465	0,00250	33,41	0,800
LCF-Luiz1G-020-01	888	0,00200	33,41	1,000
LCF-Luiz1H-020-02	987	0,00200	33,31	1,000
LCF-Luiz1I-015-01	4950	0,00150	33,61	1,333
LCF-Luiz1J-015-02	97775	0,00150	33,23	1,333
LCF-Luiz1K-015-03	8551	0,00150	33,28	1,333
LCF-Luiz1L-015-04	19332	0,00150	33,21	1,333
LCF-Luiz1M-010-01	788684	0,00100	33,49	5,000
LCF-Luiz1N-010-02	191591	0,00100	33,57	5,000
LCF-Luiz1O-010-03	567651	0,00100	33,38	5,000

3 RESULTS OBTAINED FOR THE MATERIALS SUBMITTED TO SMITH-WATSON-TOPPER (SWT)

Table 43 - Results obtained from Correia's research; Viana bridge SWT test ($R_e=-1$); (Correia, 2014)

Specimens	Nr cycles	SWT (MPa)	Area (mm ²)	f (Hz)
LCF-viana-050-01	2845	0,79570	37,84	0,800
LCF-viana-050-02	922	0,86152	37,96	0,800
LCF-viana-050-03	537	0,84724	38,52	0,800
LCF-viana-040-01	2684	0,64840	38,08	1,000
LCF-viana-040-02	581	0,60700	38,34	1,000
LCF-viana-040-03	5697	0,61994	38,68	1,000
LCF-viana-030-01	80281	0,40618	38,19	1,333
LCF-viana-030-02	49460	0,44011	37,86	1,333
LCF-viana-020-01	854096	0,23090	37,92	2,000
LCF-viana-020-02	1000000	0,26969	38,04	2,000
LCF-viana-075-01	164	1,29816	38,40	0,533
LCF-viana-075-02	153	1,34435	38,48	0,533
LCF_050_01	3012	0,77355	30,0608	0,800
LCF_040_01	4154	0,64397	31,0236	1,000
LCF_030_01	80120	0,38367	29,6946	1,333
LCF_030_02	20010	0,41260	30,5893	1,333
LCF_025_01	68911	0,28951	30,2202	1,600
LCF_007_01	68502	0,29791	29,988	15,000
LCF_006_01	192794	0,18849	31,1121	15,000
LCF_005_01	5000000	0,13365	31,0097	15,000
LCF_0055_01	984799	0,17305	29,8758	15,000
LCF_006_02	684114	0,21111	28,763	15,000
LCF_0055_02	914896	0,17351	29,766	15,000
LCF_060_01	407	1,02227	29,5715	0,667
LCF_070_01	759	1,06941	29,841	0,571
LCF_080_01	145	1,26768	30,4776	0,500
LCF_100_01	50	1,66779	28,782	0,400

Table 44 - Results obtained from Correia's research; Fão bridge SWT test ($R_\varepsilon=0$); (Correia, 2014)

Specimens	N_f cycles	SWT (MPa)	Area (mm ²)	f (Hz)
LCF-e020-01	4416	0,55486	43,86	1,00
LCF-e020-02	5433	0,57553	44,59	1,00
LCF-e020-03	8420	0,71349	34,98	1,00
LCF-e015-01	49300	0,33828	37,31	1,33
LCF-e015-02	16788	0,34633	38,60	1,33
LCF-e015-03	27731	0,38857	41,72	1,33
LCF-e040-01	374	1,26020	34,79	0,50
LCF-e040-02	452	1,39185	37,94	0,50
LCF_e025-01	290	0,76331	43,38	0,80
LCF-e025-02	2108	0,75798	38,77	0,80
LCF-e025-03	2254	0,74473	38,90	0,80
LCF-e010-01	530604	0,16697	43,37	2,00
LCF-e010-02	663962	0,13427	43,23	2,00
LCF-e010-03	74549	0,15597	38,44	2,00

Table 45 - Results obtained from Correia's research; Fão bridge SWT test ($R_\varepsilon=-1$); (Correia, 2014)

Specimens	N_f cycles	SWT (MPa)	Area (mm ²)	f (Hz)
LCF-150-01	143	2,79349	38,52	0,267
LCF-100-01	92	2,03368	39,14	0,400
LCF-100-02	955	1,52618	40,51	0,400
LCF-100-03	528	1,62479	41,87	0,400
LCF-075-01	384	1,35523	36,98	0,533
LCF-075-02	250	1,44738	37,80	0,533
LCF-075-03	507	1,29720	42,92	0,533
LCF-050-01	1106	0,70644	42,68	0,800
LCF-050-02	3454	0,87878	38,32	0,800
LCF-050-03	1195	0,82887	36,73	0,800
LCF-030-01	25560	0,45059	37,20	1,333
LCF-030-02	22618	0,41795	41,03	1,333
LCF-030-03	15517	0,40805	40,33	1,333
LCF-025-01	23878	0,32865	40,33	1,600
LCF-025-02	76677	0,25291	40,07	1,600
LCF-025-03	39998	0,29627	41,38	1,600
LCF-020-01	692177	0,21732	38,60	5,000
LCF-020-02	357127	0,21490	40,97	5,000
LCF-020-03	54116	0,21307	33,68	5,000
LCF-020-04	306129	0,24724	44,19	5,000
LCF-015-01	1000000	0,11911	35,06	5,000

Table 46 - Results obtained from Correia's research; Fão bridge SWT test ($R_{\varepsilon}=0$ and $R_{\varepsilon}=-1$); (Correia, 2014)

Specimens	N_f cycles	SWT (MPa)	Area (mm ²)	f (Hz)
LCF-e020-01	4416	0,55486	43,86	1,00
LCF-e020-02	5433	0,57553	44,59	1,00
LCF-e020-03	8420	0,71349	34,98	1,00
LCF-e015-01	49300	0,33828	37,31	1,33
LCF-e015-02	16788	0,34633	38,60	1,33
LCF-e015-03	27731	0,38857	41,72	1,33
LCF-e040-01	374	1,26020	34,79	0,50
LCF-e040-02	452	1,39185	37,94	0,50
LCF_e025-01	290	0,76331	43,38	0,80
LCF-e025-02	2108	0,75798	38,77	0,80
LCF-e025-03	2254	0,74473	38,90	0,80
LCF-e010-01	530604	0,16697	43,37	2,00
LCF-e010-02	663962	0,13427	43,23	2,00
LCF-e010-03	74549	0,15597	38,44	2,00
LCF-150-01	143	2,793493	38,52	0,267
LCF-100-01	92	2,033680	39,14	0,400
LCF-100-02	955	1,526176	40,51	0,400
LCF-100-03	528	1,624794	41,87	0,400
LCF-075-01	384	1,355232	36,98	0,533
LCF-075-02	250	1,447383	37,80	0,533
LCF-075-03	507	1,297203	42,92	0,533
LCF-050-01	1106	0,706440	42,68	0,800
LCF-050-02	3454	0,878783	38,32	0,800
LCF-050-03	1195	0,828871	36,73	0,800
LCF-030-01	25560	0,450589	37,20	1,333
LCF-030-02	22618	0,417947	41,03	1,333
LCF-030-03	15517	0,408055	40,33	1,333
LCF-025-01	23878	0,328652	40,33	1,600
LCF-025-02	76677	0,252906	40,07	1,600
LCF-025-03	39998	0,296268	41,38	1,600
LCF-020-01	692177	0,217319	38,60	5,000
LCF-020-02	357127	0,214899	40,97	5,000
LCF-020-03	54116	0,213069	33,68	5,000
LCF-020-04	306129	0,247238	44,19	5,000
LCF-015-01	1000000	0,119110	35,06	5,000

Table 47 - Results obtained from Correia's research; Trezói bridge SWT test ($R_{\varepsilon}=-1$); (Correia, 2014)

Specimens	N _f cycles	SWT (MPa)	Area (mm ²)	f (Hz)
LCF1	716	1,43601	59,04	0,400
LCF2	1626	1,04050	59,47	0,533
LCF3	5749	0,61114	59,70	0,800
LCF4	20596	0,32948	60,52	1,333
LCF5	1031126	0,16779	61,07	2,000
LCF6	15852	0,30632	60,44	1,333
LCF7	2586	0,67984	59,50	0,800
LCF8	414	2,48914	60,78	0,267
LCF9	153	3,56162	60,32	0,200
LCF10	199	4,61251	62,01	0,160

Table 48 - Results obtained from Correia's research; Luiz I bridge SWT test ($R_{\varepsilon}=-1$); (Correia, 2014)

Specimens	N _f cycles	SWT (MPa)	Area (mm ²)	f (Hz)
LCF-Luiz1A-050-01	17	1,78168	33,41	0,400
LCF-Luiz1B-050-02	28	1,78077	33,51	0,400
LCF-Luiz1C-0375-01	55	1,27818	33,39	0,533
LCF-Luiz1D-0375-02	94	1,31355	33,46	0,533
LCF-Luiz1E-025-01	325	0,83208	33,26	0,800
LCF-Luiz1F-025-02	465	0,82217	33,41	0,800
LCF-Luiz1G-020-01	888	0,64578	33,41	1,000
LCF-Luiz1H-020-02	987	0,68565	33,31	1,000
LCF-Luiz1I-015-01	4950	0,43205	33,61	1,333
LCF-Luiz1J-015-02	97775	0,43291	33,23	1,333
LCF-Luiz1K-015-03	8551	0,42663	33,28	1,333
LCF-Luiz1L-015-04	19332	0,41965	33,21	1,333
LCF-Luiz1M-010-01	788684	0,20186	33,49	5,000
LCF-Luiz1N-010-02	191591	0,20152	33,57	5,000
LCF-Luiz1O-010-03	567651	0,17475	33,38	5,000